Pointing Acquisition and Stabilization Test Bed
by
Stephan Jay Feldgoise

Submitted to the
Department of Electrical Engineering and Computer Science
in partial fulfillment of the requirements
for the degree of
Master of Science
at the
Massachusetts Institute of Technology
August, 1993

Signature of Author_____
Department of Electrical Engineering and Computer Science, August, 1993

Certified by _____
Professor James Roberge

Certified by _____
Dr. T. T. Chien

Accepted by _____
F.R. Morgenthaler, Chair, Department Committee on Graduate Students

Pointing Acquisition and Stabilization Test Bed

by

Stephan Jay Feldgoise

Submitted to the Department of Electrical Engineering and Computer Science in partial fulfillment of the requirements for the degree of Master of Science at the Massachusetts Institute of Technology, July, 1993.

Abstract

Acquisition and stabilization are key features in pointing and tracking systems. For this thesis, acquisition and image stabilization are analyzed and demonstrated by the implementation of a high bandwidth loop using an Optical Reference Gyro and a Fast Steering Mirror. In addition, the setup will show that targets can be acquired and stabilized in the presence of platform disturbance and other noise sources.

Technical Supervisor: Dr. Tze-Thong Chien
Principal Member Technical Staff
Charles Stark Draper Laboratory

Thesis Supervisor: Professor James Roberge
Dept. of Electrical Eng. and Computer Science

Acknowledgments

I would first like to thank the Charles Stark Draper Laboratory for funding my graduate work in addition to providing my undergraduate summer employment.

I would like to thank Dr. T.T. Chien for his superior guidance and Professor James K. Roberge for his time and advice.

There were many people who assisted me in my efforts. Most importantly, without the help of Dale Woodbury and Mike Luniewicz the project certainly wouldn't have gone far. The combination of Dale's crafty hands-on expertise and Mike's ease at translating theory in hardware were invaluable throughout the entire process.

There were several others who made significant contributions and I would like to mention them by name: Greg Capeillo, Ernie Nolan, Mike Depiero, Chris Doerr, Paul Tuck, Tony Badessa, and Ralph Pupa.

This thesis was prepared at The Charles Stark Draper Laboratory, Inc., under Independent and Development Project No. 432.

Publication of this thesis does not constitute approval by Draper or the sponsoring agency of the findings or conclusions contained herein. It is published for the exchange and stimulation of ideas.

I hereby assign my copyright of this thesis to The Charles Stark Draper Laboratory, Inc., Cambridge, Massachusetts.

Stephan Feldgoise

Permission is hereby granted by The Charles Stark Draper Laboratory, Inc., to the Massachusetts Institute of Technology to reproduce any or all of this thesis.

Table of Contents

List of Figures

Page

List of Tables

List of Acronyms and Variables

ADS	Angular Displacement Sensor
B(s)	Coupling Transfer Function Between Table and FSM
CCD	Charge Coupled Device
CSDL	Charles Stark Draper Laboratory
DYNAC	Dynamic Autocollimator
F(s)	FSM Dynamics
FPA	Focal Plane Array
FSM	Fast Steering Mirror
G(s)	FSM Controller
IRU	Inertial Reference Unit
LED	Light Emitting Diode
LITE	Laser Intersatellite Tracking Experiment
LOS	Line of Sight
mr	milli-radians
ORG	Optical Reference Gyroscope
PID	Proportional-Integral-Derivative
PSD	Power Spectral Density
RMS	Root Mean Square
s	Frequency Representation
S(s)	Table Follow Up Loop Controller
T(s)	ORG Loop Controller
ur	micro-radians
Θ_{BI}	Table Platform Angle
Θ_{TI}	Target Angle
η_{PH}	Photopot Noise
η_{RI}	ORG Noise
e1	Error Detected at Photopot (Target Angle)
e2	Error Det. by Quad Cell in FSM Loop (ORG Beam Angle)
e3	Error in .1Hz Follow-Up Loop
e4	Error Detected by Receiver

Chapter 1: Introduction

The main objective of this thesis is to systematically develop a pointing acquisition and stabilization test bed modeling an optical intersatellite communications platform. The concept has several practical applications. Most importantly is the potential application for optical space based communications. Optical communications allows for significantly higher data rate transmission in comparison with RF systems. In order for intersatellite communications to be possible, the platforms must be able to track one another as well as attenuate individual platform disturbances. This thesis provides a platform that demonstrates the pointing and stabilization properties that would be necessary in order for optical intersatellite communications to be feasible. The work in this thesis builds upon the LITE experiment conducted by MIT's Lincoln Laboratory [6]. The major difference from [6] is the use of the Optical Reference Gyroscope (ORG). The ORG is a dry-tuned gyro implemented with a light source and a collimating optics assembly on the spinning rotor. The rotor is inherently inertially stable because of the gyroscopic characteristics of a spinning member. The light beam passes through the spinning, collimating optics on the rotor producing an inertially stable reference beam, which when coupled with a fast steering mirror, is utilized for both the tracking and stabilization.

The thesis begins with the system configuration description in Chapter 2. Using the described configuration a computer simulation in both the frequency and time domains was designed and implemented. From the simulation and analysis, it was possible to predict the transfer functions, Power Spectrum Densities (PSDs), and transients for the system. The design and implementation of the analysis and simulation is described in Chapter 3. The system required the design and implementation of three controllers. The first is a high-bandwidth loop to control the fast steering mirror

(FSM). The second controls the ORG torquer for the pointing loop. The third controls the spacecraft in order to prevent mirror "windup". The hardware setup for the system, the component characterization, and the design, construction and testing of the three controllers is shown in Chapter 4. The results of the analysis, simulation and hardware tests are shown in Chapter 5. The conclusions are shown in Chapter 6. Finally, a current project is under way to build an enhanced ORG. Chapter 7 details this work and provides simulated results using the new enhanced ORG. Included in the Appendices is the simulation code used to find the analytical transfer functions, PSDs and transients.

Chapter 2: System Configuration

The systems level concept is shown in Figure 2.1-1. This diagram shows the main components and their symbolic geometric relationships. Also included is the incorporation of a roll gyroscope giving the system full attitude determining capabilities.

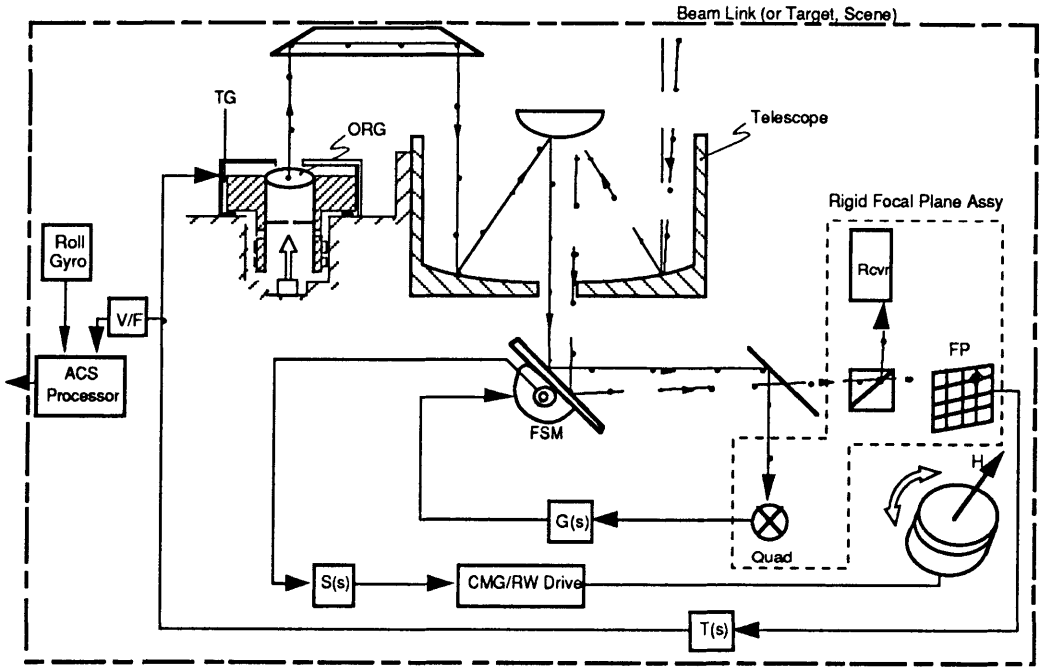

Figure 2.1-1: Pointing Stabilization System Level Configuration

The beam link or target beam represents the communication beam being transmitted between the satellites. This beam is received through a telescope and then reflected off the Fast Steering Mirror (FSM). It is desired to track the target beam as well as to remove the platform jitter injected as the beam is received by the system. The system tracks the target beam via the pointing loop.

The jitter stabilization is achieved by using the ORG (see Section 4.2 for description) in conjunction with the FSM (see Section 4.4 for description). The inertially stable reference beam from the ORG is sent through the telescope to the FSM. It is key to note that

this is the same optical path that the target beam follows. From the telescope, both the reference beam and the target beam are sent off the FSM to their respective angle detectors. The angle detector for the ORG reference beam is the Quad and for the target beam, the detectors are the receiver (Rcvr) and the focal plane (FP). Since both beams are sent off the FSM, any directional changes by the FSM will identically affect both beams. The Quad measures the reference beam detector error. Since the Quad is fixed the spacecraft, platform jitter will be the primary source of the reference beam detector error. This error signal through the FSM controller is used to drive the mirror in a closed loop to remove the injected jitter from the reference beam. Since the target beam and the reference beam are identically affected by the FSM, the attenuation of the jitter in the reference beam, by the FSM, will also remove the jitter in the target beam. Thus, the closed loop with the quad and the FSM serves to eliminate the platform jitter in the reference beam as well as the target beam. In summary, the stabilization system significantly attenuates the platform jitter in the target beam detected at the receiver thereby increasing its signal to noise ratio and image clarity. The system configuration using just the FSM loop to attenuate base disturbance will be termed the stabilization system configuration.

The pointing stabilization system configuration is accomplished by incorporating a pointing loop with the stabilization system. The pointing is necessary in order to minimize the target beam offset error which is detected by the receiver (Rcvr) and the FP. Without a tracker, the target beam would no longer be centered on its receiver as the communicating satellites moved with respect to one another, thus causing a break in the communications link. As previously noted, the target beam is sent from the FSM into a corner cube which divides the signal between a receiver (abbreviated Rcvr in Figure 2.1-1) and the focal plane (abbreviated FP in Figure 2.1-1). The focal plane or photopot detector generates the target beam offset error. This signal is sent through the ORG controller

(abbreviated T(s)) to the torquer generator of the ORG rotor. The torquer generator enables the target beam offset error from the photopot, through the ORG controller, to steer the rotor assembly of the ORG. The steering of the rotor adds an angular input to the reference beam. The angular steering of the reference beam is detected by the Quad in the FSM loop, thus commanding the FSM to null the target beam error seen at the receiver and at the photopot. Therefore, the FSM is used to remove the jitter in the stabilization loop as well as to provide tracking in the pointing stabilization configuration.

The continued tracking of a moving target beam will cause the FSM to "windup" as it holds the target beam aligned on the photopot. The Kaman error signal, from the Kaman sensors on the mirror, is proportional to how far the mirror has moved in a given direction. This signal through the platform controller, S(s), drives the satellite in a closed loop fashion nulling the Kaman error signal, thus preventing the mirror from hitting its mechanical stops.

In order to test the principles outlined by the system concept, a test-bed configuration was implemented as shown in Figure 2.1-2.

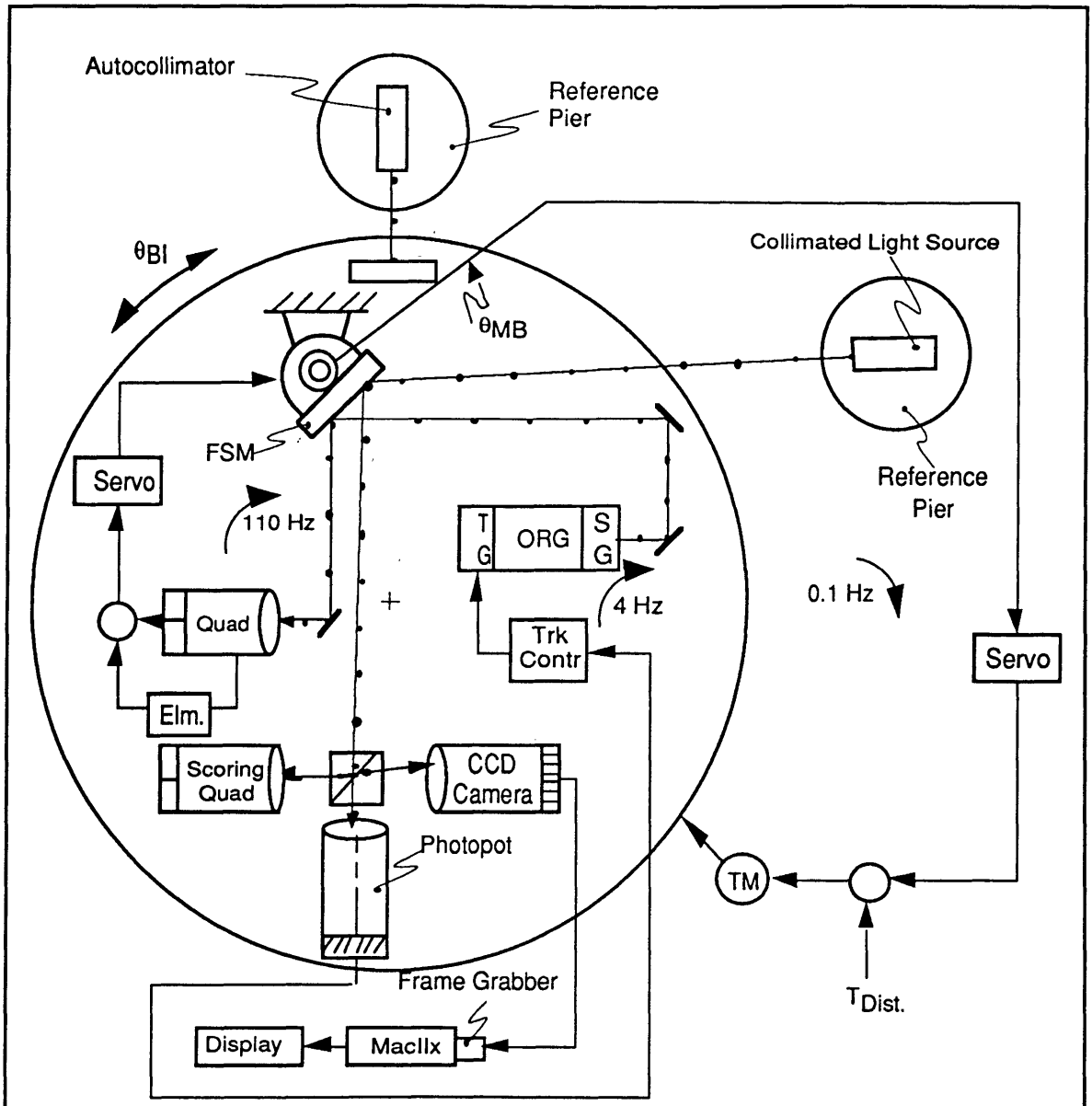

Figure 2.1-2: Pointing Stabilization Test Bed Configuration

The ORG provides the inertially stable reference beam which is directed off the FSM into the Quad. The reference beam from the ORG has a large noise characteristic at the spin speed of 90Hz. The Eliminator (Elm.) conditions the reference beam detector error from the Quad to remove the 90Hz characteristic. The conditioned signal

from the Quad is sent to the Servo controller (abbreviated G(s)). The Servo controller is the FSM controller. In turn, the FSM controller commands the FSM to null the reference beam detector error, thus removing the jitter from the reference beam as well as from the target beam. The bandwidth of the FSM loop was designed to be 110Hz (See Section 4.6 for 110Hz compensator design). The target beam is shown as the Collimated Light Source which originates from an inertially stable platform fixed to the Reference Pier. The Collimated Light Source is directed off the FSM into the Scoring Quad, the CCD Camera, and the Photopot. The Scoring Quad is used to numerically score the 110Hz stabilization system configuration. The CCD Camera provides a means to visually score both the stabilization configuration and the pointing stabilization system. By viewing the CCD signal through a Frame Grabber to the Macintosh Display, both the stabilization and pointing of the target beam can be viewed. Lastly, the Photopot acts as the Focal Plane (FP) sensor for the tracking loop. The Photopot provides the tracker controller (Trk Contr) with the target beam offset error. The tracker controller is also called the ORG controller. In turn, the tracker controller uses the target beam offset error in a 4 Hz closed loop to steer the ORG rotor. The steering of the ORG rotor steers the reference beam. The change in angle of the reference beam is detected by the Quad in the 110 Hz FSM loop. Thus, the mirror is commanded to remove the platform jitter in the stabilization mode and to track the target beam via the pointing loop.

The Kaman sensors on the FSM provide the Kaman sensor error which is a measurement of the mirror position with respect to the platform. In order to prevent "mirror windup", which is caused by tracking a moving target, the Kaman sensor error is used, via the platform controller, to drive the platform. A .1 Hz platform loop is used to "unwind" the FSM.

An autocollimator is used as an independent measurer of platform position. The autocollimator is fixed to an independent reference pier.

Chapter 3: Analytical Modeling

Section 3.1: Analytical System Model

An analytic block diagram of the system test setup shown in Figure 2.1-2 was constructed as shown in Figure 3.1-1.

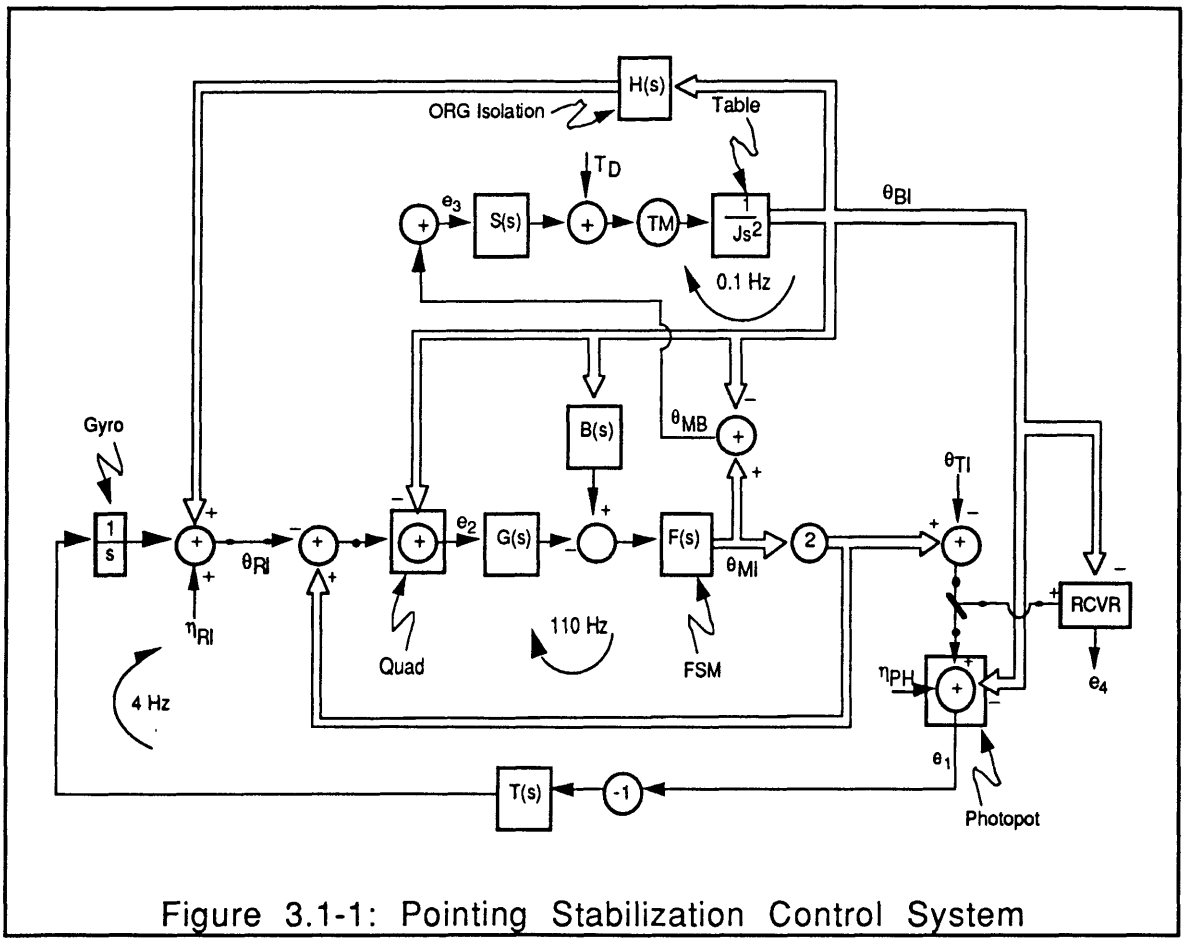

Figure 3.1-1: Pointing Stabilization Control System

The block diagram in Figure 3.1-1 was analyzed in both the frequency and time domain. In Figure 3.1-1, the signal flows are shown as well as the transfer function blocks.

Section 3.2: Variable Description

In the figure, Θ_{TI} corresponds to the angle of the target beam, Θ_{MI} is the FSM mirror angle with respect to the inertial reference frame, Θ_{MB} is the FSM angle with respect to the platform, and Θ_{BI} is the base motion disturbance angular input (injected by the test table as T_D). The torque motor constant for the test platform is abbreviated TM, S(s) is the platform compensator transfer function and J is its inertial constant. The error signals are as follows: e1 is the target beam error detected by the photopot, e2 is the reference beam error detected by the Quad, e3 is the Kaman signal from the FSM and is equivalent to Θ_{MB}, and e4 is the target beam error detected by the receiver. The abbreviations F(s) and G(s) are the FSM plant and FSM compensator transfer functions, respectively. The abbreviation B(s) is the equivalent base motion coupling into the FSM and T(s) represents the pointing servo compensator transfer function.

The reference beam detector error, e2, is composed of two terms: the beam noise Θ_{BI} and the ORG residual base motion coupling error H(s). In Figure 3.1-1, H(s) is the ORG Isolation. The ORG isolation transfer function was measured to be a pure gain of -32 dB as shown in Figure 4.2-4.

The system's stabilization performance is evaluated as the receiver residual jitter error, e_4, in Figure 3.1-1. The signal e4 and e1 measure the same signal except that e4 is corrupted by the Photopot noise. As a comparison, both the equations for e1 and e4 will be derived. There are three main error sources contributing to the receiver jitter error. They are the base motion disturbance Θ_{BI}, the photopot noise η_{PH}, and the ORG sensor noise η_{RI}. The overall system performance for both the stabilization configuration and the pointing-stabilization is computed by deriving the transfer functions relating e4 to the three critical error sources.

Section 3.3: Equations Derivations

In order to derive the expression for e4 we begin with the equations for Θ_{MI}, Θ_{BI}, e1 and e2. They are shown in Equations 3.3-1 through 3.3-4.

$$e1 = -\Theta_{TI} + 2\Theta_{MI} - \Theta_{BI} + \eta_{PH} \quad \text{Eq. 3.3-1}$$

$$e2 = -\Theta_{RI} + 2\Theta_{MI} - \Theta_{BI} \quad \text{Eq. 3.3-2}$$

$$\Theta_{MI} = -F(s)G(s)e2 + F(s)B(s)\Theta_{BI} \quad \text{Eq. 3.3-3}$$

$$\Theta_{RI} = -\frac{T}{s}e1 + H(s)\Theta_{BI} + \eta_{RI} \quad \text{Eq. 3.3-4}$$

Substituting (3.3-3) into (3.3-2) yields:

$$e2 = -\left(\frac{1}{1+2F(s)G(s)}\right)\Theta_{RI} + \left(\frac{2F(s)B(s)-1}{1+F(s)G(s)}\right)\Theta_{BI} \quad \text{Eq. 3.3-5}$$

Subtracting (3.3-2) from (3.3-1) gives:

$$e1 = e2 - \Theta_{TI} + \Theta_{RI} + \eta_{PH} \quad \text{Eq. 3.3-6}$$

and substituting (3.3-5) into (3.3-6) yields:

$$e1 = -\left(\frac{2F(s)G(s)}{1+2F(s)G(s)}\right)\Theta_{RI} + \left(\frac{2F(s)B(s)-1}{1+F(s)G(s)}\right)\Theta_{BI} - \Theta_{TI} + \eta_{PH} \quad \text{Eq. 3.3-7}$$

Substituting 3.3-4 into 3.3-7 yields the expression 3.3-8 which shows e1 as a function of the target angle Θ_{TI}, the table disturbance Θ_{BI}, the gyro noise η_{RI}, and the photopot noise η_{PH}.

$$e1 = \frac{1}{\Delta(s)}\left(\left(\frac{2F(s)B(s)-1}{1+2F(s)G(s)} + \frac{2H(s)F(s)G(s)}{1+2F(s)G(s)}\right)\Theta_{BI} + \left(\frac{2F(s)G(s)}{1+2F(s)G(s)}\right)\eta_{RI} - \Theta_{TI} + \eta_{PH}\right) \quad \text{Eq. 3.3-8}$$

where $\Delta(s)$ is expressed in equation 3.3-9

$$\Delta(s) = \left(1 + \frac{T(s)}{s}\frac{2F(s)G(s)}{1+2F(s)G(s)}\right) \quad \text{Eq. 3.3-9}$$

The relation of e4 to e1 is shown by Equation 3.3-10:

$$e4 = e1 - \eta_{PH} \quad \text{Eq. 3.3-10}$$

Thus, the relation of e4 to the target angle Θ_{TI}, the table disturbance Θ_{BI}, the gyro noise η_{RI}, and the photopot noise η_{PH}. is shown by equation 3.3-11.

$$e4 = \frac{1}{\Delta(s)}\left(\left(\frac{2F(s)B(s)-1}{1+2F(s)G(s)} + \frac{2H(s)F(s)G(s)}{1+2F(s)G(s)}\right)\Theta_{BI} + \left(\frac{2F(s)G(s)}{1+2F(s)G(s)}\right)\eta_{RI} - \Theta_{TI} + \eta_{PH}\right) - \eta_{PH}$$

Eq. 3.3-11

It is important to note that equations 3.3-8 and 3.3-11 are identical with the exception of the η_{PH} term. The individual terms of equations 3.3-8 and 3.3-11 can be isolated in order to understand their contributions to the overall transfer functions.

The term of Equations 8 and 11 respectively relating e1 and e4 to the platform disturbance, Θ_{BI}, is shown by equations 3.3-12 and 3.3-13.

$$\frac{e1}{\Theta_{BI}} = \left(\frac{1}{\Delta(s)}\left(\frac{2F(s)B(s)-1}{1+2F(s)G(s)} + \frac{2H(s)F(s)G(s)}{1+2F(s)G(s)}\right)\right) \quad \text{Eq. 3.3-12}$$

$$\frac{e4}{\Theta_{BI}} = \left(\frac{1}{\Delta(s)} \left(\frac{2F(s)B(s)-1}{1+2F(s)G(s)} + \frac{2H(s)F(s)G(s)}{1+2F(s)G(s)} \right) \right) \quad \text{Eq. 3.3-13}$$

The first term of Eq. 3.3-12 and Eq. 3.3-13, with the B(s), is the error coupling term between the platform and the FSM. This is representative of a sensitivity transfer function. The second term, with the H(s), is a result of the ORG isolation. If the ORG has no coupling between the case and the rotor then H(s) would equal zero and the second term would not exist. From the test data, the ORG isolation was -32dB. This value is a lower bound of the disturbance isolation.

The term of Equations 3.3-8 and 3.3-11 respectively relating e1 and e4 to the gyro noise , η_{RI}, is shown by equations 3.3-14 and 3.3-15.

$$\frac{e1}{\eta_{RI}} = \left(\frac{1}{\Delta(s)} \left(\frac{2F(s)G(s)}{1+2F(s)G(s)} \right) \right) \quad \text{Eq. 3.3-14}$$

$$\frac{e4}{\eta_{RI}} = \left(\frac{1}{\Delta(s)} \left(\frac{2F(s)G(s)}{1+2F(s)G(s)} \right) \right) \quad \text{Eq. 3.3-15}$$

The term of Equations 3.3-8 and 3.3-11 respectively relating e1 and e4 to the gyro noise , η_{PH}, is shown by equations 3.3-16 and 3.3-17

$$\frac{e1}{\eta_{PH}} = \frac{1}{\Delta(s)} \quad \text{Eq. 3.3-16}$$

$$\frac{e4}{\eta_{PH}} = \frac{1}{\Delta(s)} - 1 \quad \text{Eq. 3.3-17}$$

For analytical purposes the stabilization configuration is shown by the above equations with T(s)=0. The pointing-stabilization configuration analysis uses T(s) as the ORG controller as described in Section 4.7.

Using the derived transfer functions, frequency and time based simulations were constructed in the Matlab environment. The frequency analysis code was constructed using the derived transfer function equations. The Power Spectrum Densities (PSDs) were found using the derived transfer functions and known disturbance spectrums detailed in Section 5.3. The code for the frequency and time analysis is shown in Appendix A. The code for the PSDs is shown in Appendix B. The time based simulations were carried out using the derived transfer function equations in addition to the object oriented software package called Simulink. The results of the frequency and time based analysis are shown in Chapter 5.

Chapter 4: Testbed Assembly and Component Characterization

Section 4.1 Hardware Setup

Following the completion of the analysis and simulation, the system shown in Figure 3.1-1 was implemented as a hardware test facility. The hardware was used as a more realistic measure of the system capabilities as well as being a validation of the analytical results. A photograph of the hardware assembly is shown in Figure 4.1-1. Following the photograph of the test setup, the instruments utilized are described in detail.

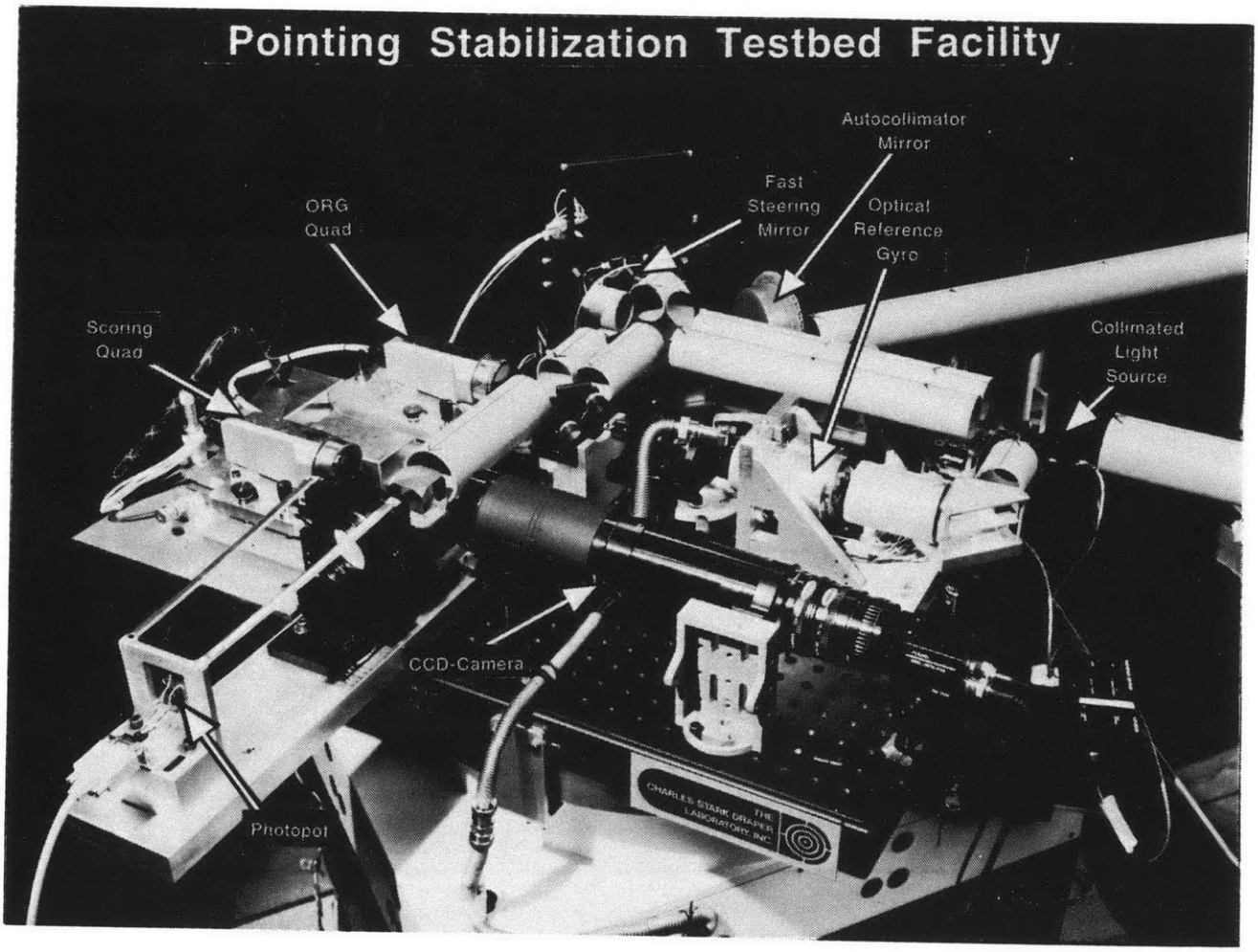

Figure 4.1-1: Hardware Testbed Photograph

Section 4.2: Optical Reference Gyroscope (ORG)

The ORG is essentially a conventional, two-degree-of-freedom dynamically tuned gyro (DTG) with a laser light source providing a collimated inertially stabilized reference beam. A cross-section of the ORG is shown in Figure 4.2-1.

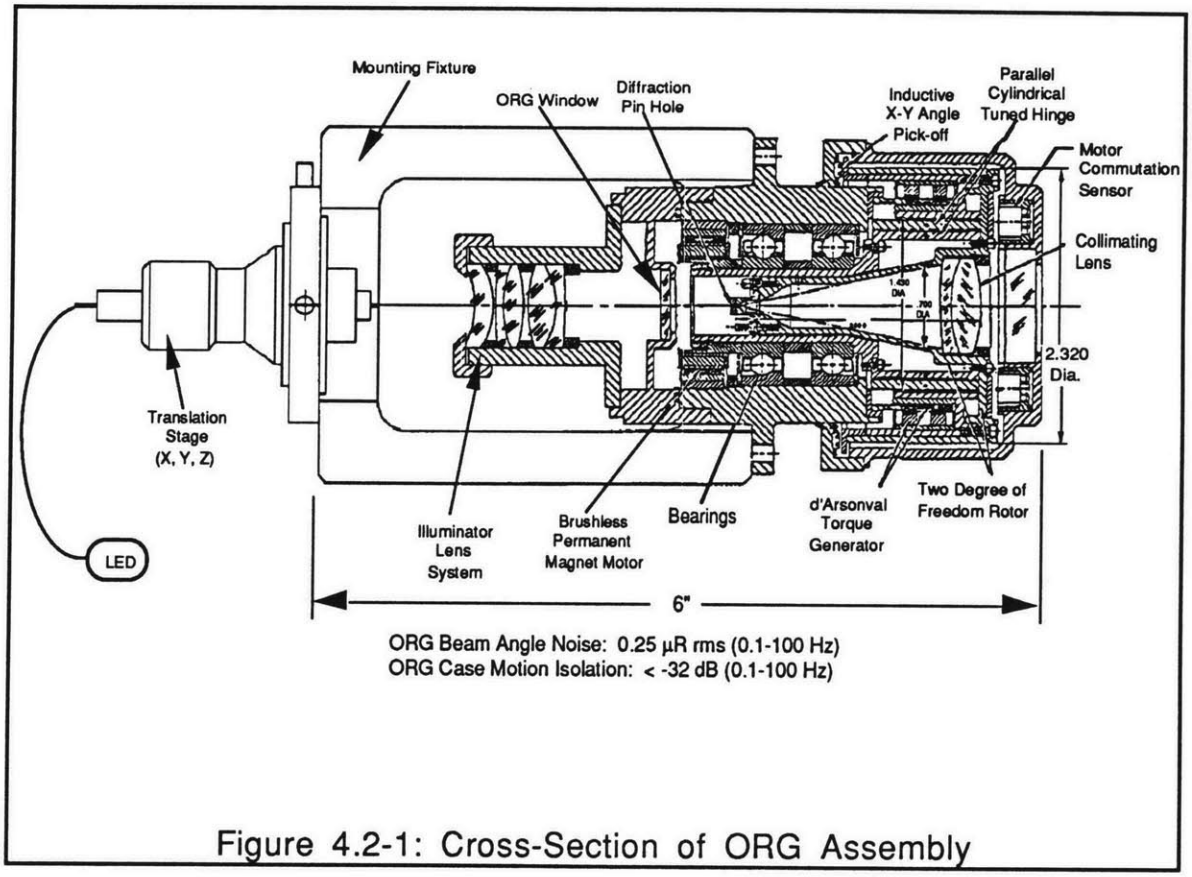

Figure 4.2-1: Cross-Section of ORG Assembly

The ORG rotor is supported on the gyro spin shaft through a double gimbaled cylindrical hinge. At the designed spin speed the rotor is said to be "tuned". This means that the rotor is an inertially spinning body decoupled from the motions of the case. The ORG used in the hardware implementation will be called the prototype ORG and the new ORG under development will be called the enhanced ORG. The tuned spin rate of the prototype ORG is 89.5 Hz.

The Optics assembly of the prototype ORG is shown in Figure 4.2-2.

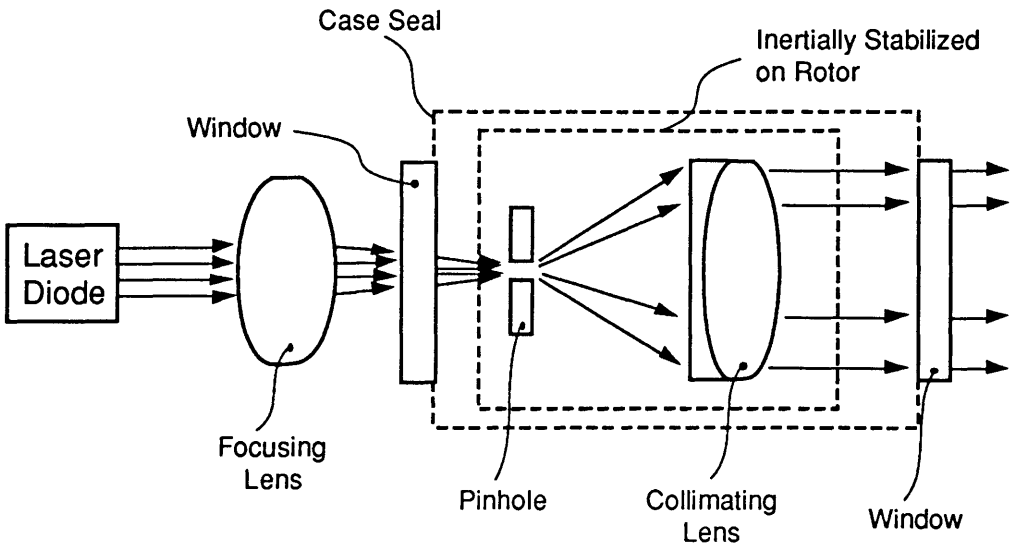

Figure 4.2-2: Optical Reference Gyro Optics Schematic

The laser light source is fixed to the platform and aligned to emit the optical beam along the gyro rotor spin axis. The reference beam from the light source is diffracted as it passes through the pinhole. From the pinhole it passes through a large collimating lens. The collimated output serves as the reference beam for the 110 Hz FSM loop. The optics design of the ORG decouples the reference beam from its source on the platform and effectively places the source on the rotor. The source is effectively on the rotor because the pinhole is as small as the diffraction limited spot size of the output lens.

The ORG has a permanent magnetic torque generator (TG) and an inductive, electromagnetic signal generator (SG) for rotor torquing and angle measurement. A permanent magnet motor provides the gyro spin axis drive. The drive shaft is supported on a high reliability, low noise spin axis bearing to minimize spin axis runout and rotor angle noise.

The prototype ORG was built at The Charles Stark Draper Laboratory in 1981 with Army and internal IR&D funding. In 1989, with IR&D funding, the prototype ORG was refurbished with a fiber-coupled light source and improved electronics.

The key measurement of the ORG is how well the rotor is isolated from the case motion. The ORG isolation is directly measured as a transfer function from the ORG case motion to the reference beam jitter output. The test setup used to measure the ORG isolation is shown in Figure 4.2-3

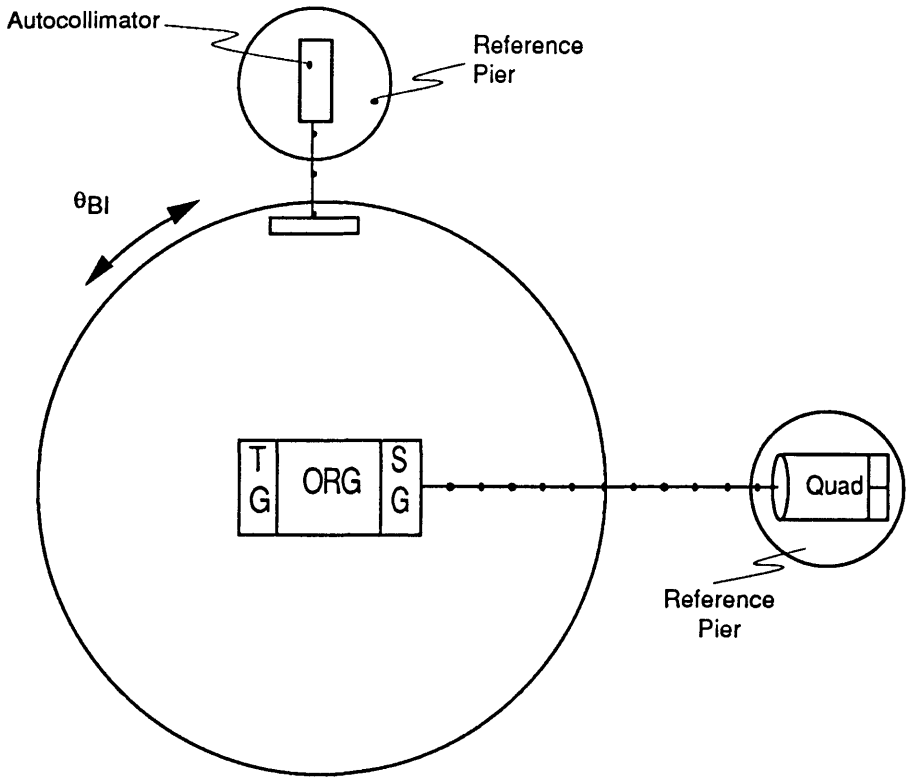

Figure 4.2-3: ORG Isolation Test Setup

Figure 4.2-4 shows that the prototype ORG provides a base motion isolation capability of -32 dB over a measured frequency range of 0.1 - 100 Hz.

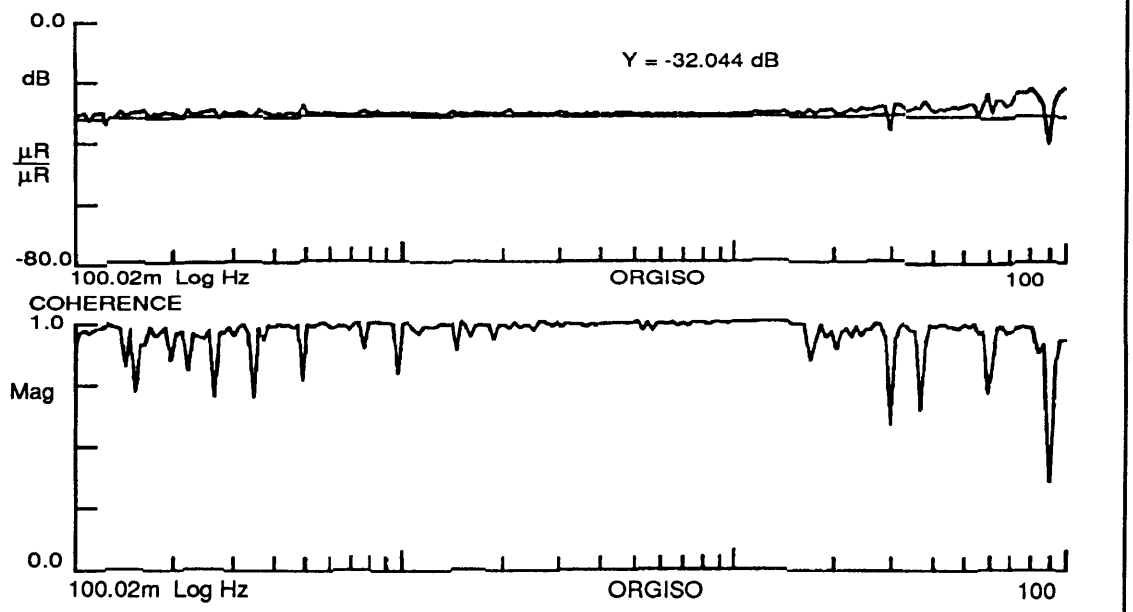

Figure 4.2-4: ORG Beam Isolation Measurement

Because the reference beam was not perfectly collimated, the reference beam isolation is not only a function of the gyro dynamic mistuning effect, but it is also a function of translation motion coupling. A perfectly collimated beam will demonstrate no translation effects when measured by an angle sensor.

The measured performance of the prototype ORG is summarized in Table 4.2-1.

Angle noise (optical)	244 nR rms, 0.1-100 Hz
Drift Stability	<0.020 deg/h
Spin speed	89.5 Hz
Rotor/case isolation	-32 dB, 0.1-100 Hz
Slew capability	8 deg/s
G-capacity (@ hinge)	100 g
Motor power	0.8W
Torquer power	2.5W (@ 8 deg/s)
Light source	Fiber-coupled laser diode
Wavelength	670 nm
Optical power out	15 mW
Optical power at source	5 mW
Beam exit diameter	0.25 in filled 0.7 in clear aperture
Pinhole diameter	8 um
Wavefront quality	NA
Beam divergence	NA
Size	2.5 in dia x 6 in length
Weight	28 oz

Table 4.2-1: Prototype ORG Parameters

Section 4.3: The Eliminator

The reference beam acquires the ORG noise characteristic at the rotor spin speed. This noise is successfully nulled with an eliminator circuit. This eliminator uses a phase-locked and automatic gain control loops that create an artificial notch filter at a desired frequency. The narrow notch has almost no phase or gain distortion beyond a ±5 Hz band around the spin speed frequency. In the stabilization configuration and in the pointing stabilization system configuration, the eliminator was used to filter out the 90 Hz discrete in the reference beam detector error. The 90Hz discrete was picked up as the reference beam passed, from the light source, through the optics on the rotor of the ORG.

Figure 4.3-1 illustrates the noise characteristics of the reference beam after it passes through the ORG as detected on the Quad. Two noise power spectra are shown. The top figure shows the beam noise of 10.8 mr rms without the use of the discrete noise eliminator. The bottom figure, with the discrete noise eliminator, shows that the reference beam noise performance is improved to 0.244 mr rms.

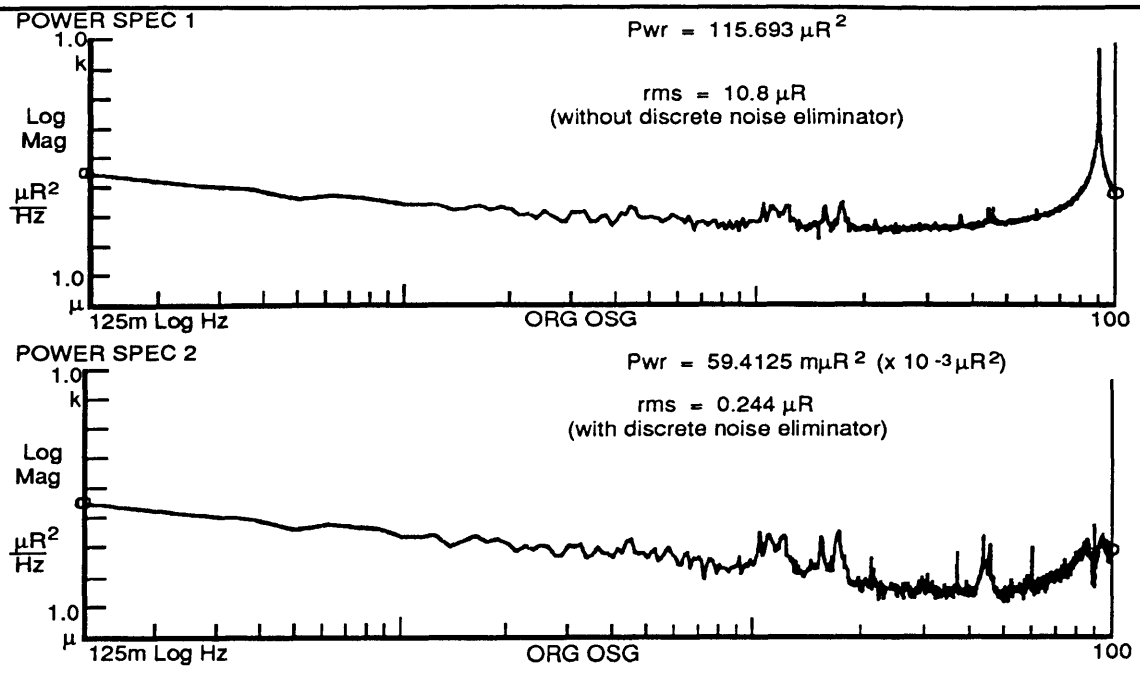

Figure 4.3-1: ORG Beam Noise Measurement With & Without Eliminator

Section 4.4: Fast Steering Mirror (FSM)

The Fast Steering Mirror (FSM) was designed and constructed by the Hughes Aircraft Corporation. It has a 5 inch mirror face with a rms surface roughness of approximately $\frac{\lambda}{10}$. The mirror face is driven by four permanent magnet voice coil accuators. The mirror is mounted on a cross blade fixture as described in [7]. The mirror position is determined via kaman sensors. The hardware tested transfer function of the mirror is shown in Figure 4.6-1. The electronics package for the mirror has the capability to fix the mirror to the case using internal compensation. In addition, the mirror can be driven using external inputs for feedback control.

Using the model described in [5], the lumped dynamics of the FSM are shown in Figure 4.4-1. The input drive signal to the FSM is abbreviated U, F(s) is the FSM plant transfer function and B(s) is the coupling transfer function between the platform and the FSM. The platform angle is Θ_{BI} and Θ_{MI} is the resulting mirror angle with respect to the inertial reference frame.

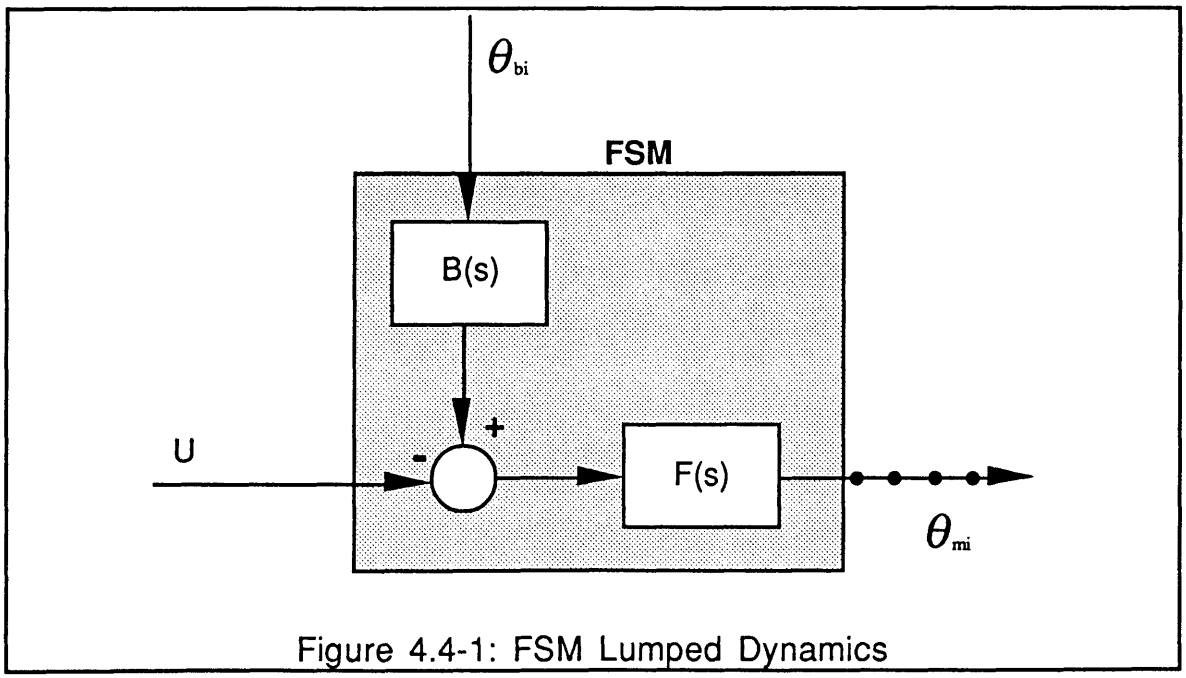

Figure 4.4-1: FSM Lumped Dynamics

Section 4.5: The Photopot

The photopot is a two-dimensional photo-sensing device. The incident light on the photopot generates a current proportional to position. There are four cells used on the detector. After the normalizing electronics an analog x and y position is outputted. The mount used to hold the photopot is shown in Figure 4.5-1.

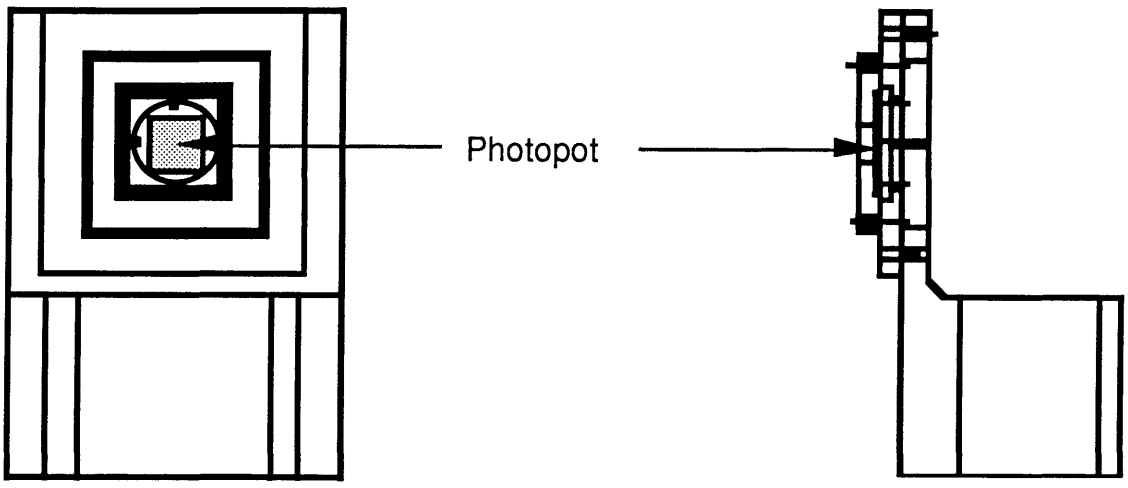

Figure 4.5-1: Photopot Mount Front View and Side View

The photopot was coupled with focusing optics for the hardware implementation. The photopot assembly with the focusing optics is shown in Figure 4.5-2.

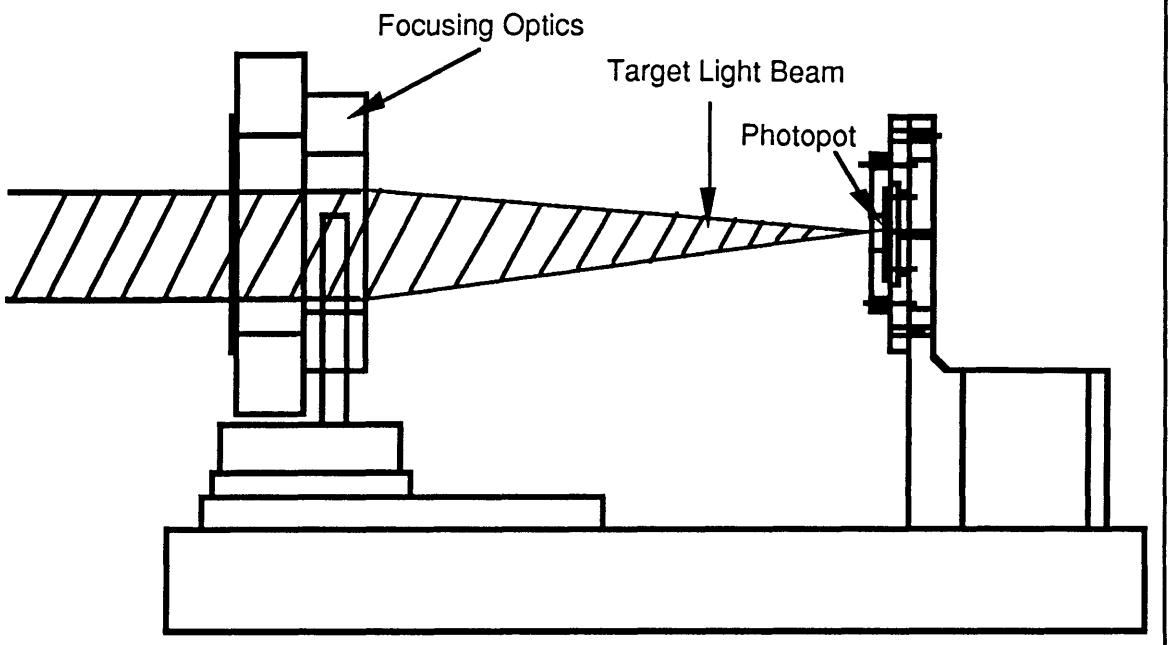

Figure 4.5-2: Focusing Optics and Photopot Hardware Assembly

Table 4.5-1 summarizes the characteristics of the Photopot.

Electrical Noise	.5 uR rms, 0.1-100 Hz
Active Area	2 cm x 2 cm
Noise Current	1.3 nAmps
Capacitance	7 pF
Internal Resistance	10 KOhms
Rise Time	.02 sec.
Non-Linearity	0.3-.8 %

Table 4.5-1: Photopot Parameters

Section 4.6: 110Hz Mirror Controller (G(s))

The 110 Hz FSM loop controller is used to condition the signal from the ORG reference beam detector before it passes to the FSM. The FSM uses the signal from the controller to null out the platform disturbances in both the reference beam and the target beam. The bandwidth of the FSM loop controller was limited by the loss of signal caused by the eliminator at the ORG spin speed of 90 Hz. The 90Hz noise characteristic was acquired by the ORG reference beam as it passed through the optics on the rotor assembly of the ORG. The large noise characteristic was removed from the reference beam signal by the eliminator (see Section 4.3). This loss of information due to the eliminator would cause instability in the loop if the bandwidth was pushed beyond 110 Hz. A higher loop bandwidth is desirable in order to increase the attenuation of base disturbances by the 110 Hz FSM loop. A new ORG is currently being designed with a higher rotor frequency to allow the FSM loop bandwidth to be increased (See Chapter 8).

The components of the FSM loop are the ORG reference beam, the ORG quad detector, the FSM compensator, and the FSM. The FSM is the plant of the system. The analytical FSM dynamics are shown in Figure 4.6-1. The FSM model in Figure 4.6-1 has the transfer function shown by Equation 4.6-1 with a damping ratio=.2408 and a natural frequency of 74.1 rad/sec.

$$\text{Mirror Transfer Function} = \frac{111430}{(s^2 + 17.8571s + 5500)} \qquad \text{Eq. 4.6-1}$$

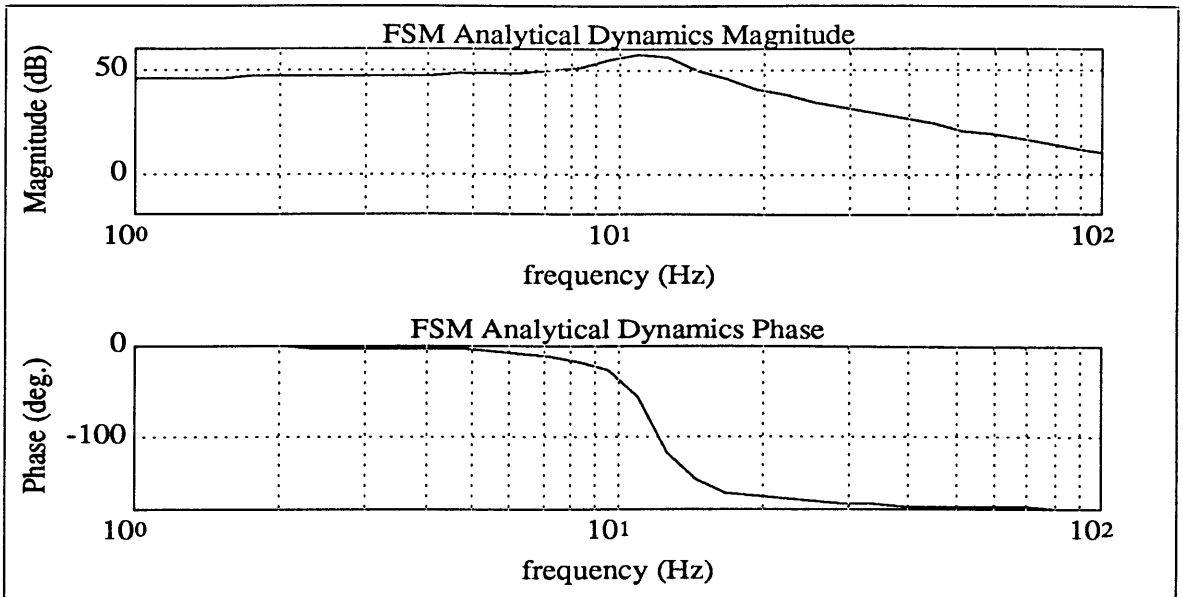

Figure 4.6-1: FSM Analytical Dynamics, Magnitude and Phase

The hardware tested FSM dynamics are shown in Figure 4.6-2.

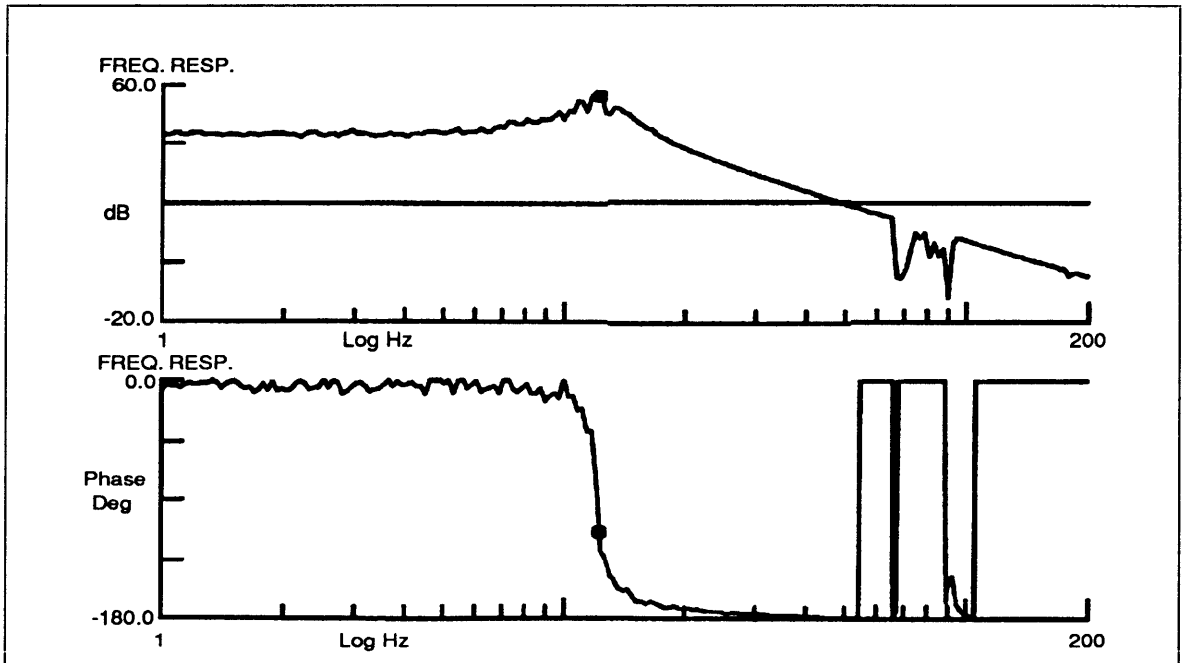

Figure 4.6-2: Hardware FSM Dynamics, Magnitude and Phase

The loss of information from approximately 70-100Hz is the notch effect of the eliminator.

For the original simulations, before the hardware was constructed, a straight PID controller was utilized. It was originally designed using the following parameterization described in greater detail in [5]. The parameterization specifies the compensator values for the PID controller dependent upon the desired open loop cross-over frequency for the loop. The open loop cross-over is denoted ω_{co}. A PID controller has three coefficients, the proportional gain, denoted K_p, the integral gain, denoted K_i and the derivative gain, denoted K_d. The general transfer function for a PID controller is shown by Equation 4.6-2.

$$G(s)=\left(K_p+K_d s+\frac{K_i}{s}\right)=\frac{1}{s}\left(K_i+K_p s+K_d s^2\right) \quad \text{Eq. 4.6-2}$$

Utilizing the open loop crossover parameterization, the PID coefficients can be evaluated according to Equation 4.6-3.

$$K_p=\frac{2}{3}(.7)J\omega_{co}^2$$

$$K_i=J*\frac{\omega_{co}^3}{9} \quad \text{Eq. 4.6-3}$$

$$K_d=J*\omega_{co}$$

The J term is the mass moment of inertia for the plant that the compensator is going to control. For this case J is the mass moment of inertia of the FSM.

Starting with the PID compensator shown by Equation 4.6-2 the hardware FSM compensator was constructed. It was necessary to make alterations to the theoretical compensator model in order to implement the design. The final analog circuit construction is shown in Figure 4.6-3. From the final hardware implementation the simulation was updated.

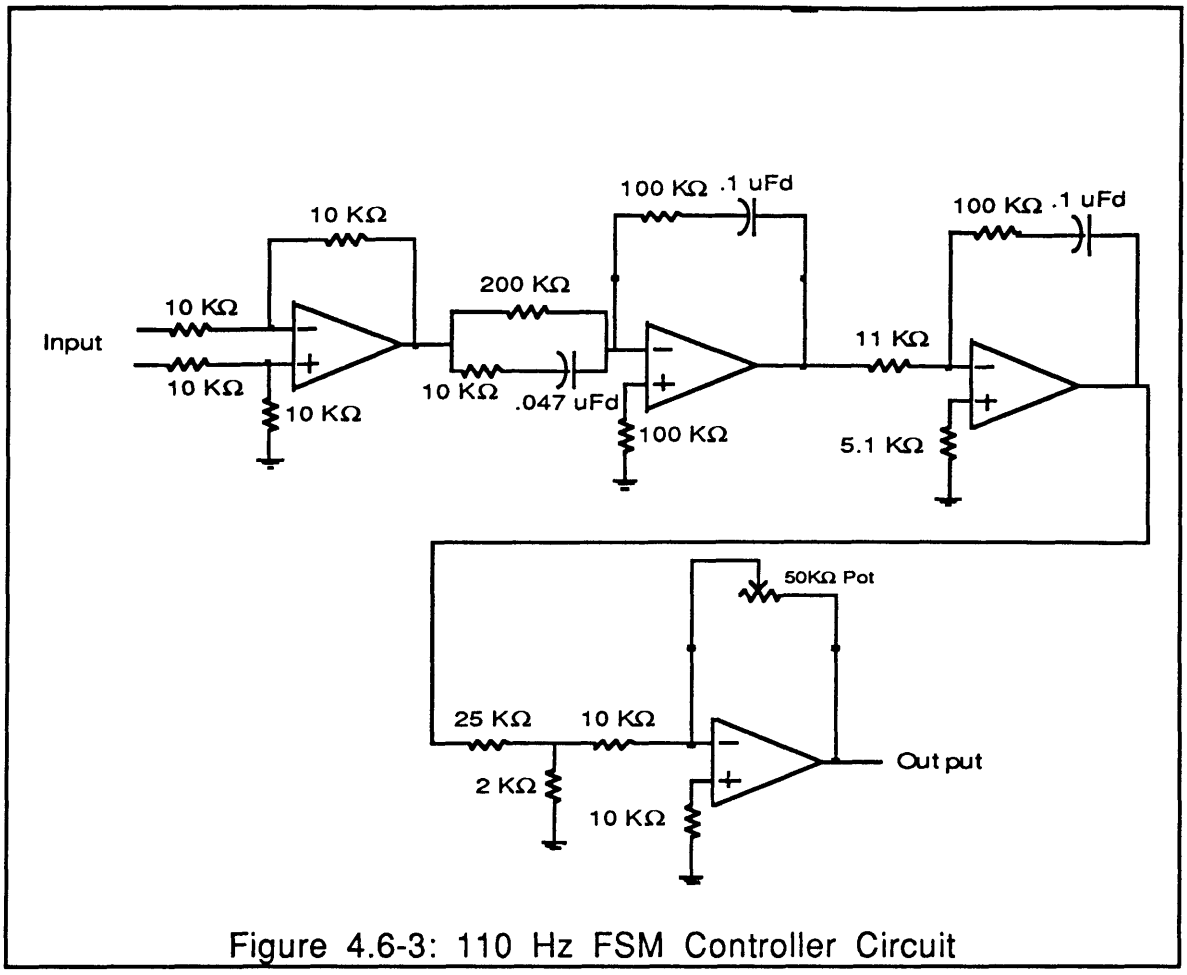

Figure 4.6-3: 110 Hz FSM Controller Circuit

For the hardware implementation, the operational amplifiers were of the make OP07EH. The transfer function in radians for the hardware implemented 110Hz compensator is shown by Equation 4.6-4.

$$G(s) = \left(\frac{10^8}{s^2}\right)\left(\frac{s+101.32}{s+2127.66}\right)\left(\frac{(s+100)^2}{1}\right) \quad \text{Eq. 4.6-4}$$

The simulated FSM compensator transfer function is shown in Figure 4.6-4 and the Hardware tested compensator transfer function is shown in Figure 4.6-5.

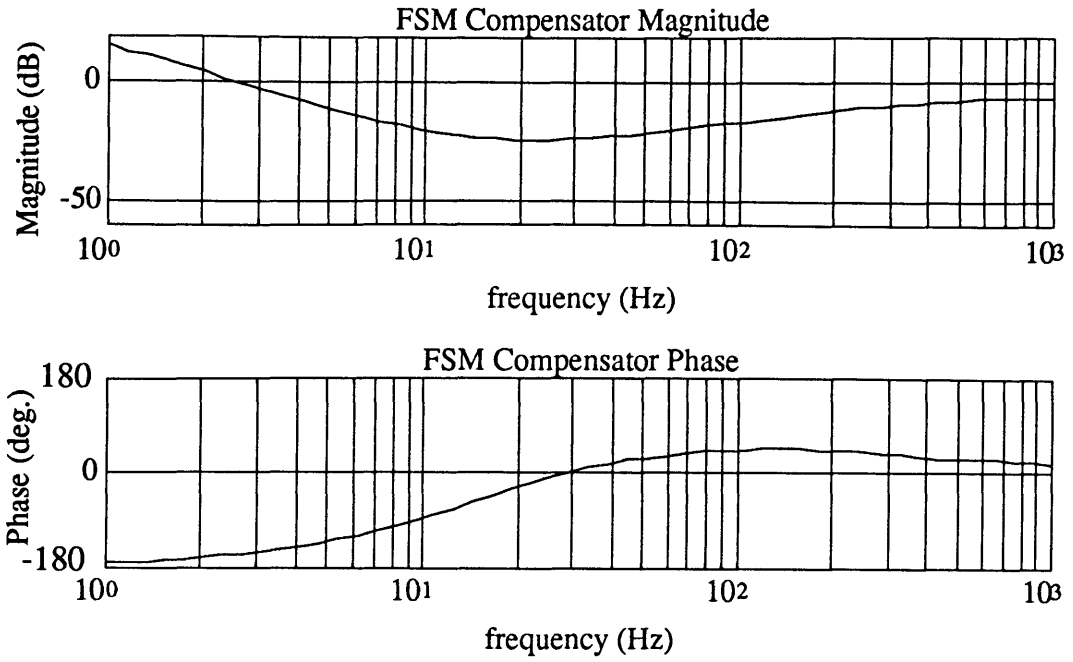

Figure 4.6-4: FSM Compensator Analytical Magnitude and Phase

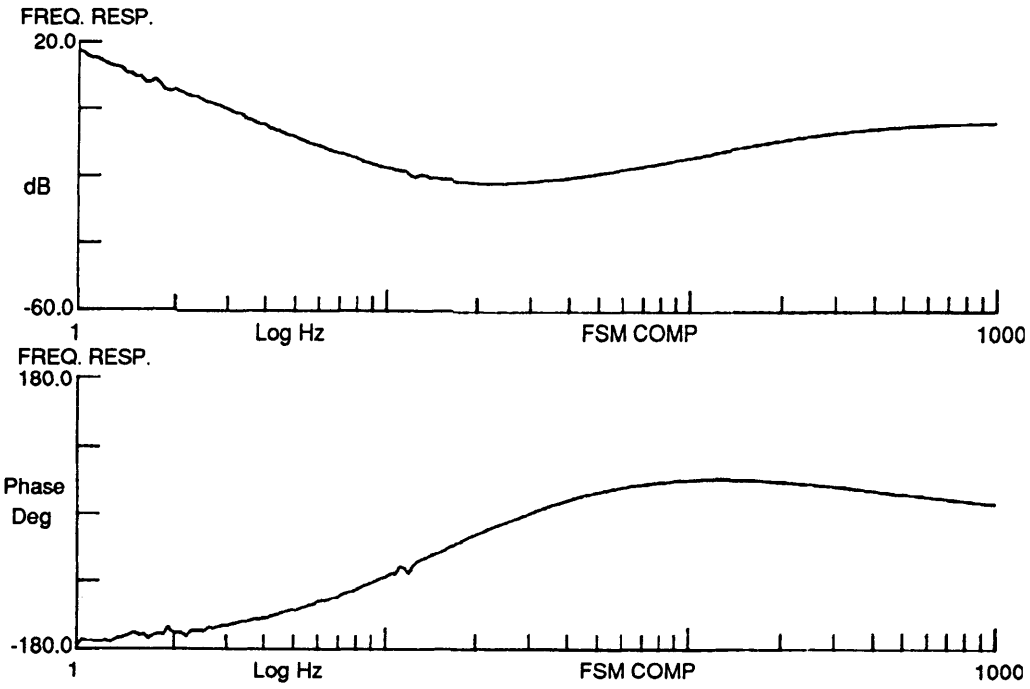

Figure 4.6-5: Hardware FSM Compensator Magnitude and Phase

The FSM loop, open loop transfer functions for the simulation and for the hardware are shown in Figures 4.6-6 and 4.6-7.

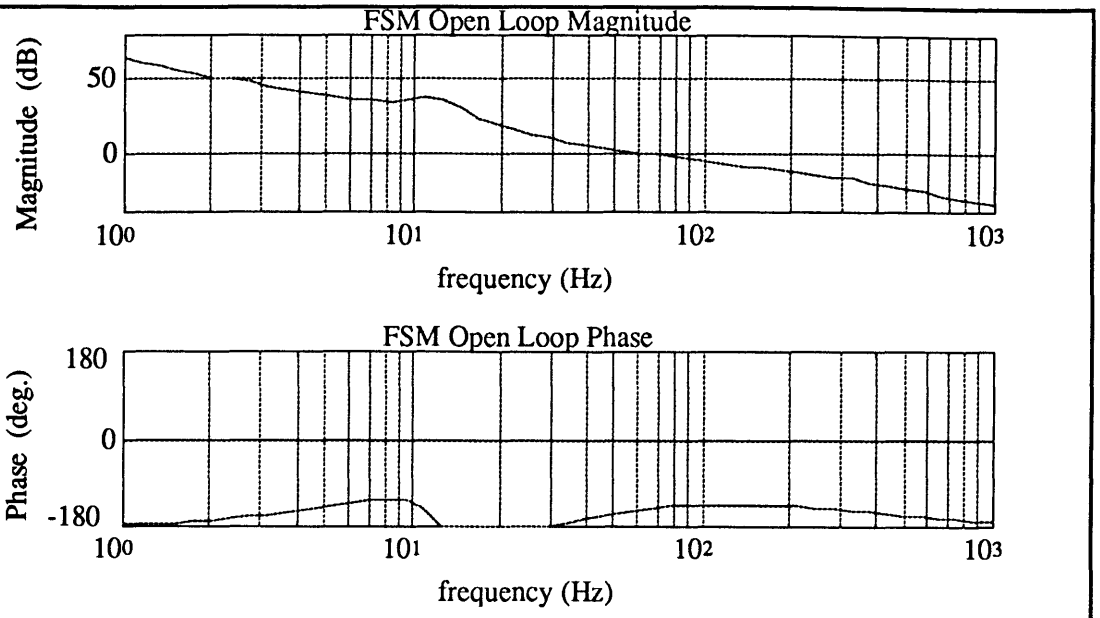

Figure 4.6-6: 110 Hz FSM Loop, Analytical Open Loop Tr. Function

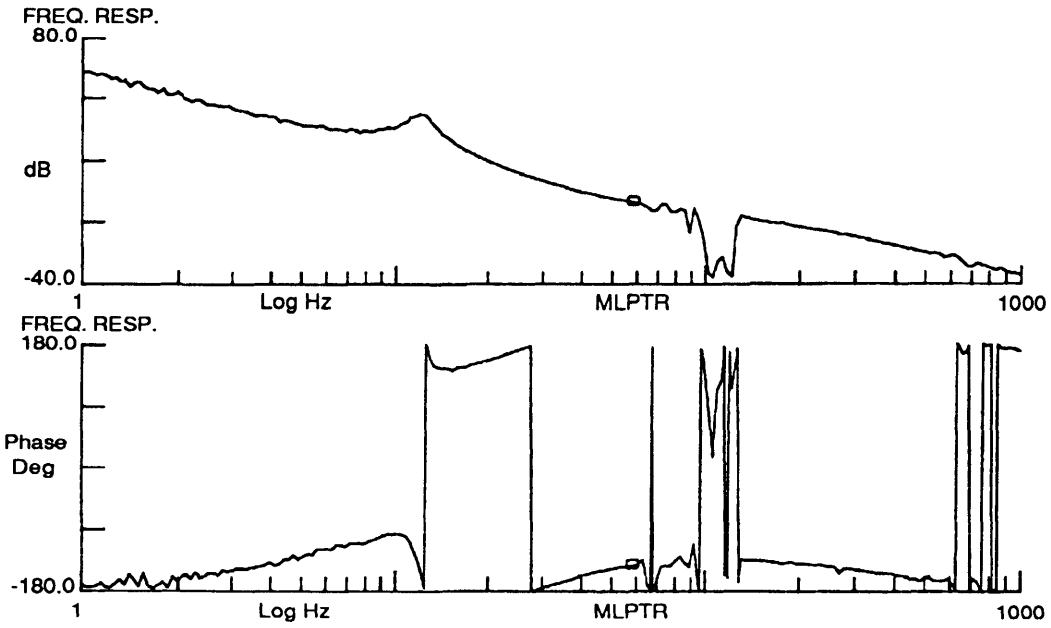

Figure 4.6-7: 110 Hz FSM Loop, Hardware Open Loop Tr. Function

Once again, the loss of information at approximately 100 Hz is due to the eliminator effects. The hardware and analytical open loop transfer functions yielded open loop cross-overs of approximately 60 Hz with phase margins of approximately 37 degrees.

The desired closed loop bandwidth was 110 Hz. The analytical closed loop transfer function is shown in Figure 4.6-8 and the hardware tested closed loop transfer function is shown in Figure 4.6-9.

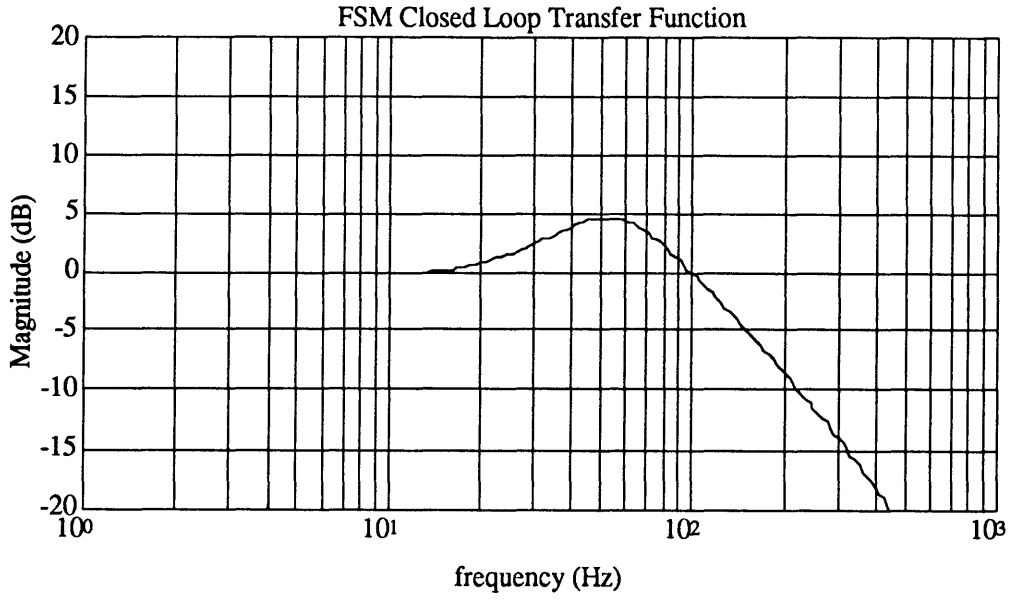

Figure 4.6-8: 110 Hz FSM Loop, Analytical Closed Loop Transfer Function

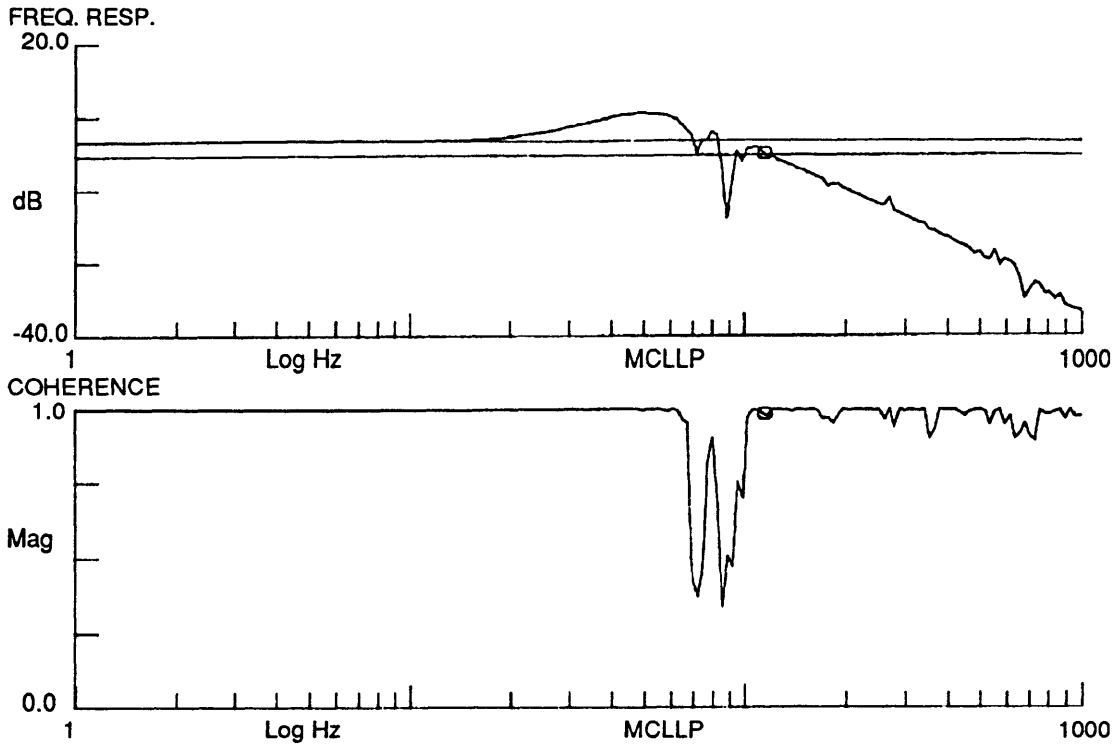

Figure 4.6-9: 110 Hz FSM Loop, Hardware Closed Loop Transfer Function

The loss of information at 90Hz is due to the effect of the eliminator. The closed loop transfer functions shown in Figures 4.6-8 and 4.6-9 provide the base disturbance attenuation for both the stabilization and the pointing stabilization configurations.

Section 4.7: 4Hz Tracker Controller

The 4 Hz ORG loop controller is used to condition the signal from the photopot detector before it passes to the ORG torquer. The photopot detector produces an analog error signal proportional to the offset of the target beam. The ORG torquer uses the signal from the controller to steer the ORG rotor which in turn steers the ORG reference beam. The steering of the ORG reference beam is an angular input which is detected by the ORG quad detector in the FSM loop. The FSM loop nulls the angle detected by the ORG quad detector by adjusting the FSM angle. This adjustment steers the target beam on the photopot nulling the target beam detector error.

The 4 Hz tracker loop consists of the target beam, the photopot, the tracker controller and the ORG. The plant of the loop is the ORG which is a simple integrator. The tracker compensator, T(s), was modeled after the system designed in [2]. For the original simulation, before the hardware construction, a simple proportional-integral controller was chosen with its transfer function shown by equation 4.7-1.

$$\frac{L_1 s + L_2}{s} \quad \text{Eq. 4.7-1}$$

In order to yield a 4 Hz loop the values of L1 and L2 were set to 15 and 400, respectively. For the hardware implementation, an additional pole was added for high frequency roll-off. The simulated tracker compensator transfer function is shown in Figure 4.7-1.

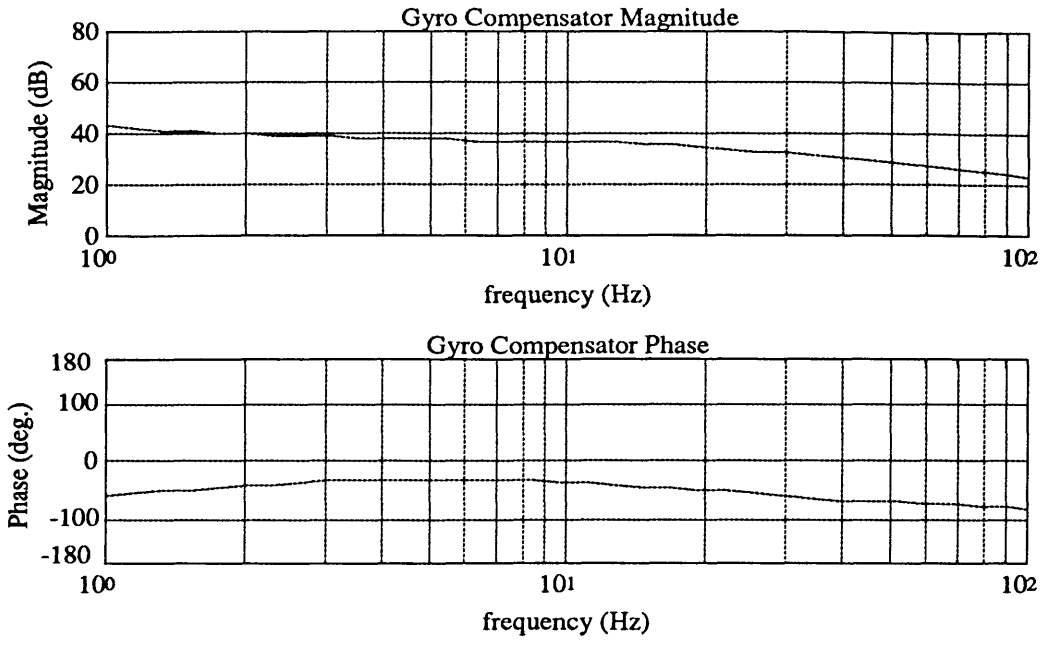

Figure 4.7-1: Simulated 4Hz Gyro Compensator Transfer Function

The hardware tested ORG compensator transfer function is shown in Figure 4.7-2.

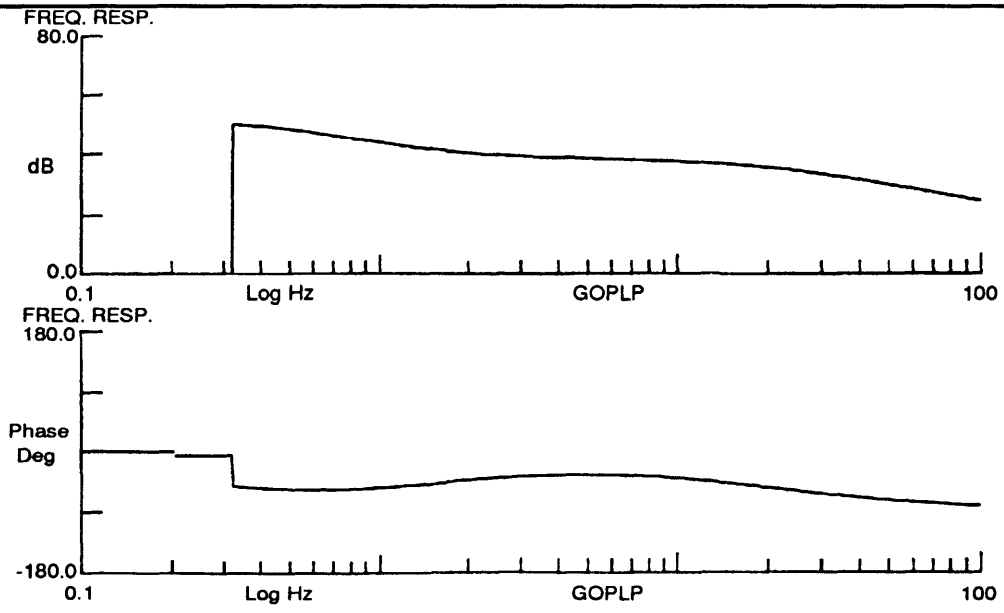

Figure 4.7-2: Hardware 4Hz Gyro Compensator Transfer Function

The analog electronics for the ORG compensator are shown in Figure 4.7-3.

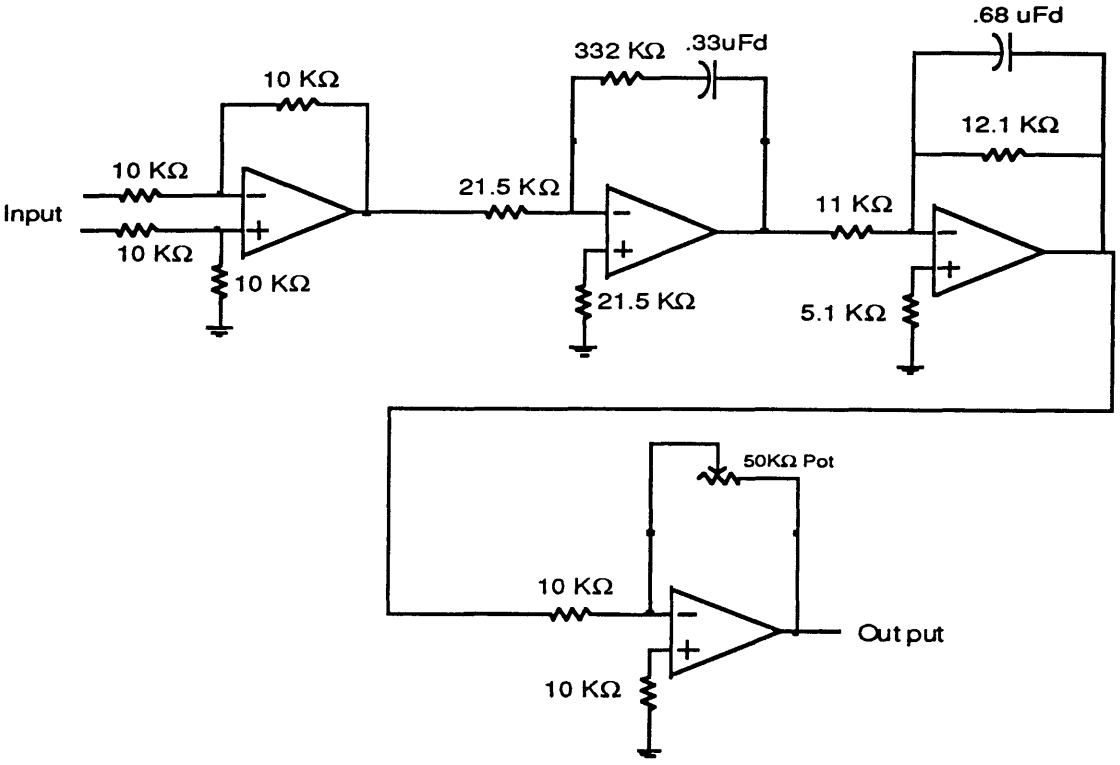

Figure 4.7-3: 4Hz ORG Compensator Analog Electronics

The hardware implemented transfer function in radians is shown in Equation 4.7-2.

$$T(s) = \left(\frac{15.8s + 141}{s}\right)\left(\frac{1}{s + 121}\right) \quad \text{Eq. 4.7-2}$$

The simulated open loop transfer function for the ORG loop is shown in Figure 4.7-4. Both the simulation and the hardware had open loop cross-overs of approximately 2.4 Hz with approximately 59 degrees of phase margin.

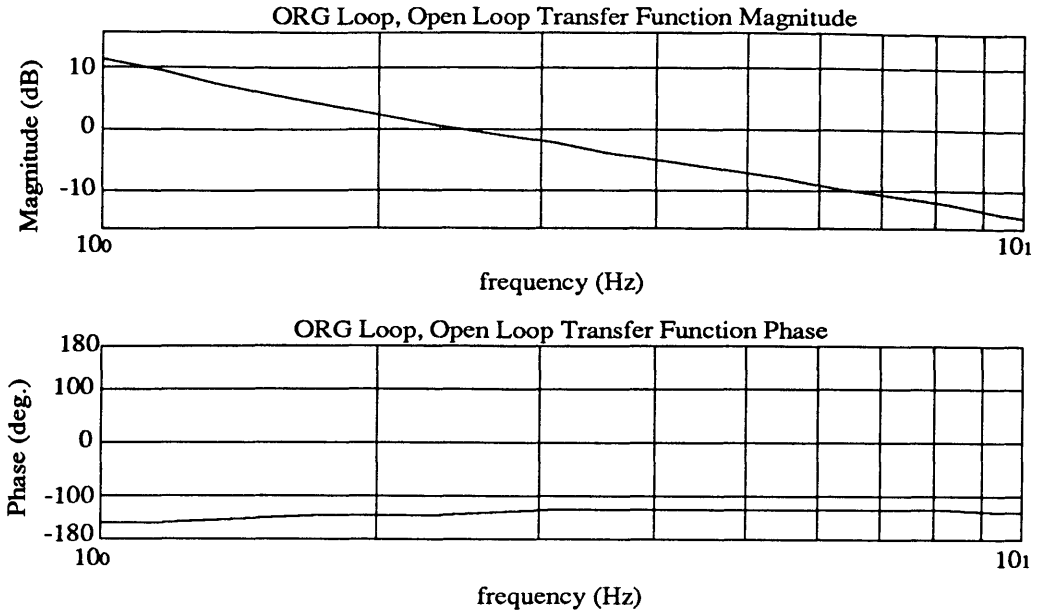

Figure 4.7-4: ORG Loop, Simulated Open Loop Transfer Function

The hardware tested open loop transfer function is shown in Figure 4.7-5.

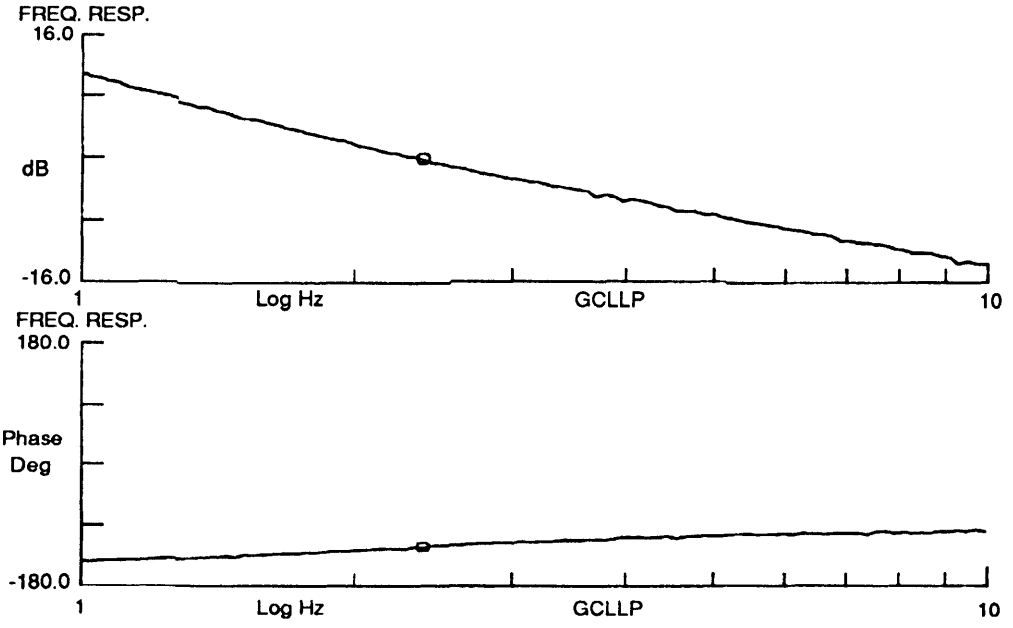

Figure 4.7-5: ORG Loop, Hardware Open Loop Transfer Function

The simulated ORG loop, closed loop transfer function is shown in Figure 4.7-6. Both the simulated and hardware tested ORG loops had closed loop bandwidths of approximately 4 Hz.

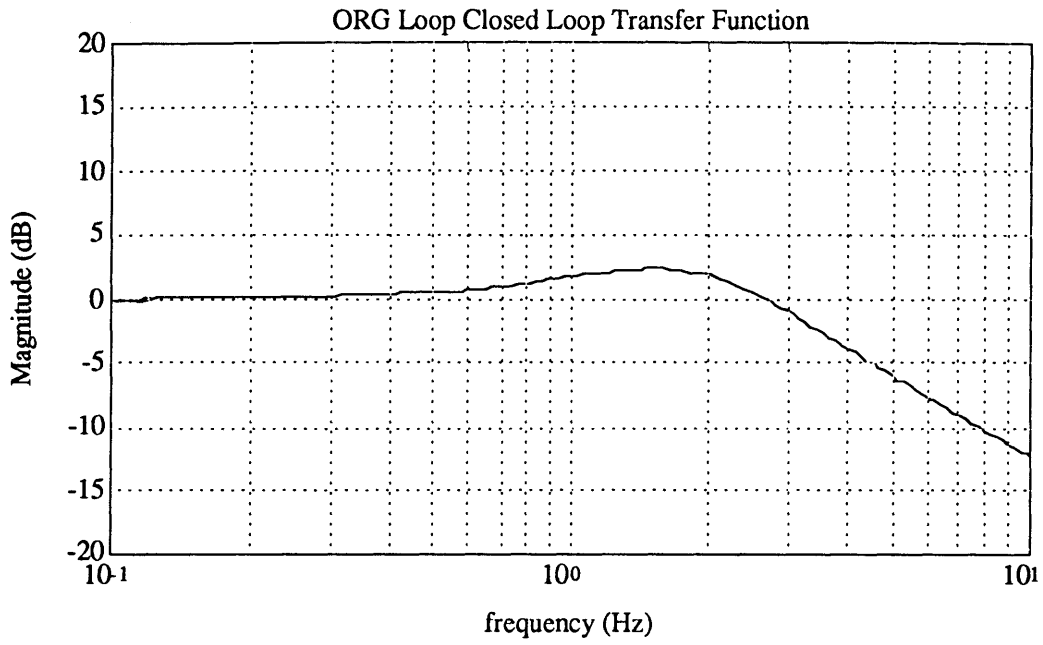

Figure 4.7-6: ORG Loop, Simulated Closed Loop Transfer Function

The hardware tested ORG loop, closed loop transfer function is shown in Figure 4.7-7.

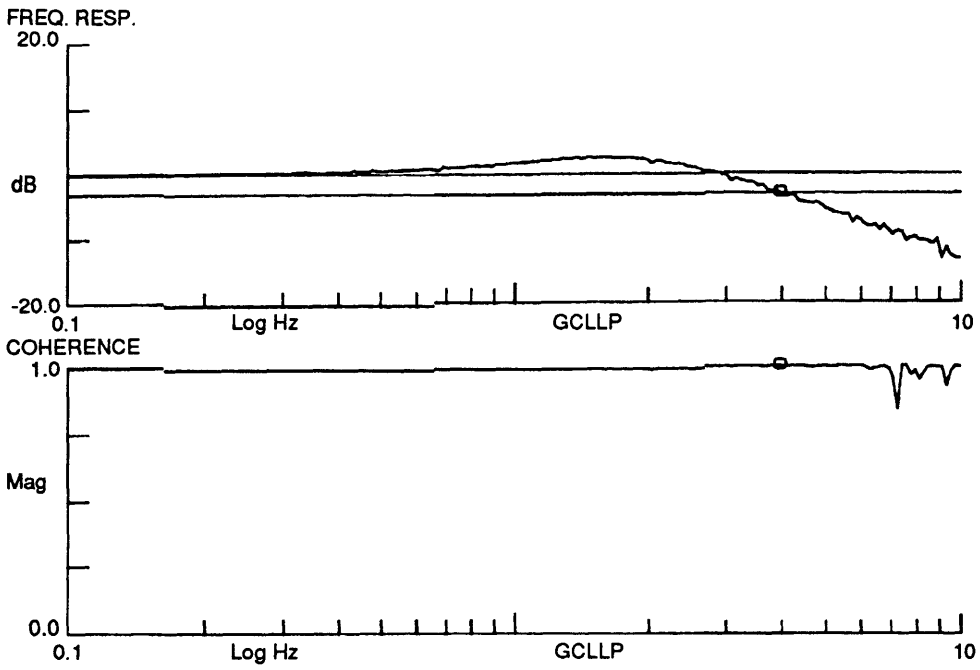

Figure 4.7-7: ORG Loop, Hardware Closed Loop Transfer Function

The closed loop transfer functions shown in Figures 4.7-6 and 4.7-7 were used in conjunction with the 110 Hz FSM Loop to form the pointing stabilization configuration. For the stabilization configuration the ORG loop was opened leaving only the 110Hz FSM loop.

Section 4.8: .1 Hz Platform Controller

As the target beam, Θ_{TI}, progresses in a given direction the ORG loop, driven by the target beam detector error, will continually adjust the mirror angle, Θ_{MI}, to maintain the target beam's alignment on the photopot. The FSM can only travel two degrees from its zero point before its motion is restricted by mechanical stops. Therefore, it is necessary to "unwind" the FSM by driving the platform beneath the FSM. By driving the platform, the target beam maintains its alignment on the photopot and the FSM is moved back to its zero position. The error signal used to drive the platform is from the Kaman sensors of the FSM. The Kaman sensors produce an analog signal proportional to mirror position. If this signal is driven to zero then the mirror will be driven to its null position.

The components of the platform loop are the Kaman sensors on the FSM, the platform compensator and the platform itself. The platform compensator is driven by the analog signal from the Kaman sensors. In turn, the platform compensator drives the platform torque-motor.

The bandwidth of the platform loop is approximately .1 Hz. The bandwidth is low in order to prevent the platform from following the high frequency motions of the FSM from the FSM loop. It is only necessary for the platform loop to follow the low frequency motions of the target beam which are detected by the 4 Hz tracker loop.

The table platform was modeled as a simple inertia. Its transfer function is shown by equation 4.8-1. Jt is the mass moment of inertial of the platform and TMt is gain of the platform torque motor.

$$\frac{TMt}{Jt * s^2} \quad \text{Eq. 4.8-1}$$

The original platform compensator was designed as a simple PID controller using the parameterization described in [6]. It was found to be impossible to implement this design for the following reason. The bandwidth of the closed loop was so low that the signal generated from the compensator was small. This small signal through the platform torque-motor was not enough to overcome the platform stictions from the wires leading from the instruments on the platform.

To overcome these stiction forces, a second compensation loop was designed. The entire platform compensator consisted of a 30Hz position loop that was commanded by a compensator that composed of a single integrator. The integrator was driven by the Kaman sensor signal from the FSM. The compensator for the 30 Hz position loop was a PID controller that was driven by the platform position. The block diagram of the platform loop is shown in Figure 4.8-1.

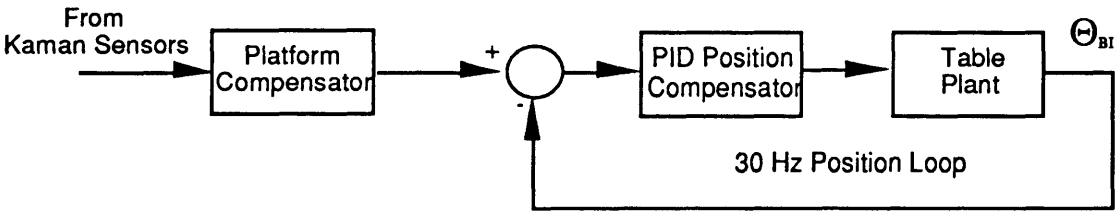

Figure 4.8-1: Platform Loop Block Diagram

In order to close the 30 Hz position loop it was necessary to have an analog signal proportional to the platform position. The analog position signal is the feedback signal in the 30Hz loop. The only output from the platform were digital pulses with one pulse being equivalent to .00001
degrees. It was necessary to convert the pulses from the platform to an analog measurement of table position. A circuit, shown in Figure 4.8-2 was designed to perform this task.

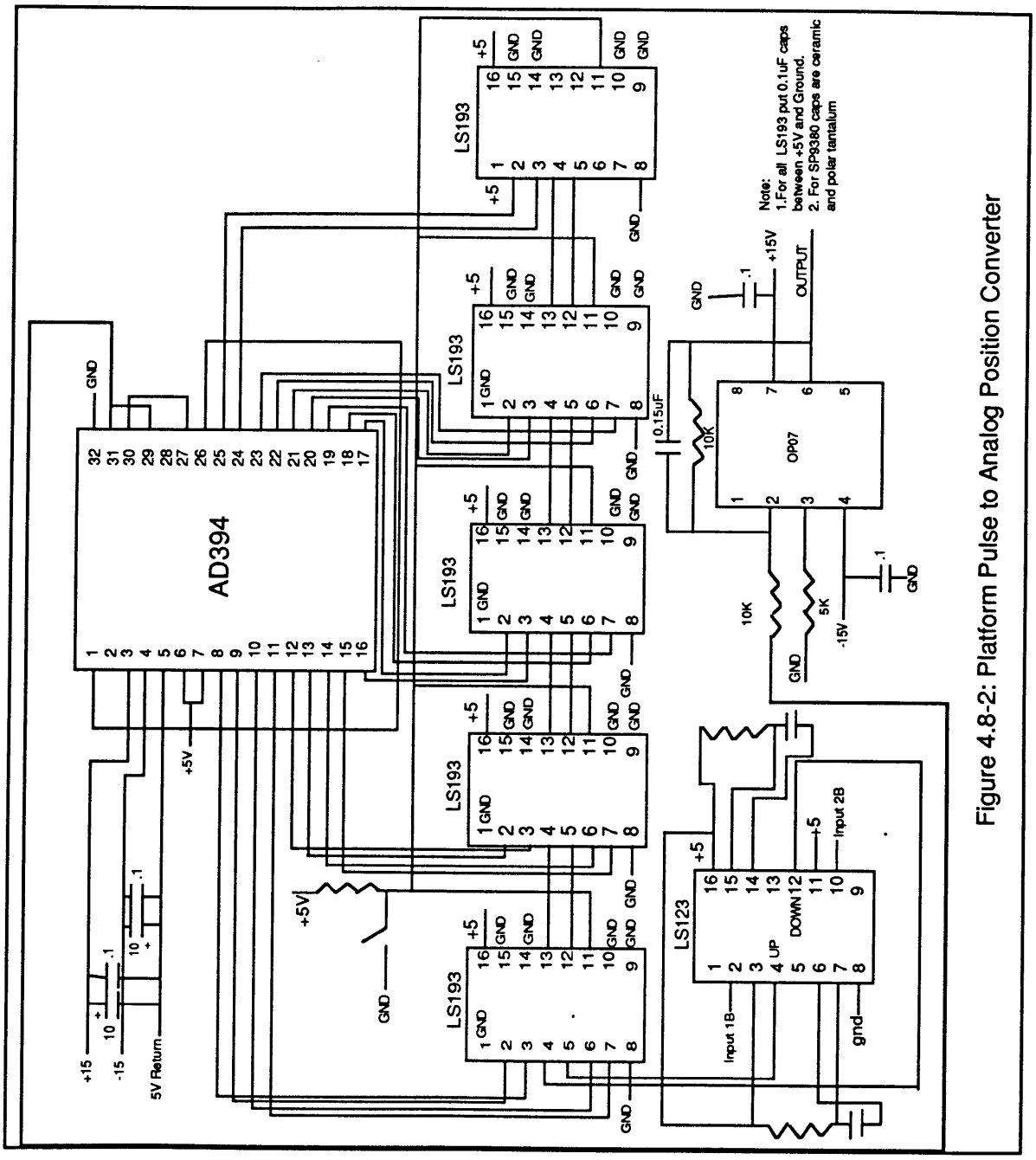

Figure 4.8-2: Platform Pulse to Analog Position Converter

The 30 Hz position compensator was PID design with an additional pole for high frequency roll-off. The transfer function for the controller is shown by equation 4.8-2.

$$\frac{s^2+32s+157.8}{s(s+6000)} \quad \text{Eq. 4.8-2}$$

The hardware implementation of the 30Hz PID position compensator was done using a state variable filter instead of operational amplifiers in series. The hardware implementation is shown in Figure 4.8-3.

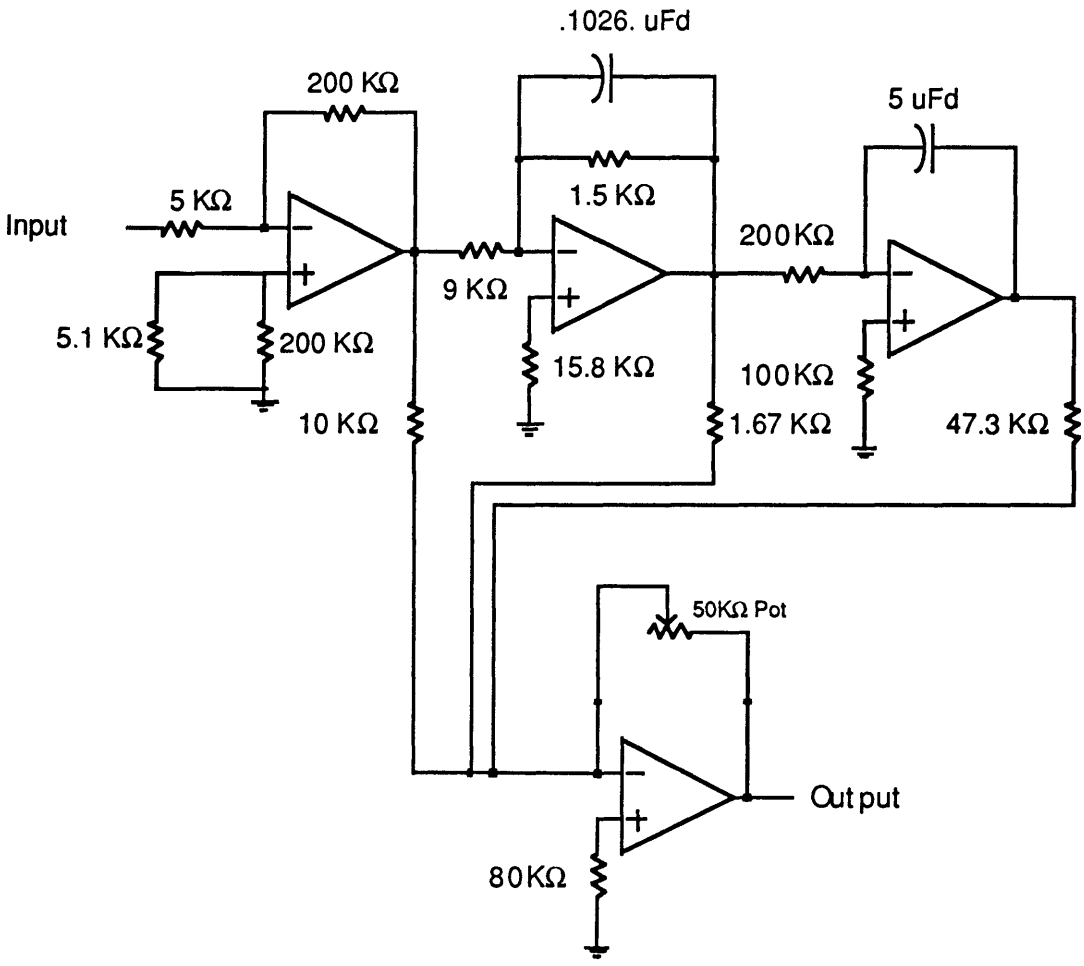

Figure 4.8-3: 30Hz PID Position Compensator

The 30 Hz position loop was driven by the signal from the Kaman sensors through the platform compensator. The platform compensator was simply an integrator and the hardware implementation is shown in Figure 4.8-4.

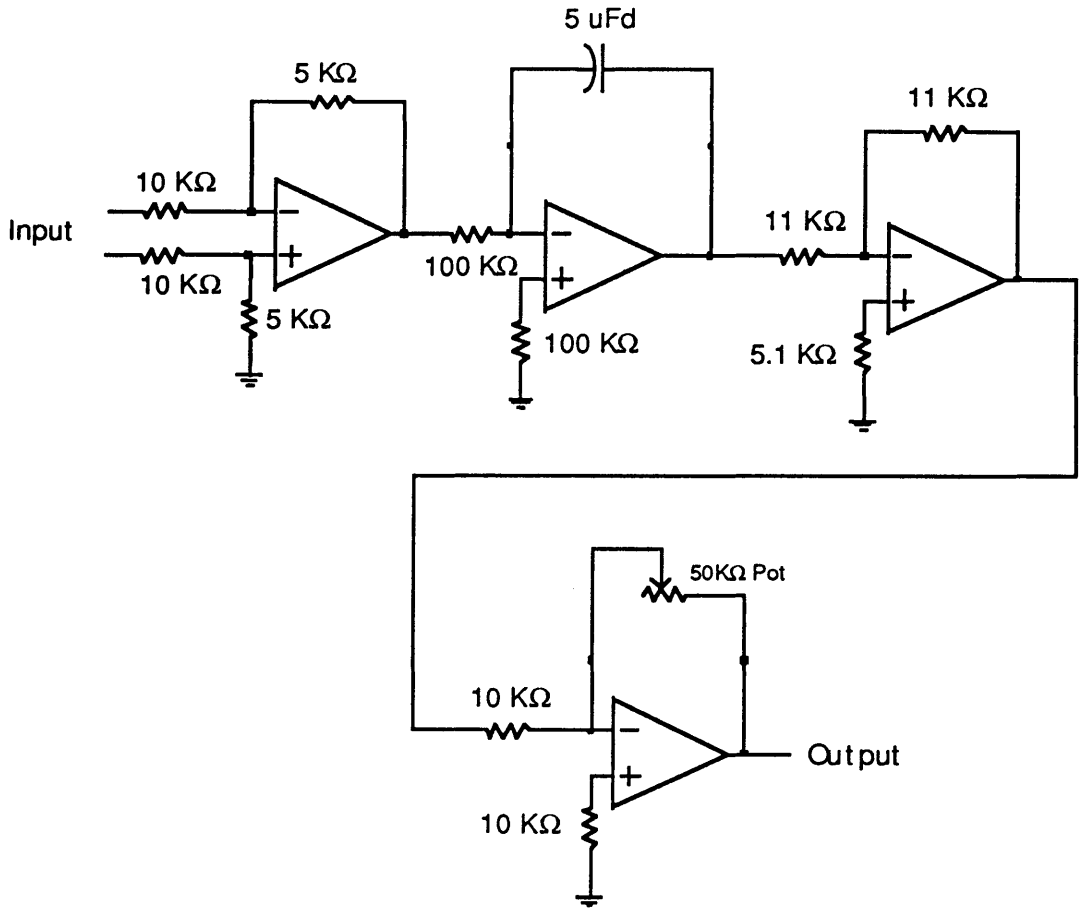

Figure 4.8-4: Platform Compensator Analog Electronics

When the platform compensator is coupled with the closed 30Hz position loop the open loop transfer function for the platform loop is yielded. The simulation and hardware system both had open loop cross-overs of approximately .1 Hz with phase margins of 90 degrees. The simulated platform loop, open loop transfer function is shown in Figure 4.8-5.

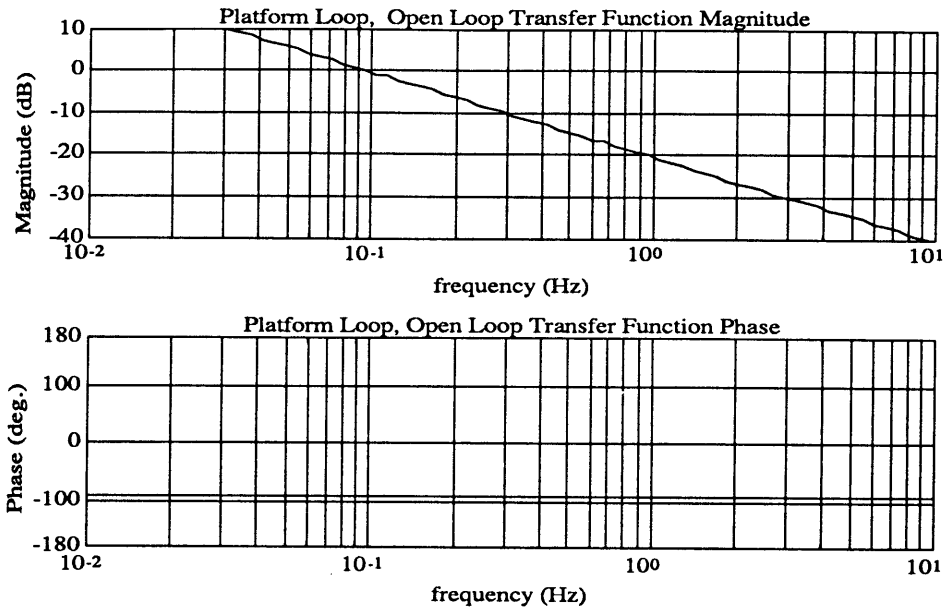

Figure 4.8-5: .1Hz Platform Loop Simulated Open Loop Transfer Function

The hardware test platform loop, open loop transfer function is shown in Figure 4.8-6. The hardware test was stopped at approximately .06 Hz because of the difficulty of testing at lower frequencies.

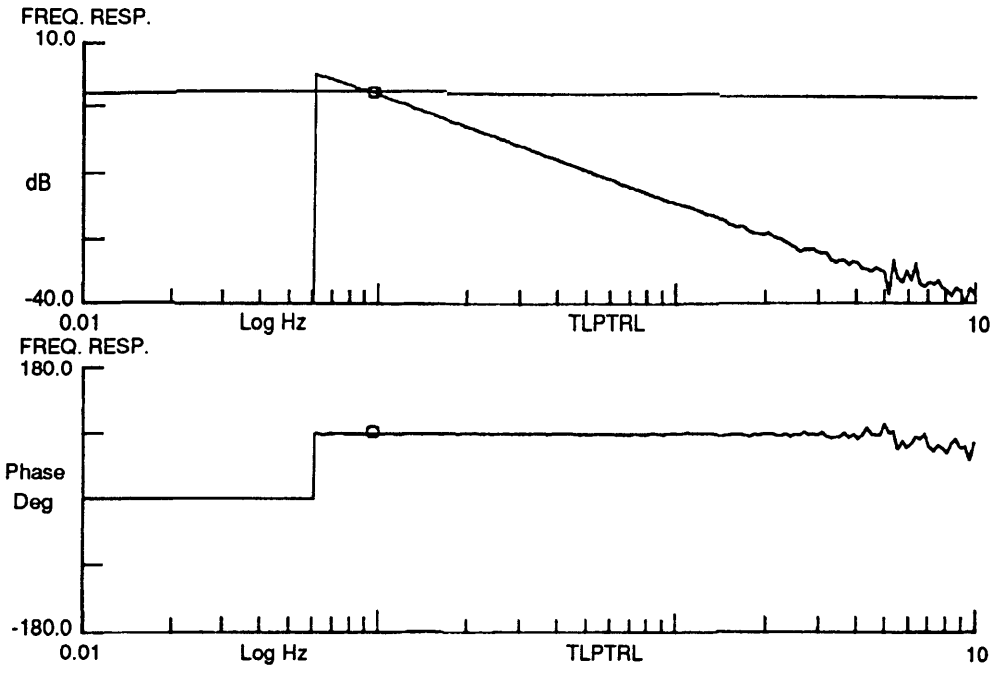

Figure 4.8-6: .1Hz Platform Loop, Hardware Open Loop Transfer Function

The resulting simulated closed loop transfer function for the platform loop is shown in Figure 4.8-7. The hardware tested platform loop, closed loop transfer function is shown by Figure 4.8-8. The approximate closed loop bandwidth for the simulation and the hardware setup was .1 Hz.

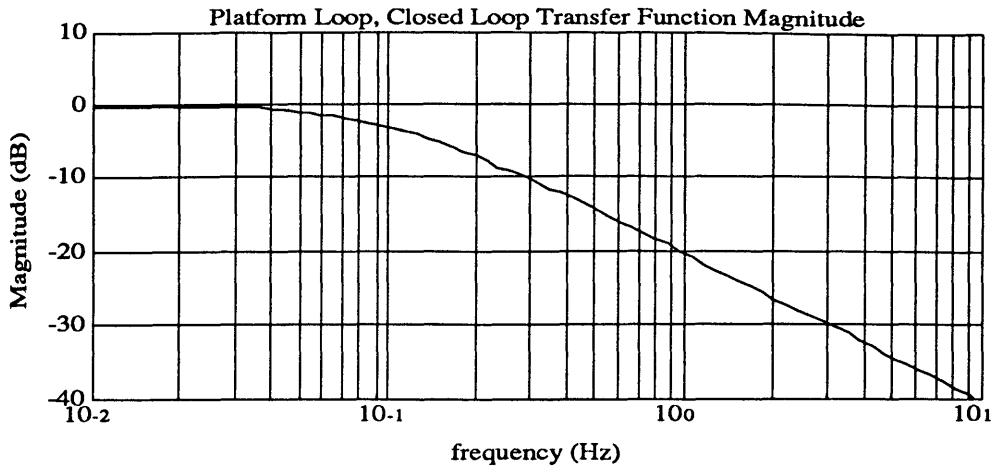

Figure 4.8-7: .1Hz Platform Loop, Simulated Closed Loop Transfer Function

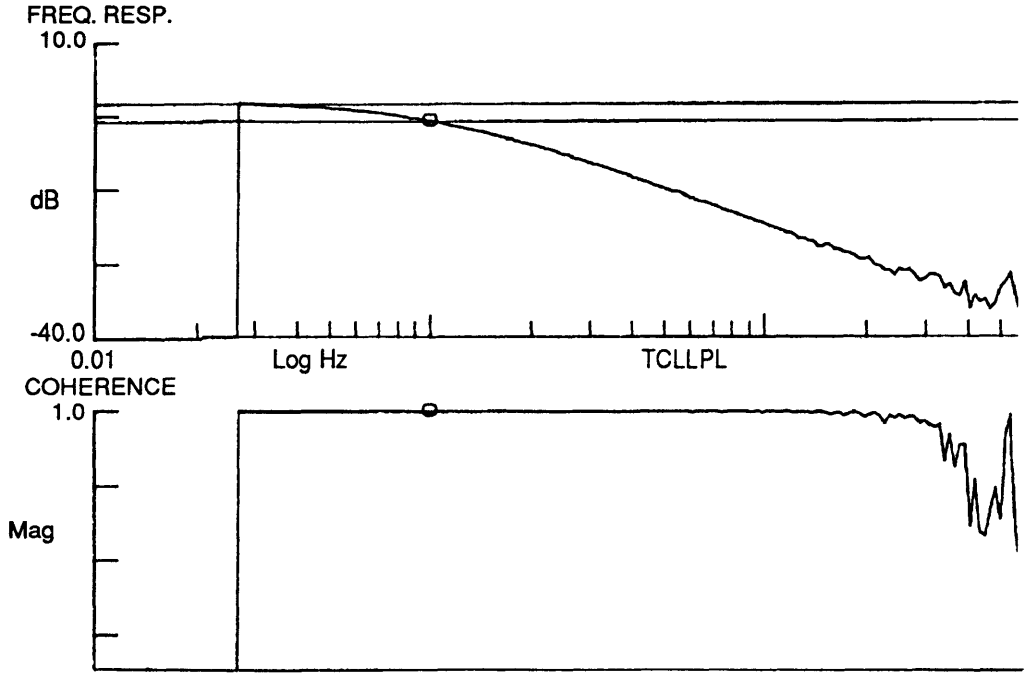

Figure 4.8-8: .1 Hz Platform Loop, Hardware Closed Loop Transfer Function

The .1 Hz platform loop with the closed loop transfer function shown in Figures 4.8-7 and 4.8-8 was used to unwind the FSM as the pointing stabilization system tracked a moving target.

Chapter 5: Results

This chapter contains the analytical, simulation and hardware test results. For clarification purposes the stabilization system is the system with the 110 Hz ORG loop closed and the tracking loop open, T(s)=0. The pointing stabilization system has both the ORG loop and the 4Hz tracking loop closed. As stated for the analysis in Chapter 3, the critical measurements were of the variables e1 and e4 The variable e1 is the measurement of the target beam on the receiver (photopot) and e4 is the same measurement made by a scoring device (target quad). The only difference between the two signals is the inherent photopot noise characteristics shown in equation 3.3-10.

Section 5.1: Analytical Transfer Function Results

The first results presented are from the stabilization system configuration (T(s)=0). The analytical stabilization transfer function corresponding to equations 3.3-12 and 3.3-13 is shown by Figure 5.1-1. This is a measure of how well the system attenuates base disturbances without the tracking loop.

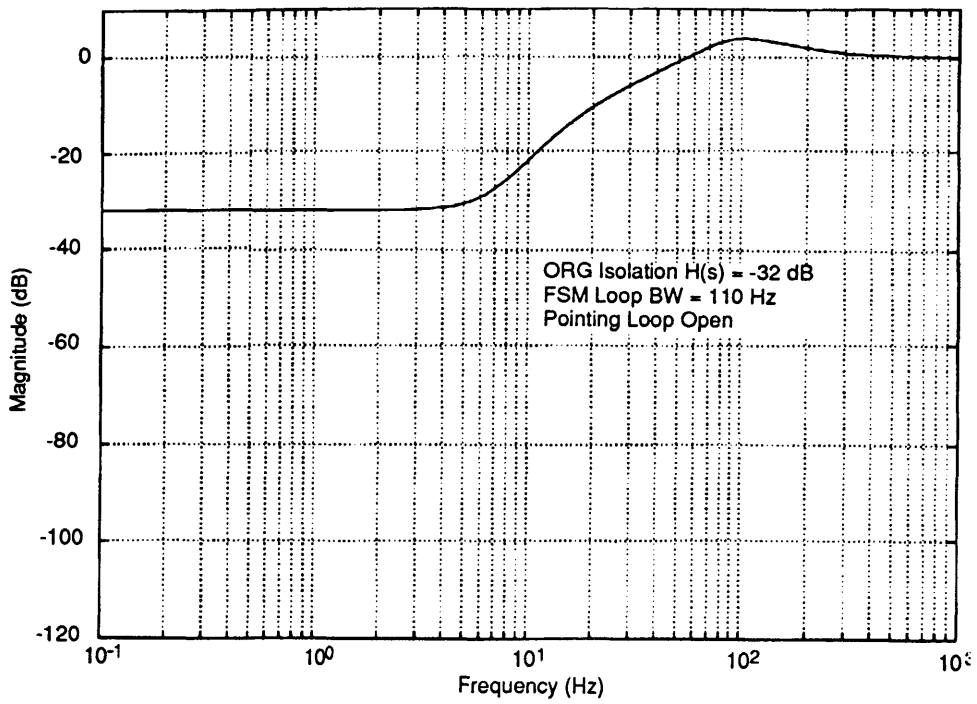

Figure 5.1-1 Analytical Stabilization System Transfer Function

The low frequency stabilization is bound by the ORG isolation of -32dB. Analytically, the isolation component corresponds to the second term of equations 3.3-12 and 3.3-13. The high frequency characteristics are dictated by the 110Hz bandwidth of the FSM loop. These dynamics are shown by the first term of equations 3.3-12 and 3.3-13. Figure 5.1-2 shows the pointing stabilization configuration transfer function. This is a measure of the base disturbance attenuation with the tracker loop. The dashed line is the stabilization configuration transfer function which is included for comparison.

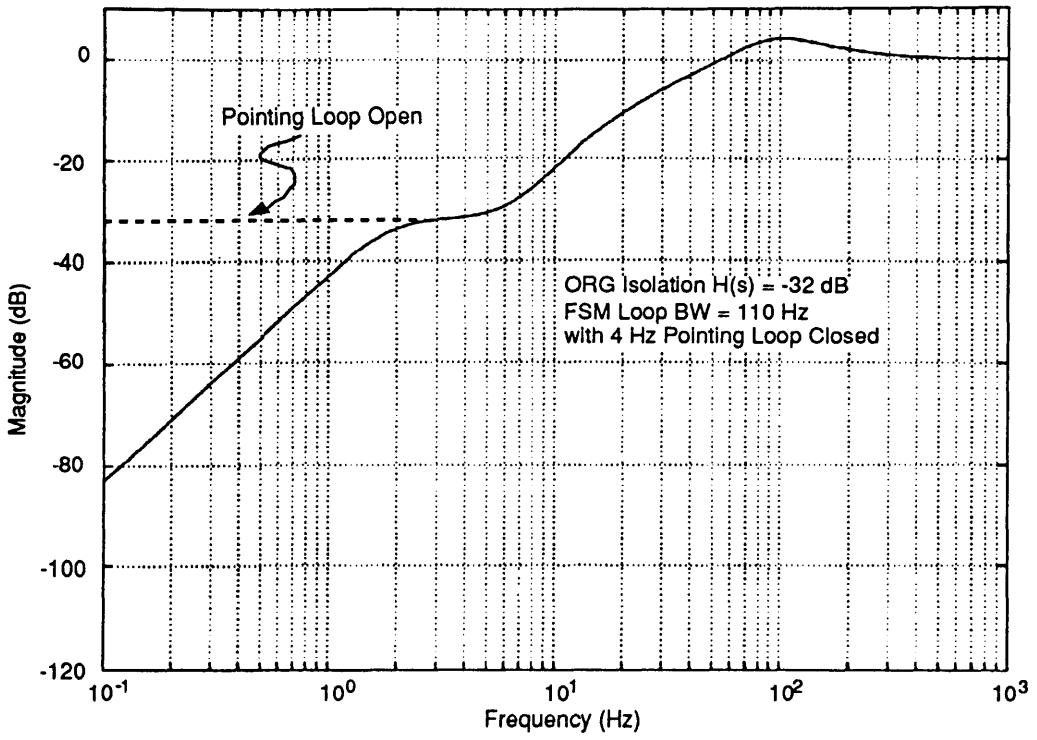

Figure 5.1-2 Analytical Pointing Stabilization System Transfer Function

As shown in Figure 5.1-2, with the 4Hz pointing loop closed the low frequency disturbances are further attenuated.

Section 5.2: Hardware Transfer Function Results

As with the analytical results, the system transfer functions were measured for the hardware setup for error signals e1 and e4. The stabilization configuration transfer function (T(s)=0) is shown in Figure 5.2-1

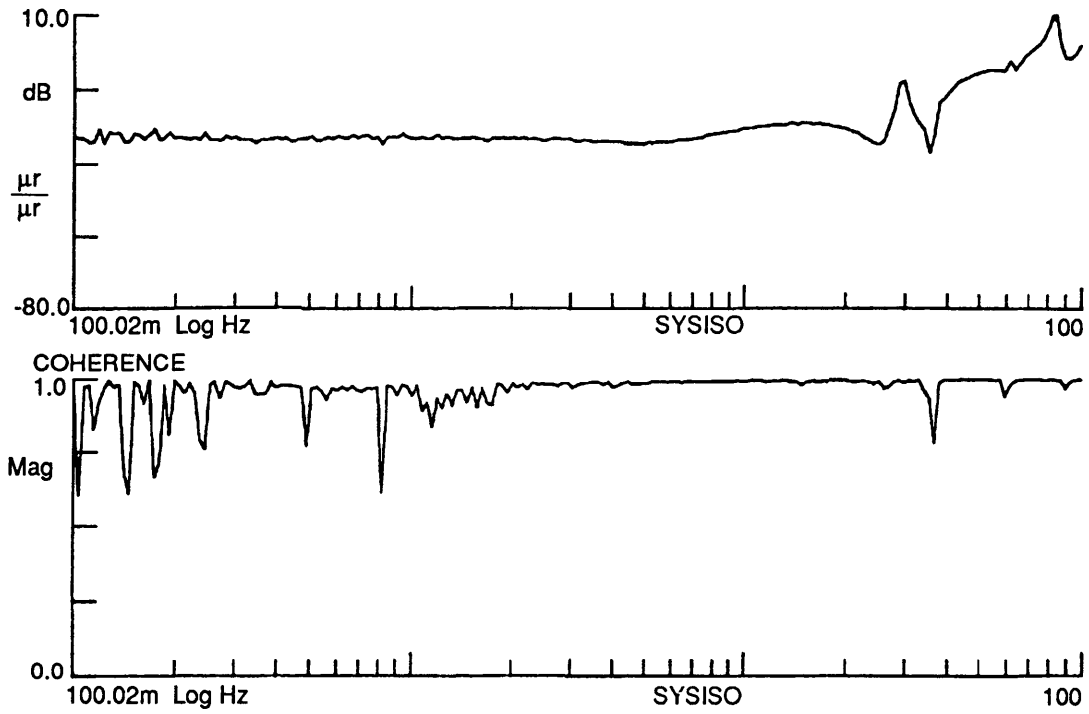

Figure 5.2-1: Hardware Stabilization System Transfer Function

The hardware test shown in Figure 5.2-1 matches closely with the similar analytical result in Figure 5.1-1, except for the frequency bands which are corrupted by the FSM dynamics and the 90 Hz eliminator notch. As in the analytical results, the low frequency is bound by the ORG isolation which was measured to be -30dB for the data shown in Figure 5.2-1. The 110 Hz ORG loop bandwidth also limits the high frequency characteristics of the hardware tests. The data shown in Figure 5.2-2 is the pointing stabilization system transfer function measured at the photopot (e1).

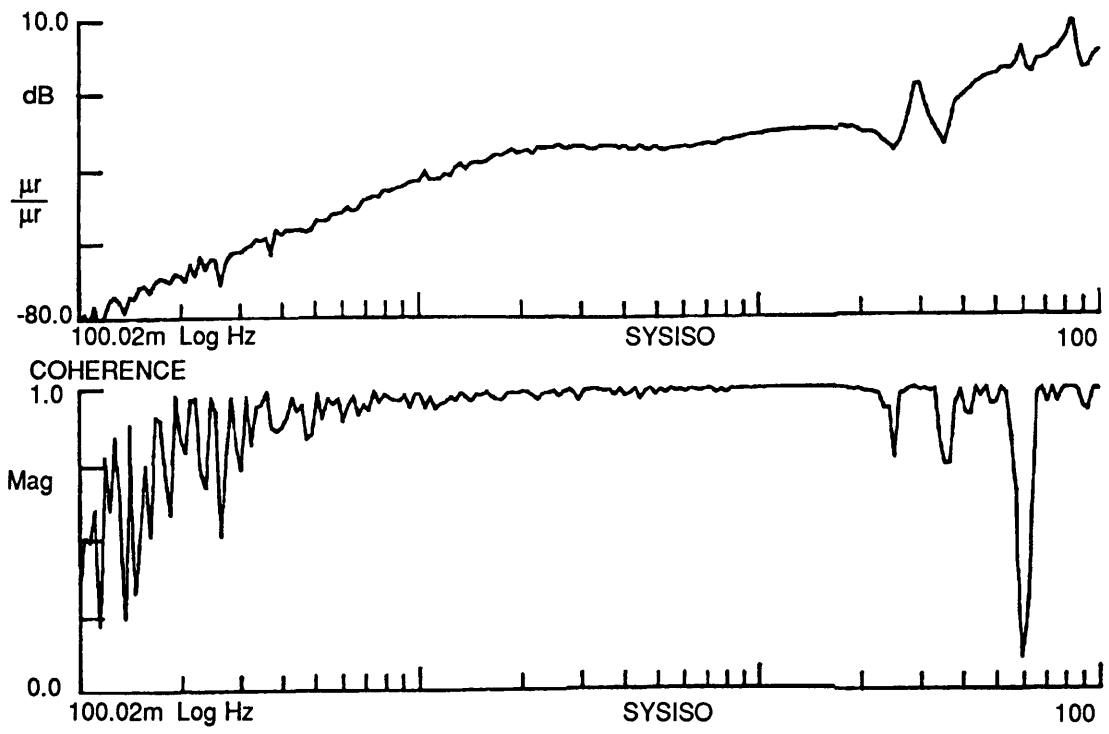

Figure 5.2-2: Hardware Pointing Stabilization System Transfer Function (measured at Photopot sensor)

Again the test results matched closely to the analytical results. The next transfer function shown is still the pointing stabilization system but it is measured at the scoring quad (e4) rather than at the photopot (e1). As shown by equation 3.3-10, e4 is corrupted by the noise from the photopot. The noise from the photopot corrupts e4 at the lower frequencies of the pointing stabilization transfer function as shown in Figure 5.2-3.

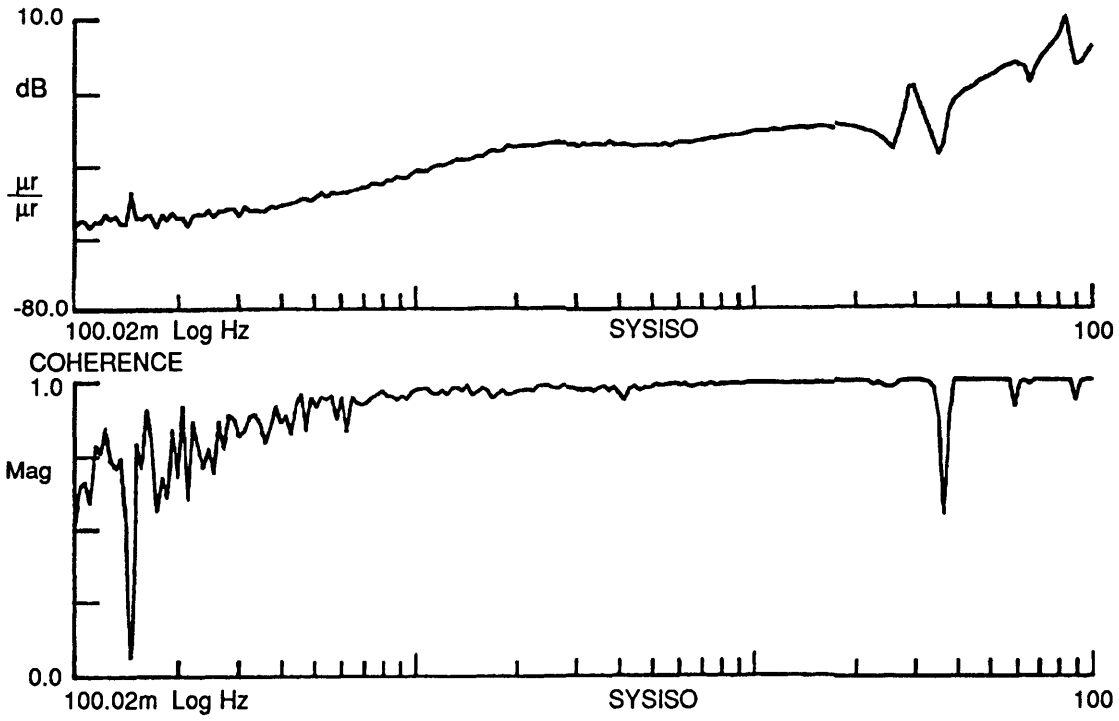

Figure 5.2-3: Pointing Stabilization System Transfer Function Measurement (measured at scoring quad)

The results shown in Figure 5.2-3 differ from the analytical result in Figure 5.1-2 at the low frequency. The data is corrupted only in the hardware tests, because the analytical results were derived using an ideal photopot without sensor noise.

Section 5.3: Quantitative Jitter Results

In order to quantitatively score the stabilization system and the pointing stabilization system the jitter error with a representative base disturbance environment, Θ_{BI}, was tested. The jitter error measurements were made by the Scoring Quad (e4). The tests were performed on the analytical models as well as on the hardware setup.

A Ball Aerospace test environment model was selected as the representative base disturbance environment for the testing. It had an rms disturbance of 30ur over a bandwidth of .1-100Hz. The Ball Aerospace test environment is shown in Figure 5.3-1.

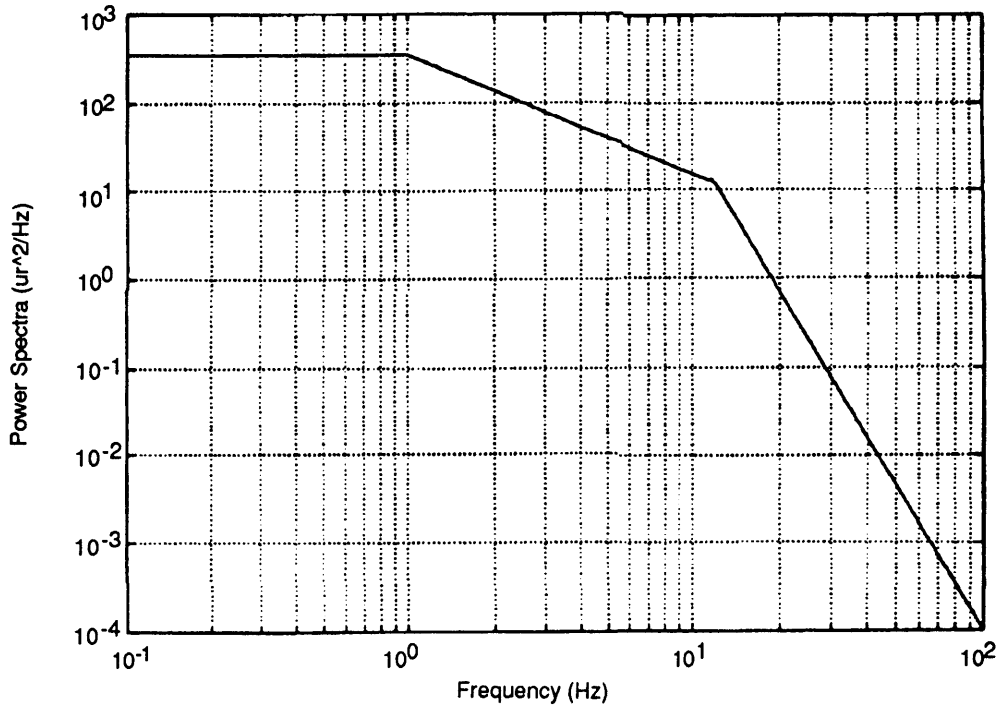

Figure 5.3-1: Base Motion Disturbance Spectrum

Section 5.3.1: Analytical Jitter Measurement Results

The Ball Aerospace base disturbance environment was applied to the analytical models for both the stabilization configuration and for the pointing stabilization configuration. Shown in Figure 5.3.1-1 is the residual stabilization error PSD for the analytic stabilization configuration.

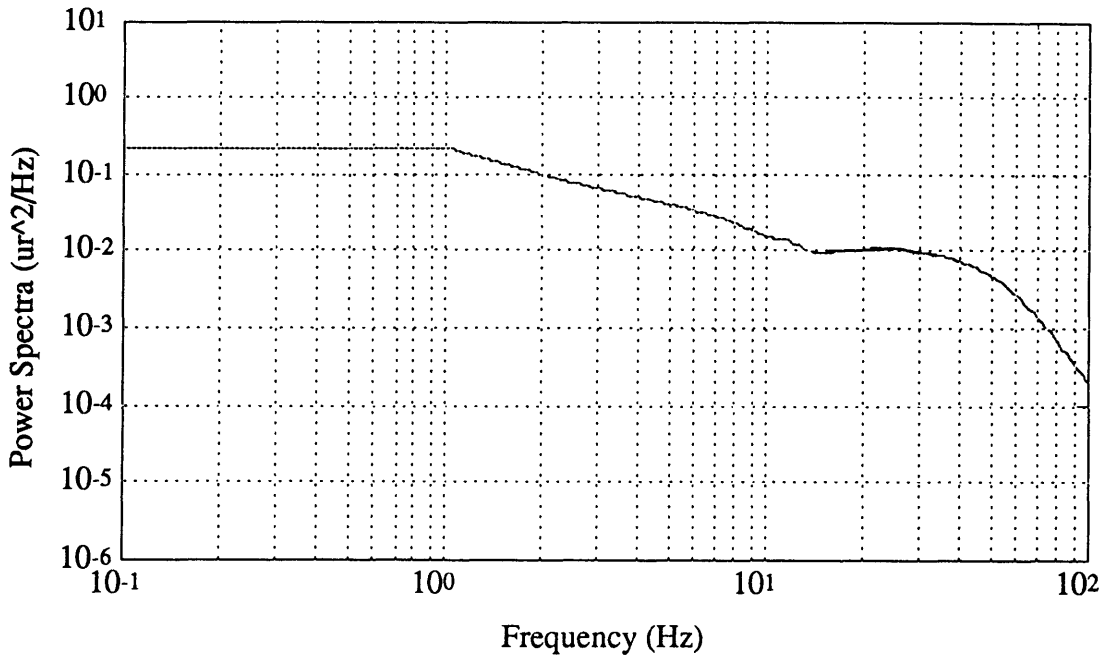

Figure 5.3.1-1: Analytical Stabilization Jitter Measurement PSD

For the analytic result in Figure 5.3.1-1 the base disturbance input spectrum was 30.3ur rms and the resulting closed loop stabilization performance was measured by the variable e4. The residual stabilization error measured at e4 was 1.54ur rms .1-100Hz.

Shown in Figure 5.3.1-2 is the analytic residual error PSD for the pointing stabilization system.

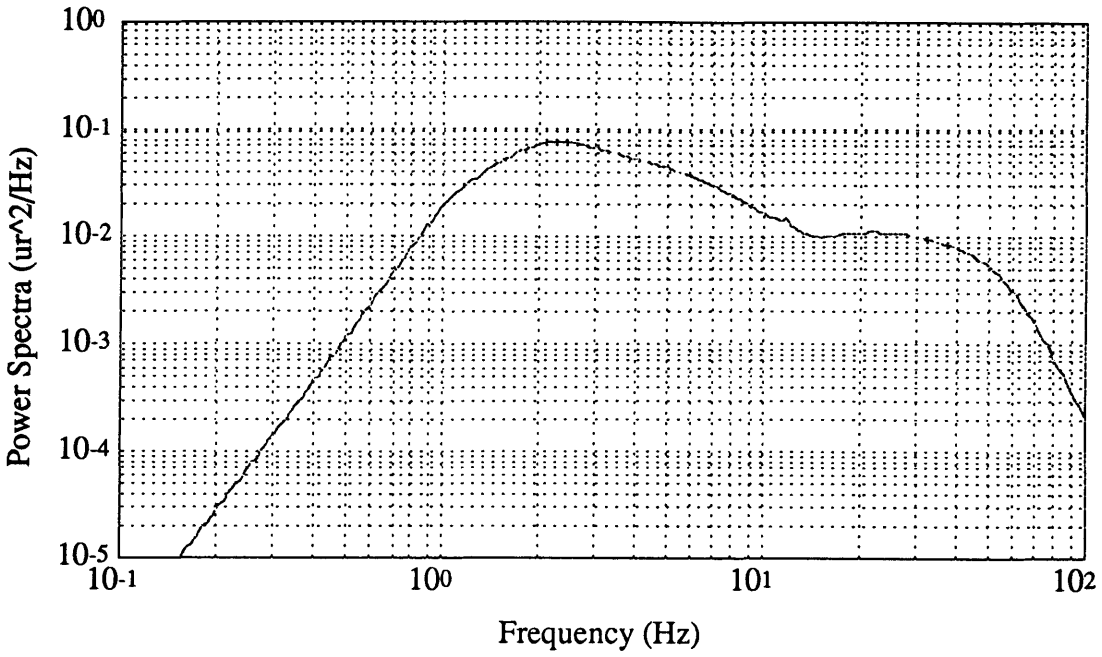

Figure 5.3.1-2: Analytical Pointing Stabilization Jitter Measurement PSD

For the analytic result in Figure 5.3.1-2 the base disturbance input spectrum was 30.3ur rms and the resulting closed loop pointing stabilization performance was measured by the variable e4. The residual pointing stabilization error measured at e4 was 1.46ur rms .1-100Hz.

Section 5.3.2: Hardware Jitter Measurement Results

The disturbance spectrum shown in Figure 5.3-1 was also applied to the hardware stabilization system and the error e4 was measured by the scoring quad. The resulting spectrum is shown in Figure 5.3.2-1.

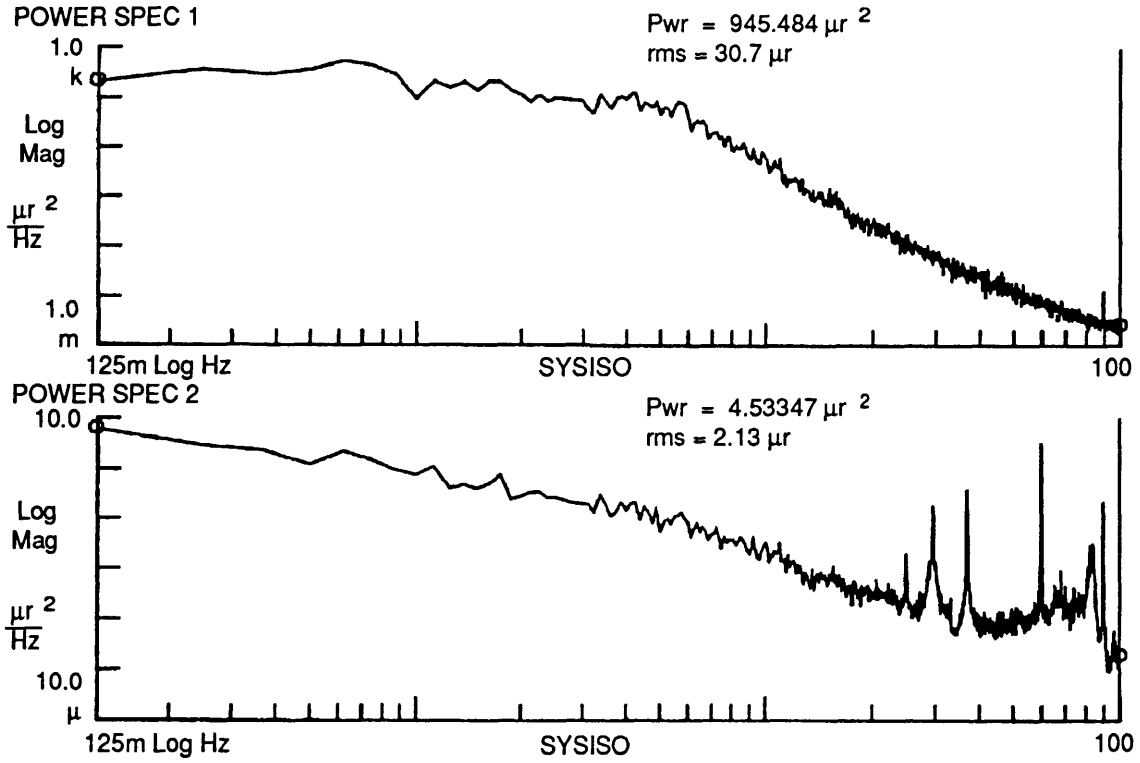

Figure 5.3.2-1: Stabilization System Residual Jitter Measurement PSD

The top plot of Figure 5.3.2-1 shows the base disturbance input spectrum of 30.7ur rms and the lower plot shows the resulting closed loop stabilization performance measured at e4. The residual

stabilization error measured at the scoring quad was 2.13ur rms .1-100Hz. The same measurement was made for the pointing stabilization system and the results are shown in Figure 5.3.2-2.

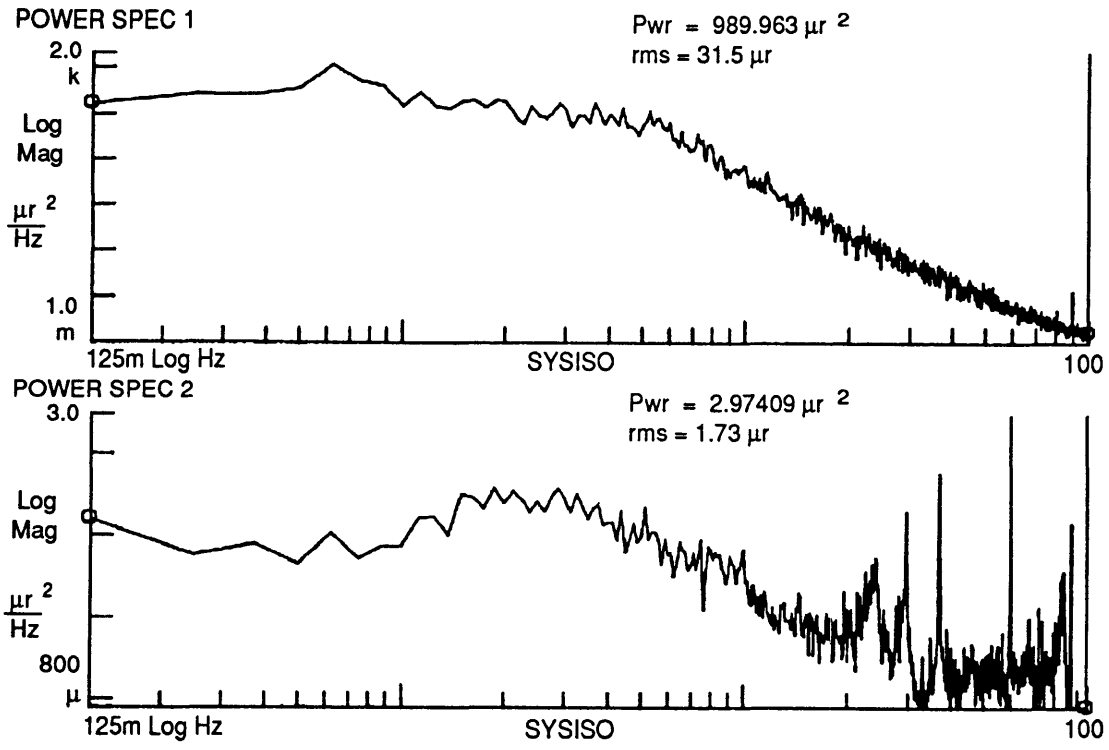

Figure 5.3.2-2: Pointing Stabilization System Jitter Measurement PSD

With the addition of the tracking loop, the performance was improved. With an input disturbance of 31.5ur rms the jitter error was reduced to 1.73ur rms from .1-100Hz.

The hardware results of the PSD measurements differ from the corresponding analytic results only at the lower frequencies. The difference is a result of the fact that it is very difficult to accurately measure the PSD spectrum at low frequencies with a hardware setup. Any small drifts or perturbations will have

significant effects on the low frequency measurements of the PSD error spectrum.

The quantitative results for both the analytical and hardware test results are summarized in Table 5-1.

Configuration		Test Results	Analytical Projections
Stabilization System H(s) = -32 dB	Input Disturbance rms, 0.1-100 Hz	30.7 μr	30.3 μr
FSM Loop BW = 110 Hz	Residual Jitter rms, 0.1-100 Hz	2.13 μr	1.54 μr
Pointing Stabilization System H(s) = -32 dB	Input Disturbance rms, 0.1-100 Hz	31.5 μr	30.3 μr
FSM Loop BW = 110 Hz Pointing Loop BW = 4 Hz	Residual Jitter rms, 0.1-100 Hz	1.73 μr	1.46 μr

Table 5-1: System PSD Performance Summary

As can be seen in Table 5-1, the analytic and hardware test results match closely verifying the analytic model. The differences in the analytical and the hardware test results can be attributed to noise sources that are not quantitatively accounted for in the

analytic model. These sources include the ORG noise, the photopot noise, the flex dynamics of the FSM and the electrical noise at 60Hz.

Section 5.4: Transient Response

In addition to the transfer functions and the PSDs, the transient response of the system was also studied. The results of two critical responses were measured. The first is a measurement of the transient time of e1 in response to a step in the target angle of .2mr. This is a measure of how much time the system requires to re-align the target beam on the receiver after the target has taken an angular step of .2 mRadians. The second measurement is for the transient motion of the platform in response to a target beam step of .2mr. In other words, this a measure of how long the system would require to track a target moving .2 mRadians without the pointing stabilization system. This is also a measure of how long the system requires to "unwind" the FSM utilizing the .1 Hz platform loop.

Shown in Figure 5.4-1 is the simulated pointing stabilization system response to a .2mr step in target angle measured at e1. In Figure 5.4-2 is the hardware test data for the same measurement.

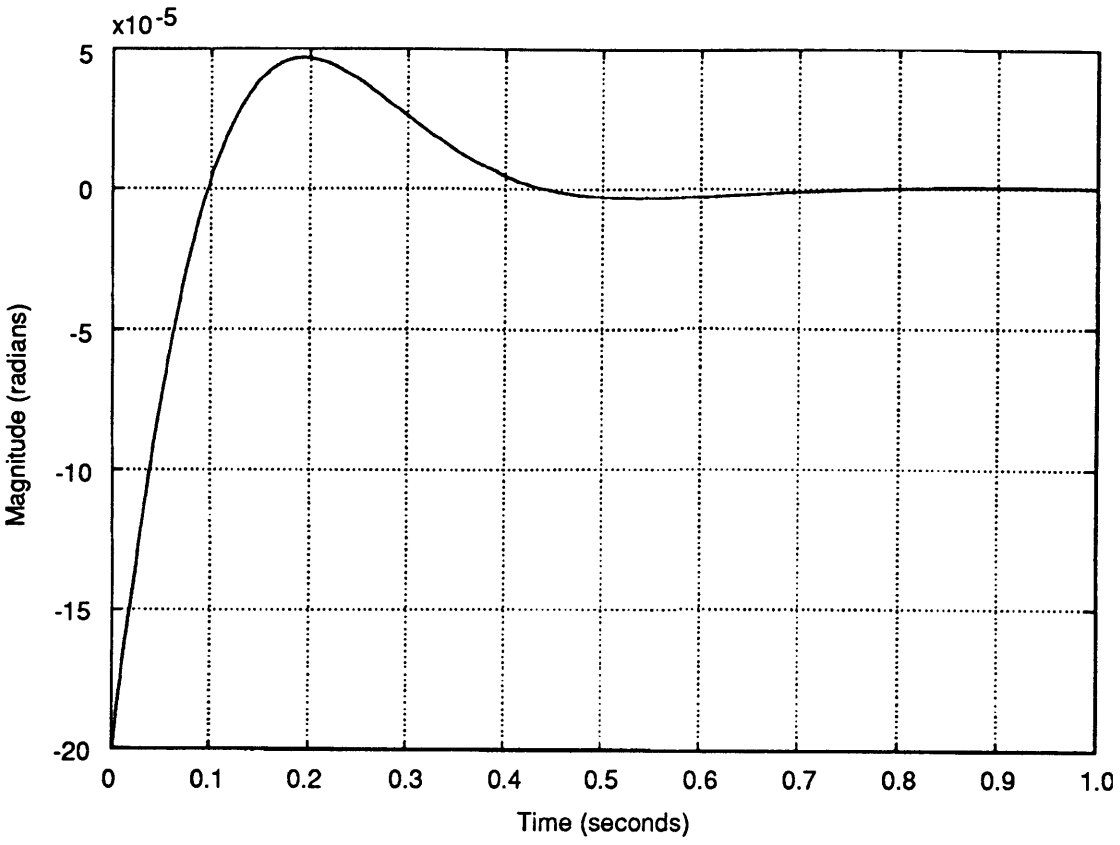

Figure 5.4-1: Analytical Pointing Stabilization Transient Response. (measured at e1)

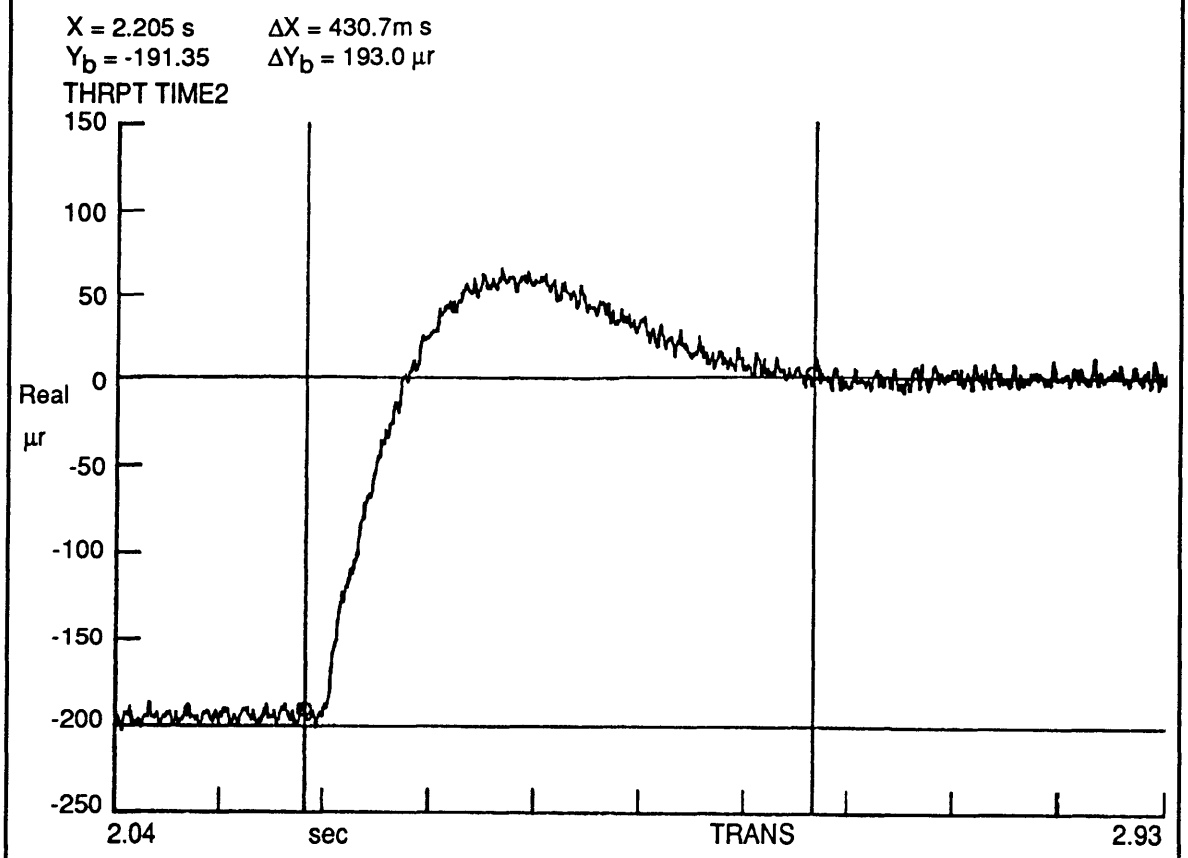

Figure 5.4-2: Hardware Pointing Stabilization Transient Response (measured at e1)

The data shows a transient time of approximately .43 seconds. The jitter on the hardware test data is due to photopot electrical noise. The simulated data and the hardware data are very well correlated.

The .1 Hz FSM "unwind" loop simulated and hardware test data are shown in Figures 5.4-3 and 5.4-4, respectively. Again, this a measure of how long the system would require to track a target moving .2mr without the pointing stabilization system.

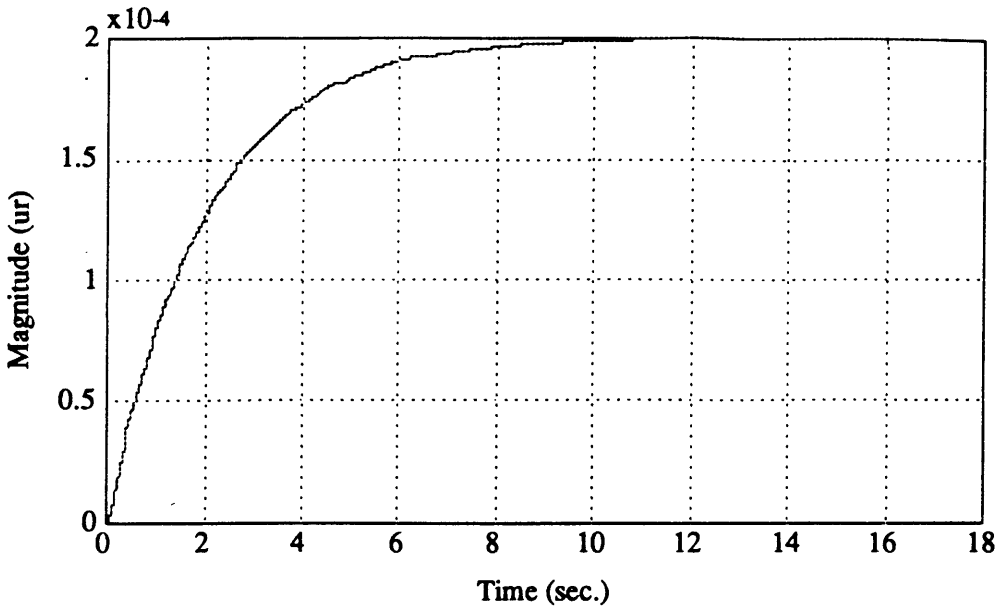

Figure 5.4-3: Simulated .1Hz Platform Loop Response

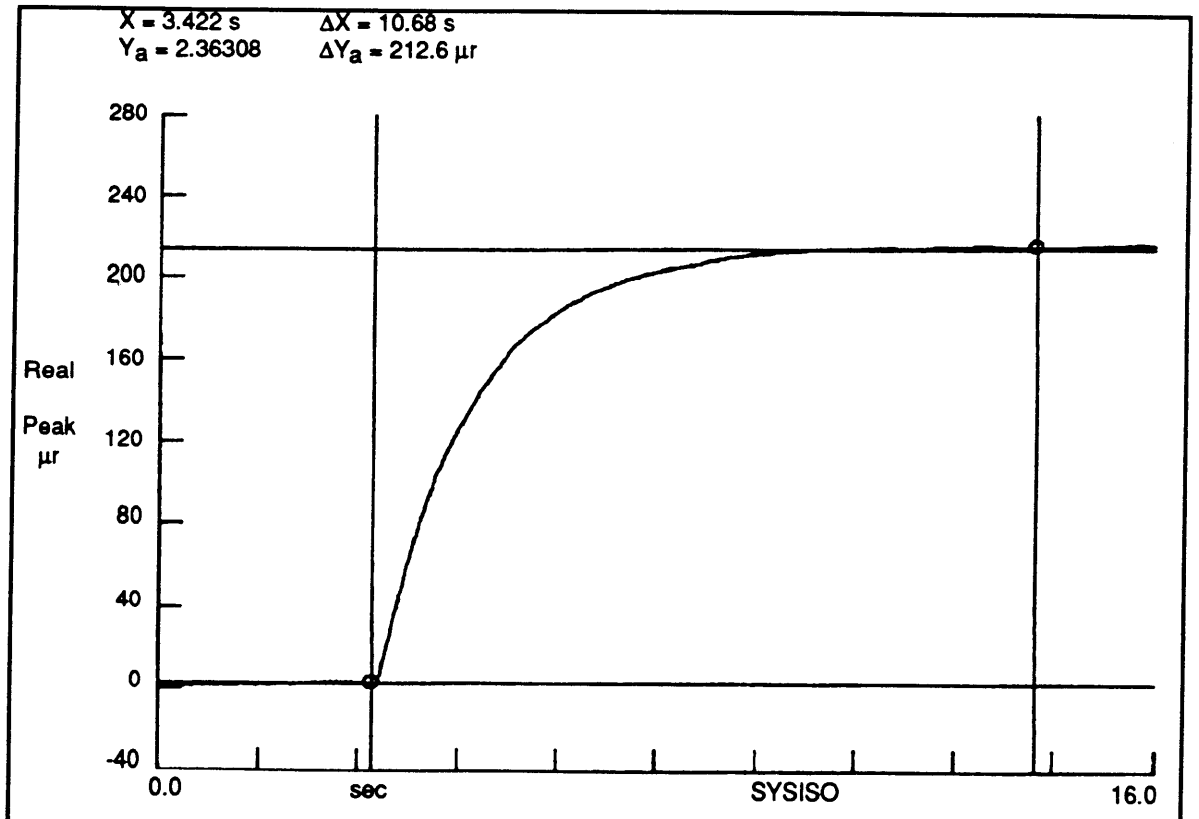

Figure 5.4-4: Hardware .1Hz Platform Loop Response

The .1 Hz platform loop reaches 2% of its steady state value in approximately 10.7 seconds. Thus, the pointing stabilization system improved the system transient time from 10.7 seconds to .43. This is a factor of improvement of 25.

Section 5.5: System Response at CCD Camera

Lastly, the stabilization and the pointing stabilization response are demonstrated by the CCD camera. The CCD views the same motion and jitter as would e1 or e4, which is the view seen by the receiver of the target beam. In Figure 5.5-1, the target beam image was smeared by a base disturbance of .75mr peak to peak at a frequency of .5 Hz. In addition, the target beam is subject to a step angular offset of 1.25mr.

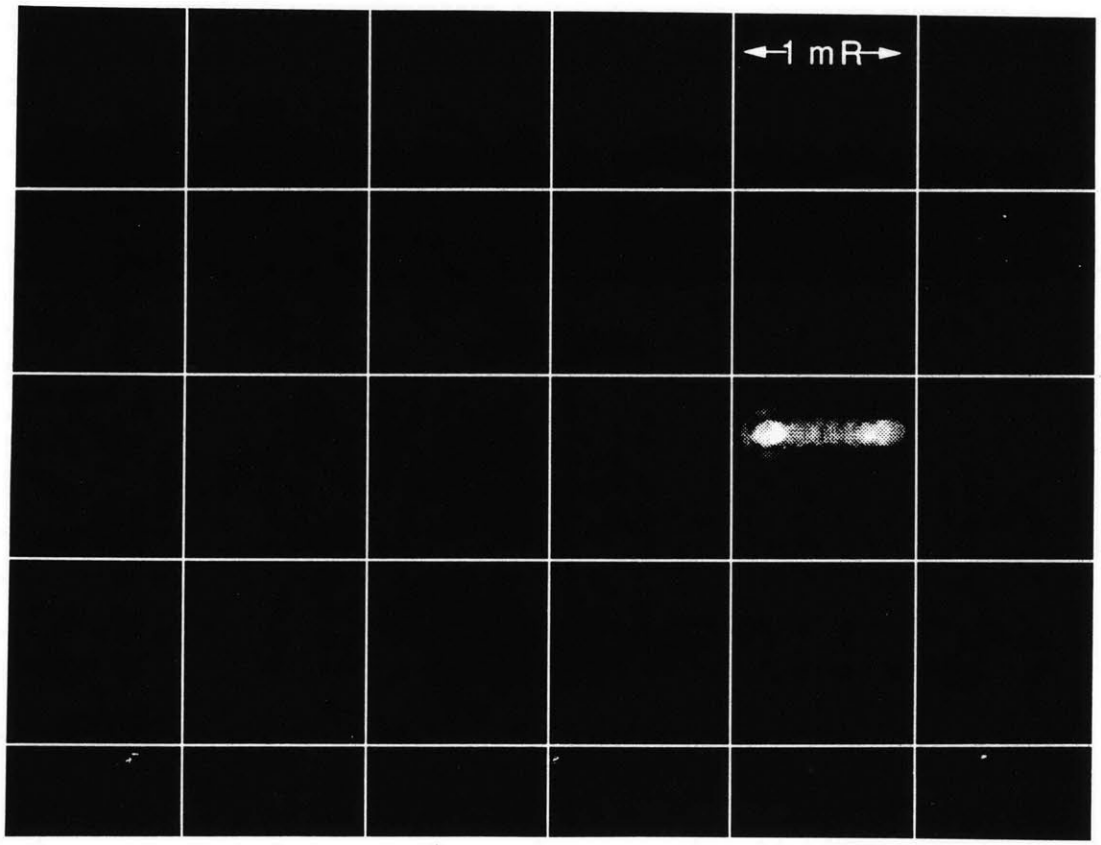

Figure 5.5-1: Image was Offset and Smeared by Base Disturbance

In Figure 5.5-2, the 110Hz FSM stabilization loop was closed thus removing the majority of the smear.

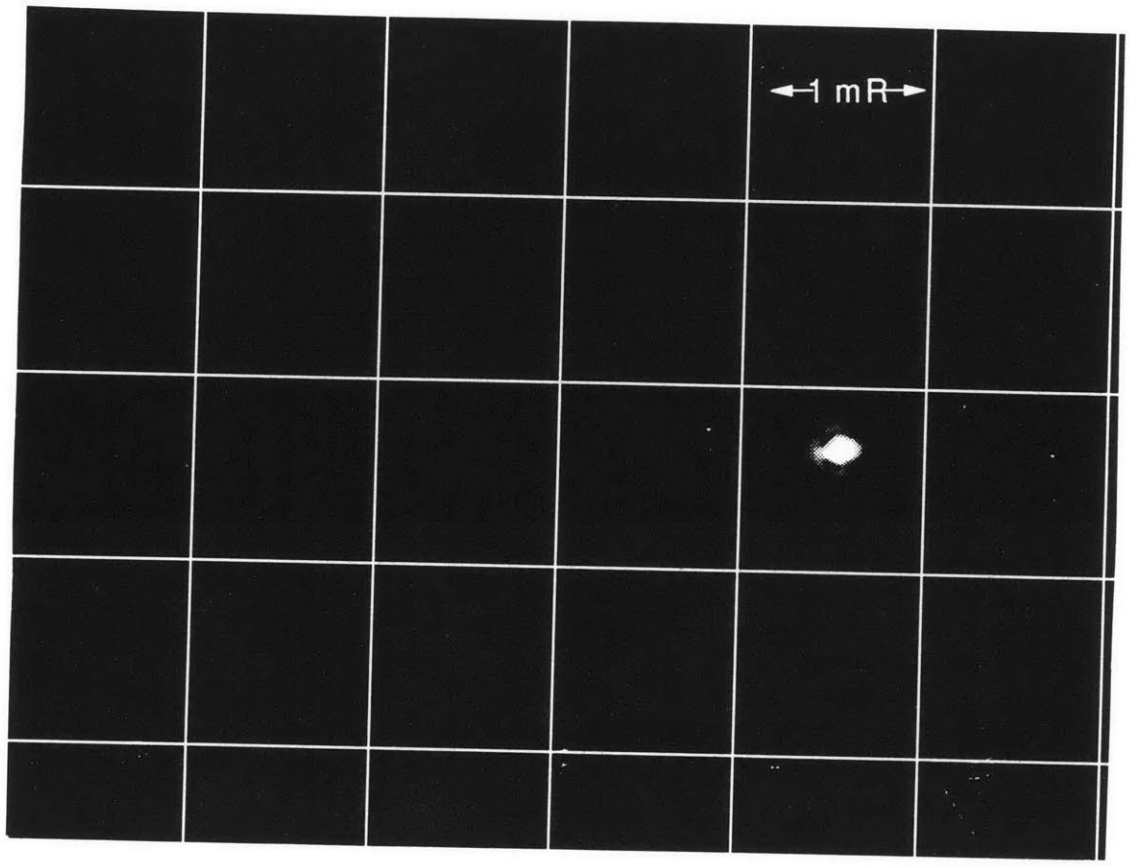

Figure 5.5-2: Image Offset but Smear Removed by Stabilization System

In Figure 5.5-3, the 4Hz pointing was also closed thus utilizing the entire pointing stabilization system. In the this configuration the image was nulled, in addition to the smear being removed.

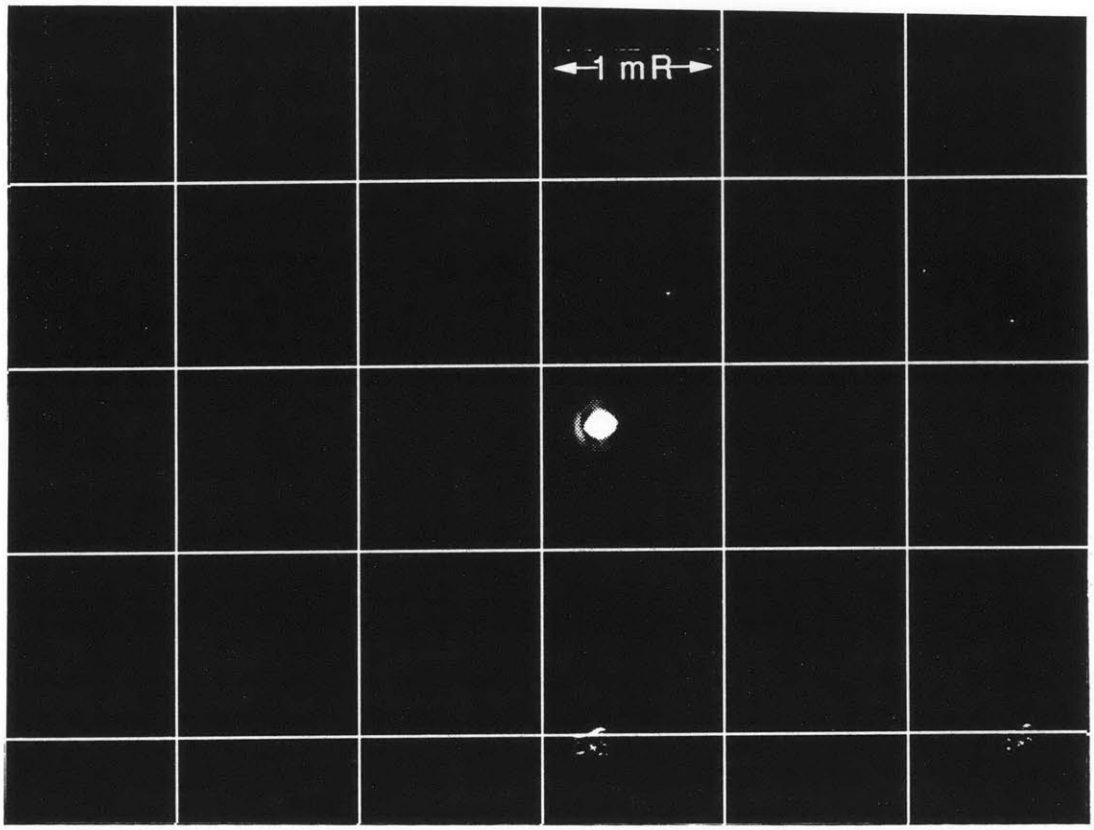

Figure 5.5-3: Image Offset Removed and Smear Removed by Pointing Stabilization System Configuration

Chapter 7: Conclusions

The pointing-stabilization system detailed in this thesis is an ideal model for the development of optical intersatellite communications. Optical communications allow for significant increases in data rate transmission with lower power requirements than current RF systems.

In this thesis, a pointing stabilization system was simulated and a hardware testbed was constructed. The system allows one satellite to follow a target beam emitted from a second satellite. In addition, the stabilization capabilities remove the individual platform disturbances significantly improving the signal to noise ratio of the received beam. The key to the system is the Optical Reference Gyroscope (ORG) which provides the inertial reference for both the pointing and stabilization functions. The analytical results gave validity to the data acquired from the testbed setup. The pointing stabilization configuration yielded an rms jitter of 1.73 uRadians in a disturbance environment of 31.5 uRadians from .1-100 Hz. This specification satisfies the 5ur stabilization specification set by the LITE experiment detailed in [6].

Chapter 8: Recommendations

In the past fiscal year, the design of an enhanced ORG has been undertaken. The goal was to improve the key parameters of the ORG as well as its overall design. As stated in Section 4.2, the key parameters of the ORG that govern the pointing-stabilization performance are the rotor spin frequency and the case to rotor isolation. For the enhanced ORG, the spin frequency has been raised to 200 Hz and the isolation has been improved to -50dB. Table 8-1 summarizes the enhanced ORG parameters.

Angle noise (Optical)	100 nR rms, 0.1 - 100Hz
Drift stability	0.005 deg/h
Spin speed	200 Hz
Rotor/case isolation	–50 dB, 0.1 - 100 Hz
Slew capability	15 deg/s
G-capability (@ hinge)	100 g
Motor power	0.95 W
Torquer power	2.5 W (@15 deg/s)
Fill gas	He at 2 psia, or evacuated
Light source	Monolithic laser diode
Wavelength	670 nm
Optical power out	1 mW
Optical power at source	2.5 mW
Beam exit diameter	0.7 in
Pinhole diameter	4.5 mm
Wavefront quality	$\lambda/6$ P- V
Beam divergence	40 ur
Size	3.25 in dia. x 7 in
Weight	35 oz

Table 8-1: Enhanced ORG Design Parameters

The higher spin frequency allows for the bandwidth of the FSM loop to be increased thus improving the base disturbance attenuation. The improved case to rotor isolation lowers the lower bound of the base disturbance attenuation by a factor of 10. To quantify the improvement in the pointing stabilization system, the analytical sections were repeated using the enhanced ORG parameters. In the analysis, an ORG isolation of H(s)=-50dB was used and the bandwidth of the FSM loop was increased to 200 Hz. Figure 8-1 shows the analytical results of the stabilization system transfer function. The results using the prototype ORG are also included for comparison.

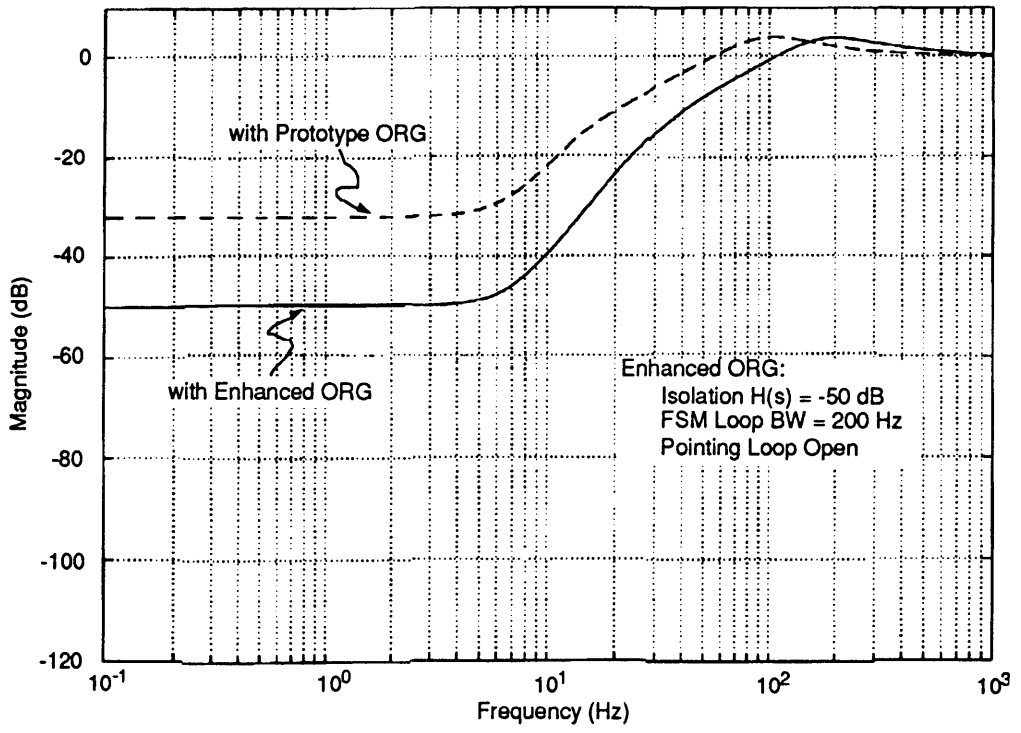

Figure 8-1: Analytical Stabilization System Transfer Function (with enhanced ORG)

The results of the pointing stabilization configuration are shown in Figure 8-2. Again the results using the prototype ORG are included for comparison.

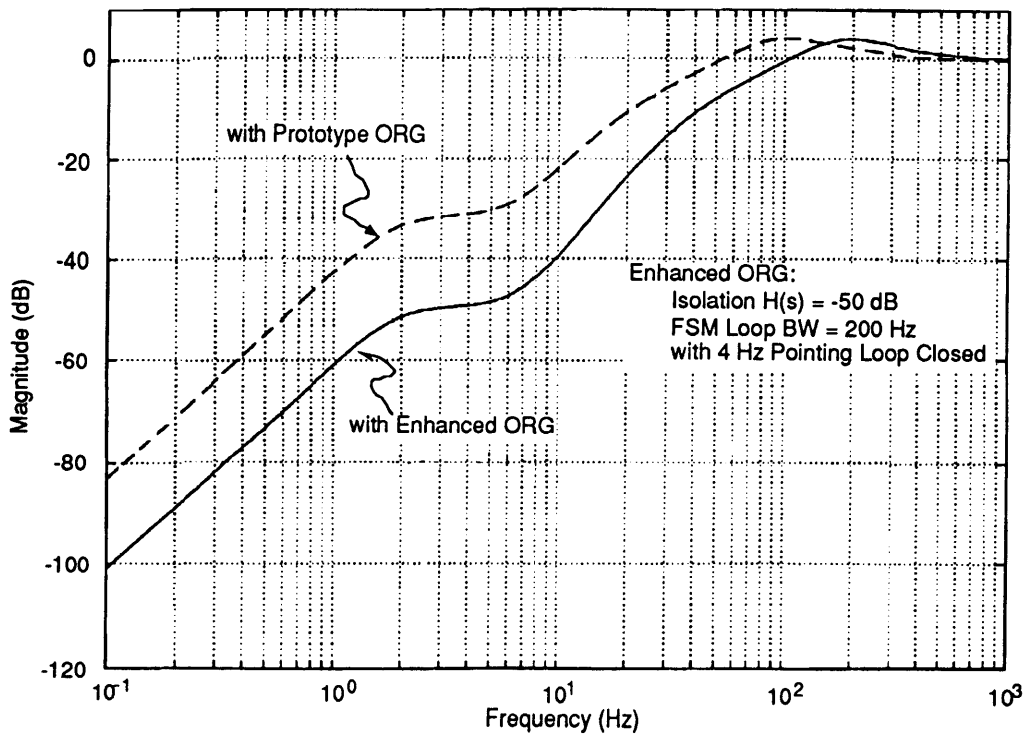

Figure 8-2: Analytical Pointing Stabilization System Transfer Function

A quantitative analysis of the stabilization and the pointing stabilization system using the enhanced ORG was also performed. In a disturbance environment of 30.3ur rms, 0.1 - 100 Hz, the projected residual jitter error is 0.35ur rms, 0.1 - 100 Hz for the stabilization system, and is 0.32ur rms, 0.1 - 100 Hz for the pointing stabilization system.

In summary, the performance analysis of the pointing stabilization system using the enhanced ORG indicates that a residual jitter of 0.32 ur rms, 0.1 - 100 Hz can be achieved in a disturbance environment of greater than 30ur rms, 0.1 - 100 Hz. This pointing stabilization system, when corrected for contributions by other error sources is projected to achieve a residual jitter of <0.5ur rms, 0.1 - 100 Hz.

Additional areas of study include the eliminator effects on the FSM loop and the FSM itself. The eliminator is essential such that the FSM loop bandwidth can be extended thus improving the disturbance isolation.

References

1. Braun, Andrew S., "Digital Signal Processing Applied to a Wideband Composite Strapdown Inertial Sensor", MIT EE&CS M.S. Thesis, June 1992.

2. Chien, Tze-Thong, "Image Stabilization with Optical Reference Gyro", Draper IR&D Project No. 328, July, 1992.

3. Doerr, Chris R., "Optical Reference Gyroscope Characterizations and Performance Enhancement", MIT EE&CS M.S. Thesis, June 1990.

4. Gilmore, Jerold P., Chien, T.T., Woodbury, Dale, Luniewicz, Mike, Feldgoise, Stephan, "Pointing Stabilization System Using the Optical Reference Gyro", Institute for Navigation, July, 1993.

5. Hamman, Jeffrey T., "Image Stabilization Performance Optimization Using an Optical Reference Gyroscope", MIT AA M.S. Thesis, June 1992.

6. Kaufmann J., Swanson E., "Laser Intersatellite Transmission Experiment Spatial Acquisition, Tracking, and Pointing System", MIT Lincoln Laboratory, September 1989.

7. Meline, Michael E., Harrell, John P., Lohnes, Kirk A., "Universal beam steering mirror design using the cross blade flexure", Hughes Aircraft Company.

Appendix A: Analytical Code

```
%part 1: Matlab Code
%Table Loop Constants for S(s) subscript t
Wcot=.13*2*pi; %Convert .1 Hz crossover to radians
Jt=3.0;
TMt=1.3;
Kit=(Jt/TMt)*((Wcot^3)/9);
Kpt=(Jt/TMt)*(2/3)*(.7)*(Wcot^2);
Kdt=(Jt/TMt)*(Wcot);
%Mirror Loop Constants for F(s),G(s),and B(s) subscript m
Bm=.006;
Jm=.0056;
Pm=.5*2.08;
Keqm=42;%10.5-(150*.064*Pm);%42
wcm=25*2*pi;  %Convert 25 Hz crossover to radians 43,80
Kpm=Jm*2/3*.7*wcm^2;
Kim=Jm*wcm^3/9;
Kdm=Jm*wcm;
am=3*wcm;

%Table Tracker Loop Constants for T(s) 4Hz Loop
L1=15;
L2=140;

%for 110 Hz Loop
R1=200000;
R2=10000;
R3=100000;
R4=96500;
C1=.048e-6;
C2=.1e-6;
C3=.33e-6;
%loading in System Transfer Functions
w=logspace(-0.2018,2.7982,300);
%w=logspace(.7979,2.099,300);
s=i*w';
m=length(w);
for  x=1:m;
                % S Compensator
                S(x)=(1/s(x))*(Kit+Kpt*s(x)+Kdt*s(x)^2);
                %S Open Loop
                %SOpLpTF(x)=(TMt/Jt)*(1/(s(x))^2)*S(x);
                %Sens(x)=TMt/(Jt*(s(x)^2)+S(x)*TMt);
                %S Closed Loop
                %SCILpTF(x)=(SOpLpTF(x))/(1+SOpLpTF(x));
                %F(s) Mirror Dynamics
                %Old one
                %F(x)=3.8*1200*(1.04)/(.0056*(s(x)^2)+.14*s(x)+35);
                %F(x)=6000*(1.04)/(.0056*(s(x)^2)+.1*s(x)+42);
```

```
            F(x)=(1.1143e+06)/(s(x)^2+17.8571*s(x)+5500);
            This is best model
            %B(s) Table to Mirror Transfer Function
            B(x)=0;%(Bm*s(x)+Keqm)/Pm;
            %External Mirror Controller G(s)
            G(x)=1.0*(3.948134e-8*s(x)^3+0.00001190016*
                  s(x)^2+0.0011952*  s(x)+0.04)  /((1.0e-
            3)*(.0001*s(x)^3+.1958*s(x)^2));
            %Mirror Loop Calculations
            MOpLp(x)=2*F(x)*G(x);
            %re(x)=real(MOpLp(x));
            %im(x)=imag(MOpLp(x));
            %MOpLpPhase(x)=atan(im(x)/re(x));
            MCILp(x)=(MOpLp(x))/(1+MOpLp(x));
            %ORG Isolation Tr. Function H(s)
            %ao=(89.4*2*pi)*120;
            %bo=(ao+6.6e5*s(x));
            %co=(790*(s(x))^2)+120*(s(x)^2);
            %H(x)=(ao*bo)/(bo^2+co^2);
            H(x)=.025;%.00315
            %Table Controller for 4Hz Gyro TG Loop
            T(x)=(L1*s(x)+L2)/(s(x));%*(125.66/(s(x)+125.66));
            %TCILp(x)=T(x)*(1/s(x))/(1+T(x)*(1/s(x)));
%Finding delta
numdelta(x)=(2*F(x)*G(x)*T(x));
dendelta(x)=(s(x)*(1+2*F(x)*G(x)));
delta(x)=1+(numdelta(x))/(dendelta(x));
e1Nph(x)=1/(delta(x));
%e1 vs Theta BI with H(s)
bb(x)=((2*F(x)*B(x)-
1)/(1+2*F(x)*G(x))+(2*H(x)*F(x)*G(x))/(1+2*F(x)*G(x)));
e1TFBi(x)=(1/delta(x))*bb(x);
%e1 vs Nri
%tfe1Nri(x)=(1/(delta(x))*(2*F(x)*G(x))/(1+2*F(x)*G(x)));
%e1 vs Nph
%e1Nph(x)=(1/(delta(x)));
%e4 vs Nph TF;
%e4Nph(x)=((e1Nph(x))-1);
%e4 vs ThetaNri TF;
%tfe4Nri(x)=tfe1Nri(x);
%e4 vs Theta BI with H(s)
%e4TFBi(x)=e1TFBi(x)
%last years e1 transfer functions
%denTF(x)=(1+2*F(x)*G(x));
%HBI(x)=(.02*F(x)*G(x))/(denTF(x));
%TFBH(x)=(2*F(x)*B(x)-1)/(denTF(x));
%e1TFBi(x)=(HBI(x)+TFBH(x));
%MOpLp(x)=2*F(x)*G(x);
            %re(x)=real(MOpLp(x));
            %im(x)=imag(MOpLp(x));
            %MOpLpPhase(x)=atan(im(x)/re(x));
```

```
%MCILp(x)=(MOpLp)/(1+MOpLp(x));
end
%Part 2, Simulink Code
function [ret,x0,str]=Thesissimulationnew(t,x,u,flag);
%THESISSIMULATIONNEW  is the M-file description of the SIMULINK system named
THESISSIMULATIONNEW.
%       The block-diagram can be displayed by typing: THESISSIMULATIONNEW.
%       SYS=THESISSIMULATIONNEW(T,X,U,FLAG) returns depending on FLAG certain
%       system values given time point, T, current state vector, X,
%       and input vector, U.
%       FLAG is used to indicate the type of output to be returned in SYS.
%
%       Setting FLAG=1 causes THESISSIMULATIONNEW to return state derivitives,
        FLAG=2
%       discrete states, FLAG=3 system outputs and FLAG=4 next sample
%       time. For more information and other options see SFUNC.
%%      Calling THESISSIMULATIONNEW with a FLAG of zero:
%       [SIZES]=THESISSIMULATIONNEW([],[],[],0),  returns a vector, SIZES, which
%       contains the sizes of the state vector and other parameters.
%               SIZES(1) number of states
%               SIZES(2) number of discrete states
%               SIZES(3) number of outputs
%               SIZES(4) number of inputs.
%       For the definition of other parameters in SIZES, see SFUNC.
%       See also, TRIM, LINMOD, LINSIM, EULER, RK23, RK45, ADAMS, GEAR.
% Note: This M-file is only used for saving graphical information;
%       after the model is loaded into memory an internal model
%       representation is used.
% the system will take on the name of this mfile:
sys = mfilename;
new_system(sys)
simver(1.2)
if(0 == (nargin + nargout))
       set_param(sys,'Location',[3,41,637,477])
    open_system(sys)
end;
set_param(sys,'algorithm',          'RK-45')
set_param(sys,'Start time', '0.0')
set_param(sys,'Stop time',          '999999')
set_param(sys,'Min step size',      '0.002')
set_param(sys,'Max step size',      '.002')
set_param(sys,'Relative error','1e-3')
set_param(sys,'Return vars',        '')
add_block('built-in/Sum',[sys,'/','aaa  '])
set_param([sys,'/','aaa  '],...
               'Drop Shadow',4,...
               'inputs','+-',...
               'position',[820,455,850,475])
add_block('built-in/To Workspace',[sys,'/',' e4  ramp'])
set_param([sys,'/',' e4  ramp'],...
               'mat-name','e4ramp',...
```

```
                'buffer','100000',...
                'position',[885,461,960,479])
add_block('built-in/To  Workspace',[sys,'/','ThetaBiThetaT'])
set_param([sys,'/','ThetaBiThetaT'],...
                'mat-name','ThetaBiThetaTi',...
                'buffer','100000',...
                'position',[890,256,965,274])
add_block('built-in/To  Workspace',[sys,'/',' thetamiramp'])
set_param([sys,'/',' thetamiramp'],...
                'mat-name','thetamiramp',...
                'buffer','100000',...
                'position',[450,521,525,539])
add_block('built-in/Note',[sys,'/','e1'])
set_param([sys,'/','e1'],...
                'position',[535,435,536,436])
add_block('built-in/Transfer  Fcn',[sys,'/','T(s)  PI2'])
set_param([sys,'/','T(s)  PI2'],...
                'Drop Shadow',4,...
                'Numerator','[10000]',...
                'Denominator','[1  200  10000]',...
                'position',[140,486,220,534])
add_block('built-in/Signal  Generator',[sys,'/','Theta  TI1'])
set_param([sys,'/','Theta  TI1'],...
                'Drop Shadow',4,...
                'Peak','5.000000',...
                'Peak Range','5.000000',...
                'Freq','20.000000',...
                'Freq  Range','1509.000000',...
                'Wave','Sin',...
                'Units','Rads',...
                'position',[65,561,95,589])
add_block('built-in/Transfer  Fcn',[sys,'/','T(s)  PI1'])
set_param([sys,'/','T(s)  PI1'],...
                'Drop Shadow',4,...
                'Numerator','[10000]',...
                'Denominator','[1  200  10000]',...
                'position',[45,376,125,424])
add_block('built-in/Note',[sys,'/',' '])
set_param([sys,'/',' '],...
                'position',[315,445,316,446])
add_block('built-in/Sum',[sys,'/','Sum'])
set_param([sys,'/','Sum'],...
                'Drop Shadow',4,...
                'inputs','++',...
                'position',[460,150,480,170])
add_block('built-in/Integrator',[sys,'/','Gyro'])
set_param([sys,'/','Gyro'],...
                'Drop Shadow',4,...
                'Initial','0',...
                'position',[30,325,50,345])
add_block('built-in/Gain',[sys,'/','Torque  Motor'])
```

```
set_param([sys,'/','Torque  Motor'],...
              'Gain','TMt',...
              'position',[530,143,570,177])
add_block('built-in/Transfer  Fcn',[sys,'/','H(s)'])
set_param([sys,'/','H(s)'],...
              'orientation',2,...
              'Drop Shadow',4,...
              'Numerator','[10e-3]',...
              'Denominator','[1]',...
              'position',[465,70,550,110])
add_block('built-in/Step  Fcn',[sys,'/','Step  Fcn'])
set_param([sys,'/','Step  Fcn'],...
              'Drop Shadow',4,...
              'Time','0',...
              'Before','0',...
              'After','.001',...
              'position',[655,265,675,285])
%    Subsystem 'S(s) '.
new_system([sys,'/','S(s)  '])
set_param([sys,'/','S(s)  '],'Location',[0,0,362,244])
add_block('built-in/Sum',[sys,'/','S(s)  /Sum'])
set_param([sys,'/','S(s)  /Sum'],...
              'inputs','+++',...
              'position',[245,57,265,93])
add_block('built-in/Gain',[sys,'/','S(s)  /D'])
set_param([sys,'/','S(s)  /D'],...
              'Gain','D',...
              'position',[95,129,115,151])
add_block('built-in/Gain',[sys,'/','S(s)  /Proportional'])
set_param([sys,'/','S(s)  /Proportional'],...
              'Gain','P',...
              'position',[120,13,140,37])
add_block('built-in/Transfer  Fcn',[sys,'/','S(s)  /Integral'])
set_param([sys,'/','S(s)  /Integral'],...
              'Numerator','[I]',...
              'Denominator','[1  0]',...
              'position',[110,57,145,93])
add_block('built-in/Derivative',[sys,'/','S(s)  /Derivative'])
set_param([sys,'/','S(s)  /Derivative'],...
              'position',[150,128,190,152])
add_block('built-in/Inport',[sys,'/','S(s)  /In_1'])
set_param([sys,'/','S(s)  /In_1'],...
              'Port','1',...
              'position',[25,65,45,85])
set_param([sys,'/','S(s)  '],...
              'Mask Display','PID',...
              'Mask Type','PID Controller',...
              'Mask Dialogue','Enter expressions for proportional, integral, and
derivative  terms.|Proportional:|Integral|Derivative:')
set_param([sys,'/','S(s)  '],...
              'Mask Translate','P=@1; I=@2; D=@3;')
```

```
set_param([sys,'/','S(s)  '],...
                'Mask  Entries','Kpt\/Kit\/Kdt\/')
%     Finished composite block 'S(s) '.
set_param([sys,'/','S(s)  '],...
                'Drop Shadow',4,...
                'position',[385,154,410,176])
add_block('built-in/Transfer  Fcn',[sys,'/','Table  Dynamics'])
set_param([sys,'/','Table  Dynamics'],...
                'Drop Shadow',4,...
                'Numerator','[1]',...
                'Denominator','[Jt  0  0]',...
                'position',[615,143,645,177])
add_block('built-in/Sum',[sys,'/','Sum1'])
set_param([sys,'/','Sum1'],...
                'Drop Shadow',4,...
                'inputs','+',...
                'position',[310,157,330,193])
add_block('built-in/Sum',[sys,'/','Sum2'])
set_param([sys,'/','Sum2'],...
                'Drop Shadow',4,...
                'inputs','+++',...
                'position',[140,317,160,353])
add_block('built-in/Sum',[sys,'/','Sum3'])
set_param([sys,'/','Sum3'],...
                'Drop Shadow',4,...
                'inputs','-+',...
                'position',[185,330,205,350])
add_block('built-in/Sum',[sys,'/','Sum4'])
set_param([sys,'/','Sum4'],...
                'Drop Shadow',4,...
                'inputs','-+',...
                'position',[235,329,255,356])
add_block('built-in/Sum',[sys,'/','Sum5'])
set_param([sys,'/','Sum5'],...
                'Drop Shadow',4,...
                'inputs','+-',...
                'position',[455,311,475,344])
add_block('built-in/Transfer  Fcn',[sys,'/','F(s)'])
set_param([sys,'/','F(s)'],...
                'Drop Shadow',4,...
                'Numerator','[Pm]',...
                'Denominator','[Jm  Bm Keqm]',...
                'position',[505,308,595,352])
add_block('built-in/Gain',[sys,'/','Mirror  Angle  Factor'])
set_param([sys,'/','Mirror  Angle  Factor'],...
                'Drop Shadow',4,...
                'Gain','2',...
                'position',[635,320,655,340])
add_block('built-in/Sum',[sys,'/','Sum6'])
set_param([sys,'/','Sum6'],...
                'Drop Shadow',4,...
```

```
                'inputs','-+',...
                'position',[730,315,750,335])
add_block('built-in/Sum',[sys,'/','Sum7'])
set_param([sys,'/','Sum7'],...
                'orientation',1,...
                'Drop Shadow',4,...
                'inputs','+-',...
                'position',[749,405,776,425])
add_block('built-in/Transfer Fcn',[sys,'/','T(s)  PI'])
set_param([sys,'/','T(s)  PI'],...
                'orientation',2,...
                'Drop Shadow',4,...
                'Numerator','[-L1  -L2]',...
                'Denominator','[1  0]',...
                'position',[455,440,510,480])
add_block('built-in/Note',[sys,'/','80 Hz Mirror Loop'])
set_param([sys,'/','80 Hz Mirror Loop'],...
                'position',[450,380,451,381])
add_block('built-in/Note',[sys,'/','4 Hz Gyro Loop'])
set_param([sys,'/','4 Hz Gyro Loop'],...
                'position',[180,440,181,441])
%    Subsystem 'B(s) '.
new_system([sys,'/','B(s)  '])
set_param([sys,'/','B(s)  '],'Location',[0,0,362,244])
add_block('built-in/Sum',[sys,'/','B(s)  /Sum'])
set_param([sys,'/','B(s)  /Sum'],...
                'inputs','+++',...
                'position',[245,57,265,93])
add_block('built-in/Gain',[sys,'/','B(s)  /D'])
set_param([sys,'/','B(s)  /D'],...
                'Gain','D',...
                'position',[95,129,115,151])
add_block('built-in/Gain',[sys,'/','B(s)  /Proportional'])
set_param([sys,'/','B(s)  /Proportional'],...
                'Gain','P',...
                'position',[120,13,140,37])
add_block('built-in/Transfer Fcn',[sys,'/','B(s)  /Integral'])
set_param([sys,'/','B(s)  /Integral'],...
                'Numerator','[I]',...
                'Denominator','[1  0]',...
                'position',[110,57,145,93])
add_block('built-in/Derivative',[sys,'/','B(s)  /Derivative'])
set_param([sys,'/','B(s)  /Derivative'],...
                'position',[150,128,190,152])
add_block('built-in/Outport',[sys,'/','B(s)  /Out_1'])
set_param([sys,'/','B(s)  /Out_1'],...
                'Port','1',...
                'position',[290,65,310,85])
add_block('built-in/Inport',[sys,'/','B(s)  /In_1'])
set_param([sys,'/','B(s)  /In_1'],...
                'Port','1',...
```

```
                'position',[25,65,45,85])
set_param([sys,'/','B(s)  '],...
                'Mask Display','PID',...
                'Mask Type','PID Controller',...
                'Mask Dialogue','Enter expressions for proportional, integral, and
derivative terms.|Proportional:|Integral|Derivative:')
set_param([sys,'/','B(s)  '],...
                'Mask Translate','P=@1; I=@2; D=@3;')
set_param([sys,'/','B(s)  '],...
set_param([sys,'/','B(s)  '],...
                'Mask Entries','Keqm/Pm\/0\/Bm/Pm\/')
%    Finished composite block 'B(s) '.
set_param([sys,'/','B(s)  '],...
                'orientation',1,...
                'Drop Shadow',4,...
                'position',[427,285,453,305])
%    Subsystem 'G(s)'
new_system([sys,'/','G(s)'])
set_param([sys,'/','G(s)'],'Location',[0,0,362,244])
add_block('built-in/Sum',[sys,'/','G(s)/Sum'])
set_param([sys,'/','G(s)/Sum'],...
                'inputs','+++',...
                'position',[245,57,265,93])
add_block('built-in/Gain',[sys,'/','G(s)/D'])
set_param([sys,'/','G(s)/D'],...
                'Gain','D',...
                'position',[95,129,115,151])
add_block('built-in/Gain',[sys,'/','G(s)/Proportional'])
set_param([sys,'/','G(s)/Proportional'],...
                'Gain','P',...
                'position',[120,13,140,37])
add_block('built-in/Transfer  Fcn',[sys,'/','G(s)/Integral'])
set_param([sys,'/','G(s)/Integral'],...
                'Numerator','[I]',...
                'Denominator','[1  0]',...
                'position',[110,57,145,93])
add_block('built-in/Derivative',[sys,'/','G(s)/Derivative'])
set_param([sys,'/','G(s)/Derivative'],...
                'position',[150,128,190,152])
add_block('built-in/Outport',[sys,'/','G(s)/Out_1'])
set_param([sys,'/','G(s)/Out_1'],...
                'Port','1',...
                'position',[290,65,310,85])
add_block('built-in/Inport',[sys,'/','G(s)/In_1'])
set_param([sys,'/','G(s)/In_1'],...
                'Port','1',...
                'position',[25,65,45,85])
set_param([sys,'/','G(s)'],...
                'Mask Display','PID',...
                'Mask Type','PID Controller',...
```

```
            'Mask Dialogue','Enter expressions for proportional, integral, and
derivative terms.|Proportional:|Integral|Derivative:')
set_param([sys,'/','G(s)'],...
            'Mask Translate','P=@1; I=@2; D=@3;')
set_param([sys,'/','G(s)'],...
set_param([sys,'/','G(s)'],...
            'Mask Entries','Kpm\/Kim\/Kdm\/')
%    Finished composite block 'G(s)'.
set_param([sys,'/','G(s)'],...
            'Drop Shadow',4,...
            'position',[275,325,305,345])
add_block('built-in/Transfer Fcn',[sys,'/','G(s)1'])
set_param([sys,'/','G(s)1'],...
            'Drop Shadow',4,...
            'Numerator','[am]',...
            'Denominator','[1 am]',...
            'position',[325,316,410,354])
add_block('built-in/Note',[sys,'/',`          '])
set_param([sys,'/',`          '],...
            'position',[155,250,156,251])
add_block('built-in/Note',[sys,'/','Theta Bi'])
set_param([sys,'/','Theta Bi'],...
            'position',[685,125,686,126])
add_block('built-in/Clock',[sys,'/','Clock1'])
set_param([sys,'/','Clock1'],...
            'position',[705,230,725,250])
add_block('built-in/Gain',[sys,'/','a'])
set_param([sys,'/','a'],...
            'Drop Shadow',4,...
            'Gain','.001',...
            'position',[720,265,740,285])
add_block('built-in/To Workspace',[sys,'/','e3ramp'])
set_param([sys,'/','e3ramp'],...
            'mat-name','e3ramp',...
            'buffer','100000',...
            'position',[375,71,450,89])
add_block('built-in/To Workspace',[sys,'/','e2ramp'])
set_param([sys,'/','e2ramp'],...
            'mat-name','e2ramp',...
            'buffer','100000',...
            'position',[340,471,415,489])
add_block('built-in/To Workspace',[sys,'/',' e1 ramp'])
set_param([sys,'/',' e1 ramp'],...
            'mat-name','e1ramp',...
            'buffer','100000',...
            'position',[565,491,640,509])
add_block('built-in/Note',[sys,'/','e2'])
set_param([sys,'/','e2'],...
            'position',[265,315,266,316])
add_block('built-in/Note',[sys,'/','e3'])
set_param([sys,'/','e3'],...
```

```
                'position',[355,140,356,141])
add_block('built-in/To  Workspace',[sys,'/','Time'])
set_param([sys,'/','Time'],...
                'mat-name','time',...
                'buffer','100000',...
                'position',[690,186,765,204])
add_block('built-in/Sum',[sys,'/','Sum8'])
set_param([sys,'/','Sum8'],...
                'orientation',2,...
                'Drop Shadow',4,...
                'inputs','-+',...
                'position',[605,250,625,285])
        if (nargin > 3)
                if (flag == 0)
                        eval(['[ret,x0,xstr]=',sys,'(t,x,u,flag);'])
                else
                        eval(['ret  =',  sys,'(t,x,u,flag);'])
                end
        else
                [ret,x0,str]  =  feval(sys);
        end
```

Appendix B: PSD Simulation

```
%Coefficients for Loading PSD's for ThetaBi (Initialization);
p1=0;
p2=0;
fo=.096;%for  .01-1000Hz
%fo=.0244;for  1-20  Hz
NoiseNrisum=0;
NoiseNphsum=0;
NoiseHzsum=0;

%Putting in Power SPec PSD's for ThetaBi;
wpsd=logspace(-0.2018,2.7982,300); %.1 to 100Hz in Radians;
%wpsd=logspace(.7979,2.099,300); 1 to 20Hz in Radians;
n=length(wpsd);
for k=1:n;
        h(k)=wpsd(k);
        h(k)=(h(k))/(2*pi);
        f=h(k);
        %if f<=1,
        %Hreal(k)=.00628/(f*2*pi*i);
        %else  Hreal(k)=.00095;
        %end
                %if f<.2, PSD1(k)=1e5;
                 %elseif (.2<f  &  f<=.3),  PSD1(k)=10^(-2.94-11.36*log10(f));
                 %elseif (.3<f  &  f<=.4),  PSD1(k)=10^(11.37+16*log10(f));
                 %elseif (.4<f  &  f<=1),  PSD1(k)=10^(3.41-4*log10(f));
                %elseif (1<f  &  f<=10),  PSD1(k)=1/f^4;
                 %else  PSD1(k)=10^(3-4*log10(f));
               %end
              %PSD1(k)=4*PSD1(k);
              if f<1,  PSD2(k)=350;
                 elseif (1<f  &  f<11.5),  PSD2(k)=10^(2.544-1.35*log10(f));
                 else  PSD2(k)=10^(7-5.5*log10(f));
        end
        %p1=p1+PSD1(k)*(f-fo);%*(f/Hz)^2;
        p2=p2+PSD2(k)*(f-fo);%*(f/Hz)^2;
        %P1(k)=p1;
        P2(k)=p2;
        %if f<.1,  NoiseNri(k)=0;
              %elseif (.1<f  &  f<100),  NoiseNri(k)=5.7e-4;
              %else  NoiseNri(k)=0;
        %end
        %NoiseNrisum=NoiseNrisum+NoiseNri(k)*(f-fo);
        %if f<.1,  NoiseNph(k)=0;
              %elseif (.1<f  &  f<30),  NoiseNph(k)=8.3e-3;
              %else  NoiseNph(k)=0;
        %end
        %NoiseNphsum=NoiseNphsum+NoiseNph(k)*(f-fo);
        %if  (f>1  &  f<4),  NoiseHz(k)=10^(1.602+1.161*log10(f));
```

```
        elseif (f>=4 & f<6.77), NoiseHz(k)=10^(3.3468-1.741*log10(f));
        elseif (f>6.77 & f<20), NoiseHz(k)=10^(5.47-(4.3*log10(f)));
        else NoiseHz(k)=0;
        end
        NoiseHzsum=NoiseHzsum+NoiseHz(k)*(f-fo);
        fo=f;
end;
sqrt(p2)
%sqrt(NoiseNrisum)
%sqrt(NoiseNphsum)
%sqrt(NoiseHzsum)

PSDe1Bi=0.00;
%PSDnoiseNri1=0.00;
%PSDnoiseNph1=0.00;
sumrmscheck1=0.00;
%PSDe4Bi=0.00;
%PSDnoiseNri4=0.00;
%PSDnoiseNph4=0.00;
%sumrmscheck4=0.00;
for k=2:n
dhz(k)=(wpsd(k)/(2*pi))-(wpsd(k-1)/(2*pi));
        freq=(wpsd(k)/(2*pi));
        e1sqBi(k)=PSD2(k)*((abs(e1TFBi(k)))^2);
        e1intsqBi(k)=PSD2(k)*((abs(e1TFBi(k)))^2)*dhz(k);
        PSDe1Bi=PSDe1Bi+e1intsqBi(k);
        %e1sqnoiseNri(k)=NoiseNri(k)*((abs(tfe1Nri(k)))^2);
        %e1intsqnoiseNri(k)=NoiseNri(k)*((abs(tfe1Nri(k)))^2)*dhz(k);
        PSDnoiseNri1=PSDnoiseNri1+e1intsqnoiseNri(k);

        %e1sqnoiseNph(k)=NoiseNph(k)*((abs(e1Nph(k)))^2);
        %e1intsqnoiseNph(k)=NoiseNph(k)*((abs(e1Nph(k)))^2)*dhz(k);
        %PSDnoiseNph1=PSDnoiseNph1+e1intsqnoiseNph(k);

        %sumnoisemotion1(k)=e1sqnoiseNri(k)+e1sqnoiseNph(k)+e1sqBi(k);
        %sumrmscheck1=sumrmscheck1+e1intsqnoiseNri(k)+e1intsqnoiseNph
                (k)+e1intsqBi(k);

        e4sqBi(k)=PSD2(k)*((abs(e4TFBi(k)))^2);
        %e4intsqBi(k)=PSD2(k)*((abs(e4TFBi(k)))^2)*dhz(k);
        %PSDe4Bi=PSDe4Bi+e4intsqBi(k);

        e4sqnoiseNri(k)=NoiseNri(k)*((abs(tfe4Nri(k)))^2);
        %   e4intsqnoiseNri(k)=NoiseNri(k)*((abs(tfe4Nri(k)))^2)*dhz(k);
        %PSDnoiseNri4=PSDnoiseNri4+e4intsqnoiseNri(k);

        %  e4sqnoiseNph(k)=NoiseNph(k)*((abs(e4Nph(k)))^2);
        %  e4intsqnoiseNph(k)=NoiseNph(k)*((abs(e4Nph(k)))^2)*dhz(k);
        %PSDnoiseNph4=PSDnoiseNph4+e4intsqnoiseNph(k);


        %sumnoisemotion4(k)=e4sqnoiseNri(k)+e4sqnoiseNph(k);%+e4sqBi(k);
```

```
        %sumrmscheck4=sumrmscheck4+e4intsqnoiseNri(k)+e4intsqnoiseNph
            (k);%+e4intsqBi(k);

end
```